

PROVENANCE OF LOWER PENNSYLVANIAN POTTSVILLE FORMATION,
CAHABA SYNCLINORIUM, ALABAMA

Except where reference is made to the work of others, the work described in this thesis is my own or was done in collaboration with my advisory committee. This thesis does not include proprietary or classified information.

Tara Peavy

Certificate of Approval:

Charles E. Savrda
Professor
Geology and Geography

Ashraf Uddin, Chair
Associate Professor
Geology and Geography

Willis E. Hames
Professor
Geology and Geography

George T. Flowers
Dean
Graduate School

PROVENANCE OF LOWER PENNSYLVANIAN POTTSVILLE FORMATION,
CAHABA SYNCLINORIUM, ALABAMA

Tara Peavy

A Thesis
Submitted to
the Graduate Faculty of
Auburn University
in Partial Fulfillment of the
Requirement for the
Degree of
Master of Science

Auburn, Alabama
December 19, 2008

PROVENANCE OF LOWER PENNSYLVANIAN POTTSVILLE FORMATION,
CAHABA SYNCLINORIUM, ALABAMA

Tara Peavy

Permission is granted to Auburn University to make copies of this thesis at its discretion, upon the request of individuals or institutions and at their expense. The author reserves all publication rights.

Signature of Author

Date of Graduation

VITA

Tara Peavy, daughter of Todd and Daisy Peavy, was born on December 3rd, 1982, in Albany, Georgia. She attended The Lakeside School, in Eufaula, Alabama, for elementary and high school and Georgia Southwestern State University, in Americus, Georgia, for a Bachelor's Degree in Geology. She moved to Auburn to complete a Masters Degree in the Department of Geology and Geography in August 2006.

THESIS ABSTRACT

PROVENANCE OF LOWER PENNSYLVANIAN POTTSVILLE FORMATION, CAHABA SYNCLINORIUM, ALABAMA

Tara Peavy

Master of Science, December 19, 2008
(B.S., Georgia Southwestern State University, 2005)

123 Typed Pages

Directed by Ashraf Uddin

The Cahaba basin, also known as the Cahaba Synclinorium, of north-central Alabama contains a thick (>2.5 km) synorogenic clastic wedge belonging to the Lower Pennsylvanian Pottsville Formation. Sediment composition and detrital geochronology reveal a provenance history for these fluvial-deltaic to shallow marine sediments.

Pottsville clastics are cyclothemtic, consisting of interbedded sandstone, siltstone, claystone, shale, and numerous coal beds, with orthoquartzite sandstone and conglomerate at the base. Basal Pottsville is dominated by quartz-rich sediments; feldspars increase upsection. Plagioclase feldspars dominate over k-spars. No obvious trend in lithic fragments was observed. Compositions of these sandstones reflect a “recycled orogenic” provenance. Heavy minerals are dominated by rutile, tourmaline, and medium-grade almandine garnets. Overall lack of chromium in the Pottsville Formation indicates that ophiolitic belts or terranes with abundant mafic igneous rocks

were not a common source for these sandstones. Mudrock geochemistry of the Pottsville units indicates a mixture of an island arc provenance and an active continental margin dominated by metamorphic rocks. $^{40}\text{Ar}/^{39}\text{Ar}$ study of detrital muscovites data reveal ages typical of all three Appalachian orogenic events (Taconic, Acadian and Alleghenian). The Western Blue Ridge, the Talladega belt, and the Cat Square terranes of the Inner Piedmont are the most probable source areas for these detrital grains.

This study confirms the suggestion that sediments of the Pottsville Formation were primarily derived from the uplifted Appalachian orogen to the east and northeast.

ACKNOWLEDGMENTS

Many people, organizations, and companies have made contributions without which my work would not have been possible. I would not have known even where to begin this thesis without the help of my principal advisor, Dr. Ashraf Uddin. He helped me to mold my topic into a workable thesis, all the while guiding and encouraging me through it. I would also like to extend my appreciation to my other committee members, Dr. Charles Savrda and Dr. Willis Hames. I would like to thank Dr. Steltenpohl, whom provided helpful information through conversations about the argon data. The Geological Society of America, especially the Southeastern section, and Gulf Coast Association of Geological Societies provided money for fieldwork and sample analyses. The Geological Survey of Alabama, with special help from Dr. Jack Pashin, and CDX Gas Co., specifically Dr. Ruppert Bodden, provided core samples and their expertise on the geology of the area. The University of Georgia Microprobe Lab, with special thanks to Mr. Chris Fleischer, and the ANIMAL facility, directed by Dr. W. Hames, all helped obtain data from the Cahaba basin. As a whole, I would like to thank the Department of Geology and Geography at Auburn University for the help and support that was required to complete this study. Finally, I would like to thank my friends and family, whom have encouraged and supported me through all of my struggles and achievements.

Style manual or journal used

Geology

Computer software used

Adobe Photoshop 7

Golden Software Grapher 3.0

Golden Software Surfer 8.0

Isoplot

Microsoft Word 2007

Microsoft Excel 2007

Rockwork 2004

TABLE OF CONTENTS

	Page
LISTS OF FIGURES.....	xii
LISTS OF TABLES.....	xviii
CHAPTER 1: INTRODUCTION.....	1
1.0 Introduction.....	1
1.1 Study area.....	2
1.2 Previous Works.....	6
CHAPTER 2: TECTONIC SETTING AND REGIONAL GEOLOGY.....	10
2.0 Introduction.....	10
2.1 Appalachians.....	10
2.1.1 Taconian Orogeny.....	11
2.1.2 Acadain Orogeny.....	12
2.1.3 Alleghenian Orogeny.....	15
2.2 Ouachita Belt.....	15
CHAPTER 3: SANDSTONE PETROGRAPHY.....	20
3.0 Introduction.....	20
3.1 Methods.....	21
3.2 Petrography.....	24
3.3 Interpretations.....	32

CHAPTER 4: HEAVY MINERAL ANALYSIS.....	40
4.0 Introduction.....	40
4.1 Methods.....	40
4.2 Results.....	42
4.3 Interpretations.....	47
CHAPTER 5: MICROPROBE ANALYSIS OF GARNETS	48
5.0 Introduction.....	48
5.1 Electron Microprobe.....	48
5.2 Methods.....	49
5.3 Results.....	50
5.4 Interpetations.....	58
CHAPTER 6: $^{40}\text{Ar}/^{39}\text{Ar}$ DETRITAL MUSCOVITE AGES.....	59
6.0 Introduction.....	59
6.1 Previous Detrital Geochronology.....	59
6.2 $^{40}\text{Ar}/^{39}\text{Ar}$ Dating.....	60
6.3 Methods.....	62
6.4 Results.....	65
6.5 Interpretations.....	67
CHAPTER 7: MUDROCK CHEMISTRY.....	69
7.0 Introduction.....	69
7.1 Methods.....	70
7.2 Results.....	70
7.3 Interpetations.....	73

CHAPTER 8: DISCUSSION AND CONCLUSIONS.....	79
REFERENCES.....	89
APPENDICES.....	97

LIST OF FIGURES

Figure 1. Location map of Cahaba Basin, located within the Cahaba synclinorium in north-central Alabama (from Pashin et al., 1995). The Cahaba basin is bounded to the northwest by the Birmingham anticlinorium and to the southeast by the Helena Thrust Fault.....	3
Figure 2a. Index map showing location of structural cross sections of the Pottsville Formation (modified from Pashin and Carroll, 1999). Cross-sections for lines A-A` through F-F` are shown in Figure 2b. Paleocurrent directions, indicated by orange arrows, are from Schlee (1963). Blue diamonds indicate locations of CDX Gas Co. drill cores; orange dot indicates location of School of Mines and Energy Development (SOMED) core obtained from the Geological Survey of Alabama	4
Figure 2b. Structural cross-sections of the Pottsville Formation in the Cahaba coal field. See Figure 2a for locations (modified from Pashin and Carroll, 1999).....	5
Figure 3. Generalized stratigraphic column for the Pottsville Formation and associated rocks (modified from Pashin and Carroll, 1999).....	8
Figure 4. Map of a portion of the Appalachians showing distribution of Ordovician sediment that experienced deformation during the Taconic orogeny (modified from Bradley, 1989)	13
Figure 5. Generalized map showing extent of Appalachian and Ouachita belts in southeastern North America. The blue oval highlights the Ouachita belt, the pink oval highlights the Appalachian belt (modified from Hatcher et al., 1989).....	17
Figure 6. Generalized stratigraphic column of the Appalachian/Illinois and the Ouachita basins (modified from Gleason et al., 1995).....	19
Figure 7. Generalized stratigraphic column of the Pottsville Formation in the Cahaba coalfield, Alabama (modified from Pashin and Carroll, 1999). Purple dots to the right of the column indicate depths at which outcrop samples were collected. Solid lines represent the depths that cores were drilled, while dots to the right show where samples were collected. Four cores were made available by CDX Gas Company (left to right: Mayberry Creek in blue; Dogwood No. 1 in red; Savage Creek in green; Radio Tower in orange). The fifth core, SOMED drill core (black), was provided by the Geological Survey of Alabama.....	22

Figure 8. Representative photomicrographs of Pottsville sandstone. (a) Rounded to sub-angular monocrystalline grains (Qm) among polycrystalline quartz (Qp), sedimentary (Ls) and metamorphic lithic (Lm) fragments, and plagioclase (plag) (sample PSS-4, crossed polars). (b) Detrital chert and polycrystalline quartz grains (Qp) among lithic grains (Ls) (sample PSS-5, crossed polars)..... 25

Figure 9. Representative photomicrographs of Pottsville sandstone. (a) Volcanic lithic fragments (Lv) with quartz (Qm) and calcite (sample PSS-5, crossed polars). (b) Very low- to low-grade metamorphic fragments (Lm) (sample PSS-3, crossed polars)..... 26

Figure 10. Representative photomicrographs of Pottsville sandstone. (a) Sedimentary rock fragment (Ls) (sample CHB-4, cross polars). (b) Plagioclase (plag) partially replaced by calcite, with monocrystalline (Qm) and polycrystalline quartz (Qp) grains (sample PSS-6, plane polar)..... 27

Figure 11. QtFL plot showing overall sandstone modes of Pottsville sandstones from the Cahaba Basin. Standard deviation polygon is drawn around the mean (shown as a red dot). Provenance fields are from Dickinson (1985). Qt=total quartz; F=feldspar; L=lithic grains. Most sands from the Pottsville Formation plot very close together within the “recycled orogenic” field..... 29

Figure 12. QmFLt plot of Pottsville sandstones from the Cahaba Basin, showing mean (red dot) and standard deviation polygon, with appropriate provenance fields from Dickinson (1985). Chert and other polycrystalline quartz are included in the total lithic counts (see Table 1). Qm=monocrystalline quartz; F=feldspar; Lt=total lithic fragments. Most sands from the Pottsville Formation also plot very close together within the “quartzose recycled” field..... 30

Figure 13. QmPK plot of Pottsville sandstones from the Cahaba Basin, showing mean (red dot) and standard deviation polygon. Qm=monocrystalline quartz; P=plagioclase feldspar; K=potassium feldspar. Most sands from the Pottsville Formation plot close to the Qm end member..... 31

Figure 14. LsLvLm plot showing variations in the composition of lithic fragments in the Cahaba Basin. Ls = sedimentary lithic fragments, Lv = volcanic lithic fragments, and Lm = low- to intermediate-grade metamorphic rock fragments..... 33

Figure 15. LsLm₁Lm₂ plot showing the mean (red dot) and standard deviation in composition of Pottsville sandstones in the Cahaba Basin. Ls = sedimentary lithic fragments, Lm₁ = very low- to low-grade metamorphic rock fragments, and Lm₂ = low- to intermediate-grade metamorphic rock fragments..... 34

Figure 16. Profile plot of changes in percentages of total quartz (Qt), feldspars (F), and lithic fragments (L) through the Pottsville Formation in the Cahaba Basin..... 35

Figure 17. Profile plot of changes in percentages of monocrystalline quartz (Qm), feldspars (F), and total lithic fragments (Lt) through the Pottsville Formation in the Cahaba Basin. Chert and polycrystalline quartz are included in total lithic fragments....	36
Figure 18. Profile plot of changes in percentages of monocrystalline quartz (Qm), plagioclase feldspars (P), and potassium feldspars (K) through the Pottsville Formation in the Cahaba Basin.	37
Figure 19. Profile plot of changes in percentages of sedimentary (Ls), volcanic (Lv), and metamorphic (Lm) lithic fragments through the Pottsville Formation in the Cahaba Basin.....	38
Figure 20. Profile plot of changes in percentages of sedimentary lithic fragments (Ls), very low- to low-grade metamorphic (Lm ₁), and low- to intermediate-grade metamorphic (Lm ₂) lithic fragments through the Pottsville Formation in the Cahaba Basin.....	39
Figure 21. Photomicrographs of heavy minerals from Pottsville Formation. (a) Rutile grain in sample RTC-1 from the conglomerate measure. (b) Zircon grain in sample DC-4 also from the conglomerate measure. Both in plane transmitted light.....	43
Figure 22. Photomicrographs of heavy minerals from Pottsville Formation, Cahaba Basin, Alabama. (a) Garnet grain in sample PSS-6 from the mudstone measure. (b) Chlorite surrounded by opaque minerals in sample PSS-12, also from the mudstone measure.....	44
Figure 23. Heavy-mineral distribution in Pottsville sandstone showing distribution of all observed heavy minerals in conglomerate, mudstone, and quartzarenite measures.....	46
Figure 24. Backscatter images from microprobe analysis of garnet grains. (a) Garnet (lighter grain, high z; high average atomic number, common for iron-rich minerals) intergrown with calcite (darker grain, low z; typical of carbonates, quartz, etc.) (b) Garnet grain (lighter grain, high z) intergrown with large calcite (darker grain, low z) crystals.....	52
Figure 25. Ternary plot showing garnet chemistry; Al=almandine; Sp=spessartine; Gr=grossular; and Py=pyrope. I=garnets with almandine and grossular with <10% pyrope; II=garnets with almandine and pyrope with <10% grossular; and III=garnets with pyrope and grossular, both >10% (modified from Morton et al., 1992).....	53
Figure 26. Ternary plot of garnet chemistry. Alm=almandine; Sp=spessartine; Gro=grossular; and Py=pyrope.	54
Figure 27. Ternary plot of garnet chemistry; Alm=almandine; Sp=spessartine;	

Py=pyrope; and Gro=grossular	55
Figure 28. Ternary plot of garnet chemistry and its relation to metamorphic grade. Alm=almandine; Sp=spessartine; Py=pyrope. APF=amphibolites facies; GNF=granulite facies; ECF=eclogite facies; Pg=pegmatite; and met=metamorphic (after Nanayama, 1997).....	56
Figure 29. Relationship between Pottsville garnet chemistry and metamorphic pressures and temperatures. Dashed black lines are isopleths of constant Fe/(Fe+Mg)calculated assuming garnet in equilibrium with biotite (from Spear and Cheney, 1989). Red shaded polygon indicates where Pottsville garnets would presumably plot if formed under Barrovian or Buchan/Abukuma.....	57
Figure 30. Decay scheme of relevant isotopes according to the $^{40}\text{Ar}/^{39}\text{Ar}$ technique. Filled boxes are naturally occurring isotopes; red arrow indicates $^{40}\text{K}\rightarrow^{40}\text{Ar}$ decay, which is a naturally occurring reaction. The blue arrow indicates the $^{39}\text{K}(\text{n,p})^{39}\text{Ar}_{\text{K}}$ reaction, which is induced in a nuclear reactor, and makes $^{40}\text{Ar}/^{39}\text{Ar}$ dating possible.....	61
Figure 31. Generalized stratigraphic column of Pennsylvanian Pottsville Formation in the study area (modified from Pashin and Carroll, 1999). Stratigraphic positions of the three samples (D2S1, D2S2, and CHB-5), used to extract muscovite grains for $^{40}\text{Ar}/^{39}\text{Ar}$ dating are shown by arrows.....	63
Figure 32. Photomicrographs of muscovite grains of samples D2S1, D2S2, and CHB-5.....	64
Figure 33. $^{40}\text{Ar}/^{39}\text{Ar}$ isotope ages for samples D2S1, D2S2, and CHB-5, in stratigraphic order. The curves show relative probability of ages. Error bars represent 1σ . Mode of CHB-5 was defined by analysis of all data using an algorithm for rejecting outliers in Isoplot (Ludwig, 2003). Modes of D2S2 and D2S1 were determined by inspection.....	66
Figure 34. Generalized stratigraphic column of Pottsville Formation in the study area (modified from Pashin and Carroll, 1999) showing depths at which samples (MC-4, PSS-11, PSS-10, PSSC-5, PSSC-4) were collected for whole-rock chemical analysis.....	71
Figure 35. Weight percentages of major oxides present in the Pottsville samples.....	74
Figure 36. Trace elements of Pottsville samples, given in parts per million.....	75
Figure 37. Plot of the log of $\text{K}_2\text{O}/\text{Na}_2\text{O}$ versus SiO_2 for Pottsville mudrock samples (modified from Roser and Korsch, 1988). Samples fall in both active continental margin and island-arc provenances. The two samples that plot in the island arc provenance are PSSC-5 and MC-4.....	76
Figure 38. Possible source rock affinities of Pottsville mudrock samples illustrated in Si-	

Ca+Mg–Na+K ternary plot (after Taylor and McLennan, 1985). Post Archean average shale (PAAS) and average crustal composition are taken.....77

Figure 39. Compositional variations of mudrock samples of Cahaba Basin illustrated in A–CN–K (Al_2O_3 –CaO+Na₂O–K₂O) compositional space triangle (after Nesbit and Young, 1984). CIA is the chemical index of alteration $[(Al_2O_3/(Al_2O_3+K_2O+Na_2O+CaO))] * 100$. Pottsville samples plot close to the Al_2O_3 apex, indicating intense chemical weathering. Kln=kaolinite; Chl=chlorite; Ms= muscovite; Bt biotite; Kfs=potassium–feldspar; Cpx=clinopyroxene; Hbl=hornblende; Pl=plagioclase; Sm=smectite.....78

Figure 40. Composite profile of petrographic data of the Pottsville Formation. In Qt–F–L: Qt=blue, F=dark red, L=yellow. In Qm–F–Lt, Q: Blue, F: Dark red, Lt: yellow. In Qm–P–K, Qm: Blue, P: Dark red, K: yellow. In Ls–Lv–Lm, Ls: Blue, Lv: Dark red, Lm: yellow. In Ls–Lm₁–Lm₂, Ls: Blue, Lm₁: Dark red, Lm₂: yellow..... 81

Figure 41. Nickel in parts per million versus ferric oxide + magnesium oxide. Pottsville samples are plotted along with samples from two separate basins in the Himalayan orogen; the Assam basin, proximal to the orogen, and the Bengal basin, more distal from the orogen. The Pottsville samples are more closely related to the Bengal basin with respect to Ni content..... 82

Figure 42. Plot of titanium oxide versus ferric oxide + magnesium oxide. Pottsville samples are plotted along with samples from two separate basins in the Himalayan orogen; the Assam basin, proximal to the orogen, and the Bengal basin, distal from the orogen. Himalayan and Appalachian samples plot relatively close.....84

Figure 43. Lower Pennsylvanian paleogeographic map of the Cahaba Basin region of Alabama and regional surroundings. Note the proximity of the region to the equator. Purple represents the Hillabee Greenstone of Alabama (Mersch and Hatcher, 2007). Green represents the Talladega Slate belt and Western Blue Ridge of the Appalachians (McDonald, 2008). Yellow represents the Tugaloo terrane and blue represents the Cat Square terrane of the Appalachians (McClellan et al., 2007). Uplifted terranes were located further to the east of Cahaba than they are today and are the primary sources of sediment (BWB: Black Warrior Basin)..... 87

LIST OF TABLES

Table 1. Recalculated modal parameters of sand and sandstones.....	23
Table 2. Normalized modal compositions of sandstones from three magnafacies of the Lower Pennsylvanian Pottsville Formation.....	28
Table 3. Normalized abundances of heavy minerals of the Pottsville Formation, Cahaba Basin, Alabama. (ZTR – Zircon-Tourmaline-Rutile).....	45
Table 4. Electron microprobe standards used in this study.....	51
Table 5. Results of whole-rock chemical analyses of Pottsville samples PSS-10, PSS-11, PSSC-4, PSSC-5, and MC-4.	72

CHAPTER 1. INTRODUCTION

1.0 INTRODUCTION

Provenance studies of sedimentary sequences deposited along the flanks of mountain systems can provide significant constraints on orogenic processes and the history of mountain belts (Uddin and Lundberg, 1998). Continental collision represents the last event in a compressional orogeny series. Crustal thickening due to convergence of plates causes intense surface relief and subsidence of flanking basins that favors rapid erosion and accumulation of clastic detritus.

Analyses of detrital sediment are vital in determining provenance. Petrofacies analyses can help discriminate various tectonic settings and interpret plate interactions in the geologic past. Composition of detrital sediments is controlled by various factors: source rocks, modes of transport, depositional environments, diagenesis, and climate (Suttner, 1974; Zahid, 2005). Provenance studies focusing on key characteristics of sediments provide important information on basin evolution and unroofing of mountain chains. Reconstruction of the provenance of a region is based on the belief that control factors—such as climate and mode of transportation—have not altered sediment grain composition.

The Pottsville Formation is part of a thick clastic wedge that accumulated during the Pennsylvanian in response to collision of Laurentia and Gondwana. Previous studies have produced conflicting interpretations for the provenance of these sediments

(e.g., Schlee, 1963; Graham et al., 1976; Mack et al., 1983; Demirpolat, 1989; Liu and Gastaldo, 1992). Accurate and precise determination of provenance is needed in order to better understand the nature and timing of regional tectonics of central Alabama.

The objective of this study is to delineate the provenance for the Pottsville sandstone located in the Cahaba coalfield region of north-central Alabama. Mack et al. (1983) suggested a provenance from the Ouachita orogen to the southwest as the dominant source for the Pottsville Formation, with minor contributions from the northeast. This current project will test their findings and suggest if instead the Appalachian orogen, located to the east-northeast, had been the predominant source.

1.1 STUDY AREA

The Lower Pennsylvanian Pottsville Formation is a classic clastic wedge stretching from New York to central Alabama (Thomas, 2006). The Pottsville Formation contains a thick succession of siliciclastic rocks that were deposited near the paleo-equator (Thomas et al., 2004). It consists of interbedded sandstones, siltstones, claystone, shale, and coal beds, with orthoquartzite conglomerate at the base. The cyclic nature of Pottsville Formation strata is interpreted to be the product of fourth-order glacial eustasy mediated by waxing and waning of the Gondwanan ice sheet (Pashin, 2006).

The Cahaba Basin, also referred to as the Cahaba coal field, is a synclinorium located in north-central Alabama (Figures 1 and 2). The Cahaba synclinorium is bordered to the northwest by the Birmingham anticlinorium. It is separated from the Coosa synclinorium (also referred to as Coosa coal field; Figure 1) to the southeast by the regionally extensive Helena fault. The Cahaba Basin is dominantly composed of Lower

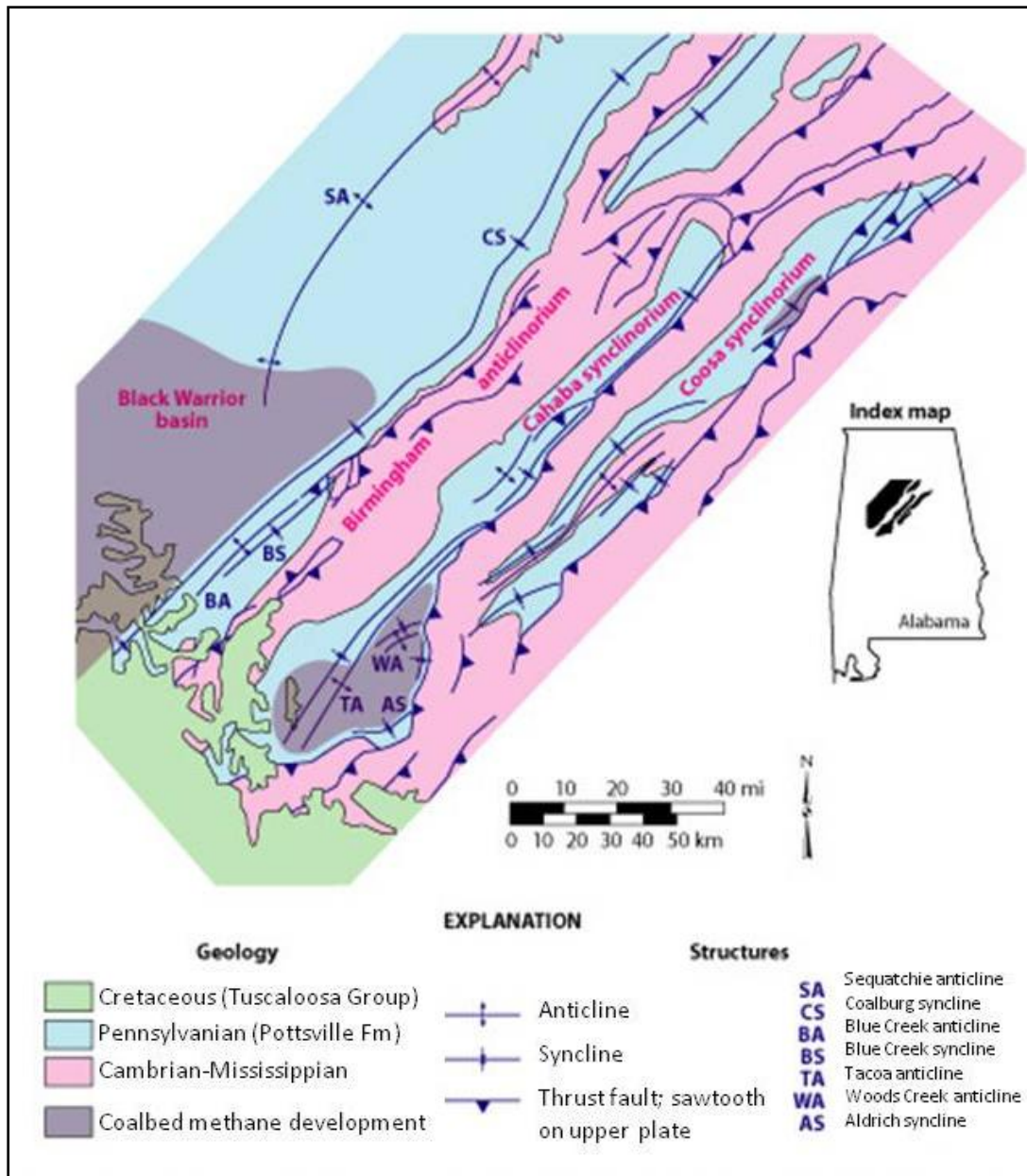


Figure 1. Location map of Cahaba Basin, located within the Cahaba synclinorium in north-central Alabama (from Pashin et al., 1995). The Cahaba basin is bounded to the northwest by the Birmingham anticlinorium and to the southeast by the Helena Thrust Fault.

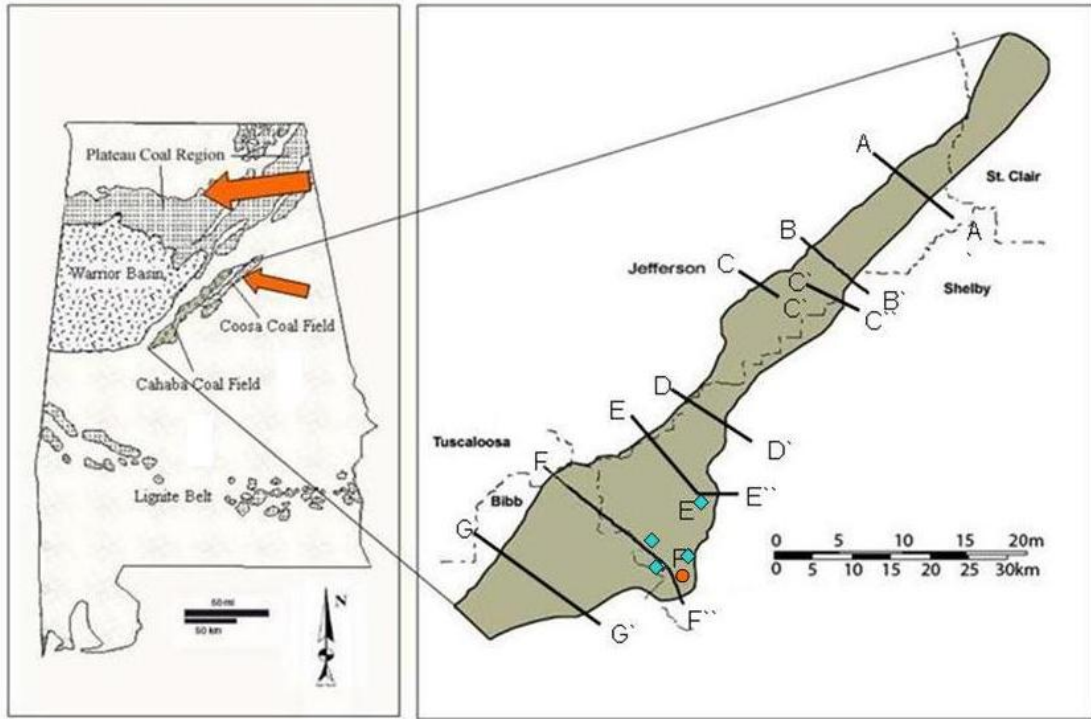


Figure 2a. Index map showing location of structural cross sections of the Pottsville Formation (modified from Pashin and Carroll, 1999). Cross-sections for lines A-A' through F-F' are shown in Figure 2b. Paleocurrent directions, indicated by orange arrows, are from Schlee (1963). Blue diamonds indicate locations of CDX Gas Co. drill cores; orange dot indicates location of School of Mines and Energy Development (SOMED) core obtained from the Geological Survey of Alabama.

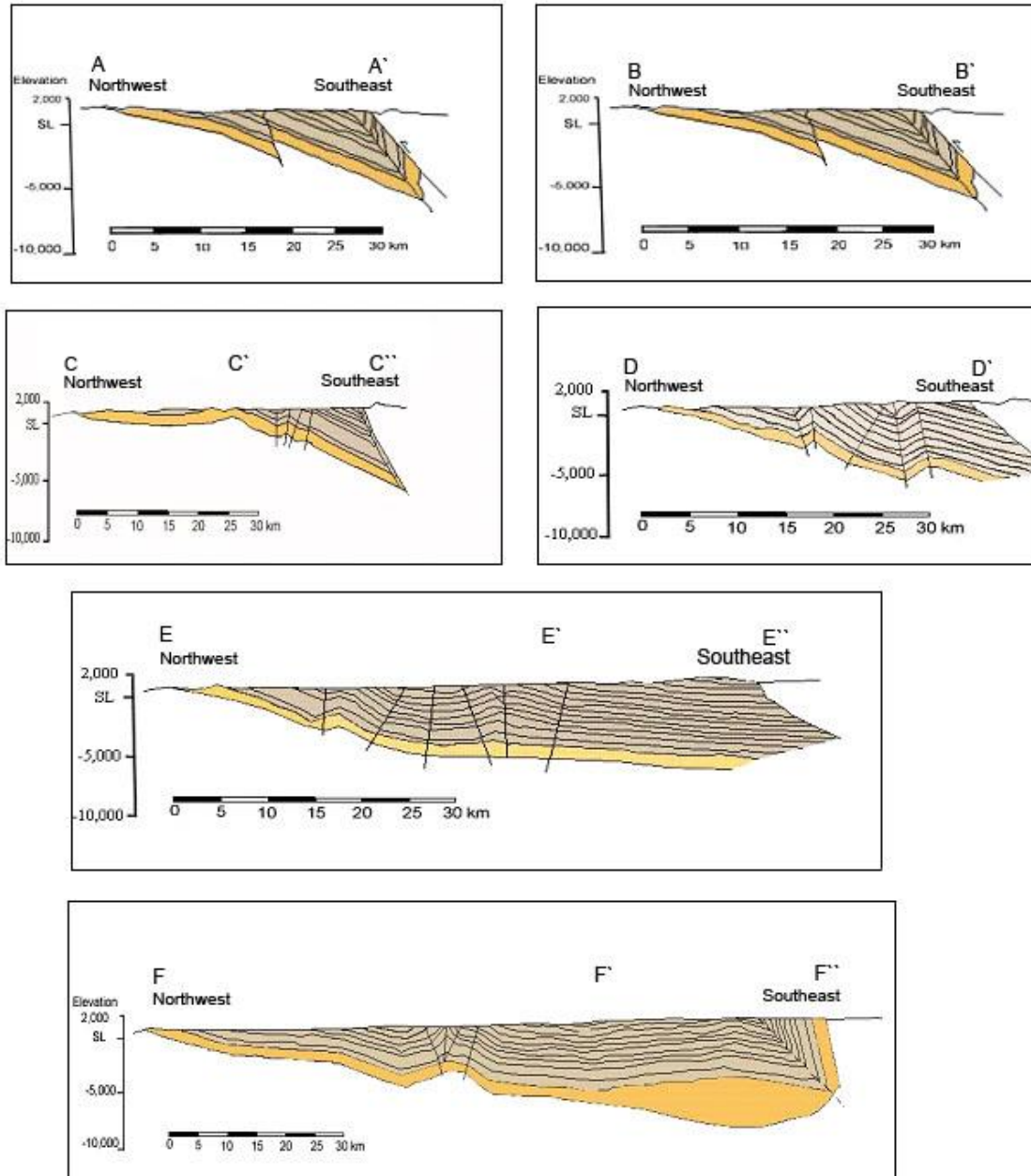


Figure 2b. Structural cross-sections of the Pottsville Formation in the Cahaba coal field. See Figure 2a for locations (modified from Pashin and Carroll, 1999).

Pennsylvanian Pottsville Formation, which contains 20 informal coal zones and has a maximum thickness that locally exceeds 2,500 meters. The Pottsville Formation overlies the Upper Mississippian-Lower Pennsylvanian Parkwood Formation throughout the Cahaba Basin. In most of the Cahaba synclinorium, the Pottsville Formation is the youngest unit. However, near the southwest end of the structure, the Pottsville Formation is unconformably overlain by the Cretaceous Coker Formation (Tuscaloosa Group) (Pashin and Carroll, 1999) (Figure 3). The southeast part of the Cahaba Basin possesses a thicker succession of sediment and greater rates of subsidence during deposition (Pashin and Carroll, 1999; Pashin, 2004).

Pashin et al. (1995) subdivided the Pottsville Formation of the Cahaba coal field into three magnafacies (Figure 3). The *quartzarenite measures* dominate the basal Pottsville Formation. The *mudstone measures* are dominated by mudstone, but contain numerous litharenite bodies and coal beds. The upper part of the formation is dominated by litharenite, mudstone, and coal. It is characterized by thick extraformational conglomerate units and is accordingly named the *conglomerate measures*. Based on previous work on the basin and the availability of outcrop and core samples of the formation provided by Dr. Jack Pashin (Geological Survey of Alabama) and by CDX Gas Company (Hoover, Alabama), the Cahaba Basin provides an excellent opportunity to evaluate provenance of the Pottsville Formation.

1.2 PREVIOUS WORKS

Previous studies have produced conflicting interpretations of provenance for the Pottsville Formation. Some workers suggested that Pottsville Formation sediments were

derived in part from the Ouachita Mountain belt (located west and northwest), while others suggested sediments were derived wholly from the Appalachians (located to the east and northeast).

Mack et al. (1983) proposed that the predominant source area of the Pottsville in Alabama, specifically in the Black Warrior basin, is the Ouachita belt, located to the southwest. Based on observations made in both the Appalachian fold and thrust belt and the Black Warrior foreland basin in Alabama, Mack et al. (1983) proposed that deposition occurred in two converging clastic wedges. A northeastward-prograding clastic wedge reached Alabama by the Middle Mississippian time. Northeastward-progradation continued with deposition of the Lower Pennsylvanian Pottsville Formation (Mack et al., 1983). The southwestward-prograding clastic wedge did not appear in Alabama until latest Mississippian time. Mack et al. (1983) found andesitic \pm basaltic and dacitic volcanic rock fragments in the sandstones of the Parkwood and Pottsville formations. Based on this observation, they suggested that sediment was derived from an arc complex associated with the Ouachita orogen.

Other workers provided evidence for an Appalachian source. Schlee (1963) measured several hundred cross-beds in basal sandstone units of the Pottsville Formation in the southern Appalachians. The paleocurrent data indicated an east-northeast source, (see Figure 2a). Graham et al. (1976) studied sandstone modal analysis of the Pottsville Sandstone in the Black Warrior Basin and suggested a source from a collisional orogen located to the northeast. Based on asymmetric ripple marks and cross-bed orientations, Demirpolat (1989) determined that sediment was transported from the southeast, which was probably the up-slope direction at the time of deposition. Liu and Gastaldo (1992)

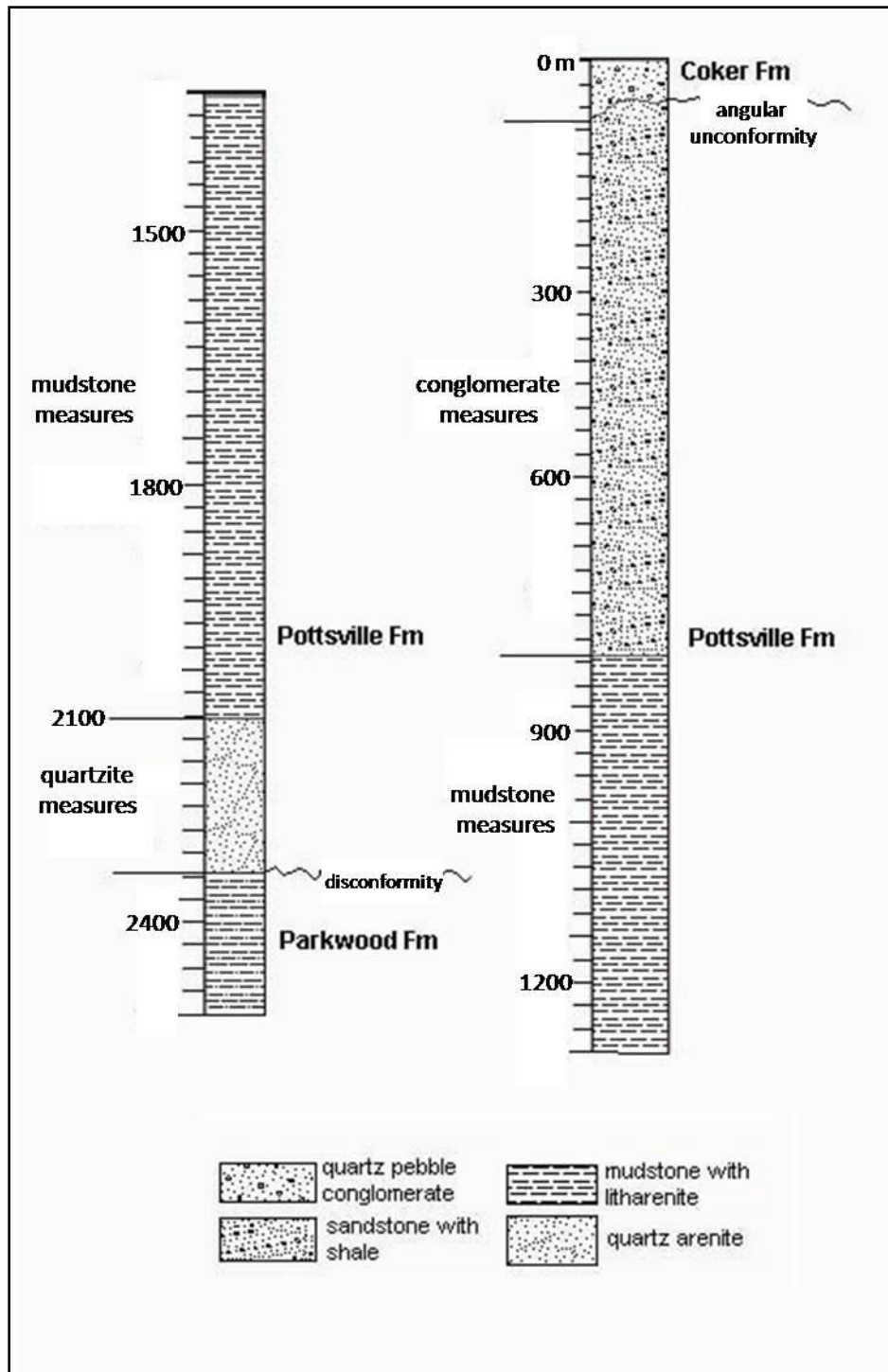


Figure 3. Generalized stratigraphic column for the Pottsville Formation and associated rocks (modified from Pashin and Carroll, 1999).

studied an unusual accumulation of gravel deposits, which provided an opportunity to characterize the rock types exposed in the source area. Based on clast lithologies, they suggested that the Pottsville Formation of the Black Warrior Basin of Alabama was derived from the deformed and uplifted southern Appalachian orogen.

CHAPTER 2: TECTONIC SETTING AND REGIONAL GEOLOGY

2.0 INTRODUCTION

Specific interpretations for the southern Appalachian-Ouachita region have linked collision of the southern margin of North America with microcontinents and/or with South America (Mack et al., 1983). The Wilson Cycle of opening and closing of ocean basins is incorporated in the cyclic assembly and dismantling of supercontinents. Alternating processes of extension and compression of continental margins provide potential for continental inheritance and overprinting (Mack et al., 1983; Thomas, 2006). Thomas (2006) recognizes a succession of two complete cycles in eastern North America: (i) the closing of an ocean and the assembly of the supercontinent Rodinia, the breakup of Rodinia and opening of the Iapetus Ocean; and (ii) the closing of the Iapetus Ocean and assembly of the supercontinent Pangaea, followed by the breakup of Pangaea and the opening of the Atlantic Ocean.

2.1 APPALACHIANS

The Appalachian orogen was constructed along the Precambrian continental margin of eastern North America by a series of collisions that began in the Ordovician and episodically spanned throughout much of the Paleozoic Era (Thomas, 2006). The process of accretion of suspect and exotic terranes, along with terrane collision and

completion of a Wilson Cycle by continent-continent collision, resulted in development of the Appalachian orogen. The Appalachian-Ouachita orogenic belt records three separate mountain-building events; the Middle Ordovician Taconic orogeny, the Devonian Acadian orogeny, and the Pennsylvanian-Permian Alleghenian orogeny.

2.1.1 TACONIAN OROGENY

The Taconic orogeny was the first of three orogenic events responsible for the Appalachian Mountains. Mid-Ordovician to Early Silurian (480–430 Ma) closing of the Iapetus Ocean resulted in the convergence of Laurentia and an arc terrane (Drake et al., 1989; Horton et al., 1989). Originally viewed as a single event, the Taconic orogeny is now known to consist of at least three episodes of collision. The first took place in the Early Ordovician near Maine and Newfoundland, the second was focused in eastern Tennessee in the Middle Ordovician, and the third occurred during the Late Ordovician, predominately in eastern Virginia, Pennsylvania, and New York (Drake et al., 1989). These diachronous events are thought to represent an oblique collision between an irregular passive margin and at least one east-dipping subduction complex (Bradley, 1989).

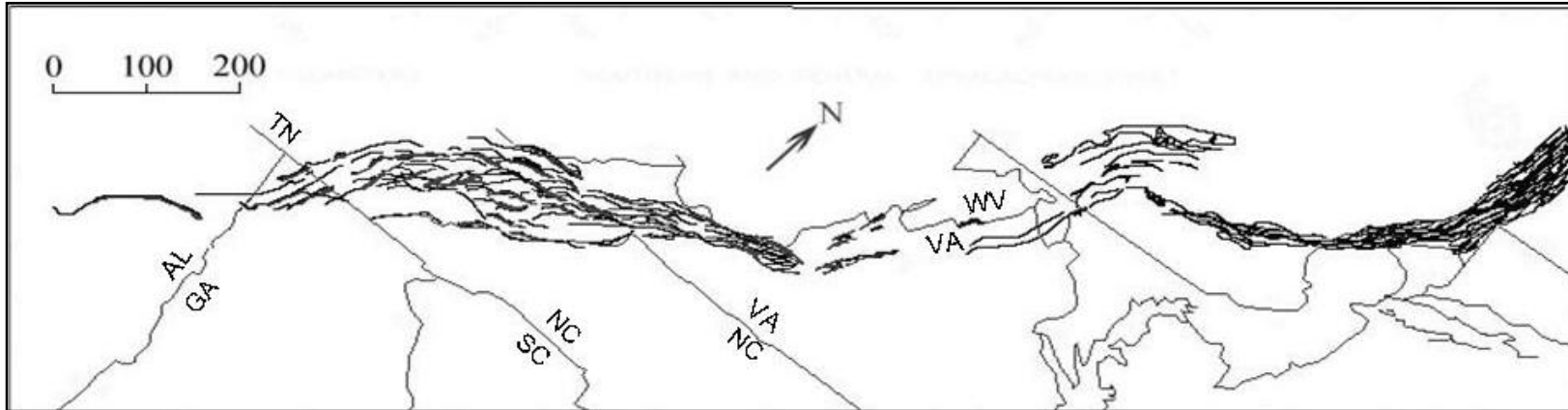
During Cambrian and Early Ordovician, the eastern margin of present-day North America was a carbonate platform that faced the Iapetus Ocean. The platform is represented by an eastward thickening, shallow-water carbonate sequence. The platform was flanked to the east by a continental slope and rise. Strata of the slope and rise sequence consist of mostly deep water argillaceous and arenaceous sediments, with minor volcanics, few carbonates, and lesser cherts, which are preserved in far traveled thrust

sheets (Rowley and Kidd, 1981). The Taconic orogeny resulted in drowning of the carbonate platform, followed by obduction of slope/rise allochthons and large ophiolite sheets (Bradley, 1989). Based on the pattern of Taconic shelf drowning, Bradley estimated the rate of convergence to have been 1 to 2 cm/yr, and the minimum width of the Iapetus Ocean to have been 500 to 900 km. Figure 4 illustrates the current distribution of synorogenic sediments deposited during the Taconic events.

Terranes located in the southern Piedmont, in vicinity of the study area, that were produced during the time of the Taconic orogeny include the Dahlonaga gold belt (NE Georgia) and the Hillabee Greenstone (NE Alabama). High-precision U/Pb zircon dating of felsic volcanics from these units (McClellan and Miller, 2000) indicate an Ordovician age (~470 Ma). Taconic clastic wedges are characterized by the Blount and Martinsburg formations in the central-northern Appalachian foreland basin and the Sevier-Paperville-Athens formations in the southern Appalachian Basin (Stevens and Wright, 1981; Thomas, 1991).

2.1.2 ACADIAN OROGENY

The Acadian orogeny has long been viewed as encompassing the most intense period of deformation, regional metamorphism, and granite intrusion affecting the northern Appalachian Mountains (Naylor, 1971). Early to Late Devonian (ca. 420–340 Ma) convergence again resulted in the closure of the Iapetus Ocean and the accretion of a Middle Ordovician volcanic arc terrane to Laurentia (Horton et al., 1989; Osberg et al., 1989).



13

Figure 4. Map of a portion of the Appalachians showing distribution of Ordovician sediment that experienced deformation during the Taconic orogeny (modified from Bradley, 1989).

The relative sequence of events began with the deposition of geosynclinal sediments as young as Early Devonian, followed by deformation and regional metamorphism, and finally emplacement of granitic plutons. The orogeny was most intense in the Merrimac area in southern New England and in Maine and extended northward to the central volcanic belt of Newfoundland. The collision of plates may have been diachronous along the front of the belt (Osberg et al., 1989). According to Osberg et al. (1989), although the deformational effects and continent collision were probably short lived, the deformational and thermal effects related to subduction of oceanic crust, specifically volcanism and plutonism, may have developed slowly over a long time span. Also, effects associated with oceanic subduction and crustal thickening may have occurred over time spans that overlap those of previous or later orogenies in distal crustal plates (Osberg et al., 1989).

An understanding of the effects of the Acadian orogeny and its role in the history of the Appalachians is poorly understood due to plutonic and metamorphic overprint, complex structural features, and the lack of stratigraphic continuity (Osberg et al., 1989). Acadian rocks are incompletely exposed in the Appalachians. More easterly sections are covered by coastal plain sediments, or exposed as deformed terranes scattered about the continental margins.

Southern Appalachian terranes formed during Acadian orogenies include the Siluro-Devonian Cat Square terrane. This terrane is made up of metapsammite and pelitic schist, with Devonian anatectic granitoid intrusions and rare mafic and ultramafic rocks (Merschhat and Hatcher, 2007). U/Pb studies of zircons indicate that Cat Square rocks have a maximum age of ~430 Ma (Merschhat and Hatcher, 2007).

2.1.3 ALLEGHENIAN OROGENY

The Carboniferous to Early Permian Alleghenian orogeny is the youngest and most pervasive event to affect the central and southern Appalachians. It commenced as an oblique–dextral collision of then continents Laurentia and Gondwana (ca. 340–270 Ma) (Secor et al., 1986; Hatcher et al., 1989). Collision with Gondwana caused thrusting of Late Proterozoic to Permian Laurentian margin and Piedmont terranes cratonward atop Laurentia (Secor et al., 1986; Hatcher et al., 1989; Hatcher, 2002).

The Alleghenian orogen includes a foreland belt of folds and thrust faults that propagated into sedimentary rocks of the North American craton in the western part of the southern and central Appalachians (Hatcher et al., 1989). Deformation stretched from Alabama to New York, and extended inward as far as Tennessee. The eastern section of the Appalachians consists of a series of allochthonous metamorphic rocks, created during the Taconic and Acadian orogenies. Alleghenian metamorphic effects are omnipresent in the Western Blue Ridge and Talladega Belt with typical $^{40}\text{Ar}/^{39}\text{Ar}$ ages of ca. 335–325 Ma (McDonald, 2008).

Large–scale thrusting resulted in considerable deposition and subsequent deformation of clastic sediments in the Appalachian foreland basin, which prograded cratonward from the central and southern Appalachians (Thomas, 1977; Hatcher et al., 1989; Hatcher, 2002). The Pennsylvanian Pottsville Formation represents the Alleghenian clastic–wedge in the southern Appalachian Basin (Hatcher et al., 1989).

2.2 OUACHITA BELT

The Ouachita Belt is an east-west trending mountain range located in west central

Arkansas and southeastern Oklahoma, with roots extending as far as central Texas (Figure 5). The now deeply eroded and largely buried mountains of the Ouachita orogenic belt were produced by the collision of Laurentia with the South American segment of Gondwana. Appalachian-Ouachita orogenesis concluded by large scale cratonward thrusting of Paleozoic rocks (Mack et al., 1983).

Middle Cambrian rifting resulted in a geographically irregular, passive margin along southern North America (Arbenz, 1989). Two promontories, Alabama and Texas, and two embayments, Ouachita and Marathon, were created with this rifting event. The Reelfoot, Oklahoma and Delaware aulacogens, which represent rift or rift transform basins, were also produced at this time (Arbenz, 1989). The Reelfoot Rift laid the groundwork for the formation of the Arkoma Basin. The paleoshelf extended westward into southwestern Oklahoma and eastern Texas, where it is intersected by large-scale displacement faults. Reconstructions loosely place the southern limit of the shelf near the Arkansas-Louisiana border (Coleman, 2000). The resulting Arkoma Basin had a minimum pre-deformation aerial extent of approximately 250,000 km² and reached depths of 1500 to 2000 m, based on sedimentary structures and lithofacies successions (Coleman, 2000). As epicontinental seas regressed, the primary sediment source for the basin is believed to be of continental origin through a topographic low associated with the Reelfoot Rift (Morris, 1989).

The geology of the Ouachita belt is different from the southern Appalachians and their unexposed connection is still enigmatic. Timing of orogenic events in the two domains also differs. It is possible that the Ouachitas were deformed by a continent-continent collision with present-day South America, while the southern Appalachians

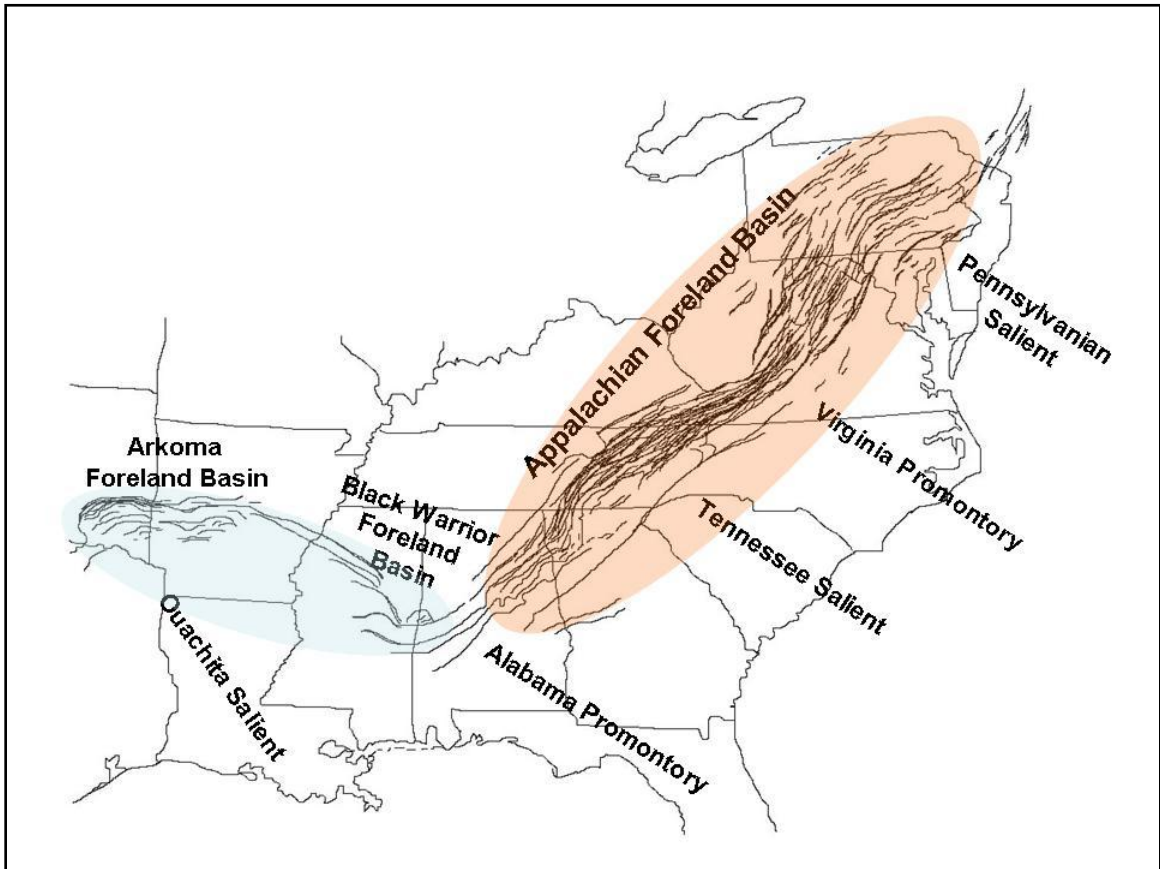


Figure 5. Generalized map showing extent of Appalachian and Ouachita belts in southeastern North America. The blue oval highlights the Ouachita belt, the pink oval highlights the Appalachian belt (modified from Hatcher et al., 1989).

were deformed by a collision with the African plate (Rast, 1984). The part of South America that today is Venezuela is believed to have formed the southern margin of the Late Paleozoic Ouachita mountain system (Bally and Palmer, 1989).

The Ouachita orogen consists of four packages of strata (Figure 6). Lower to Middle Ordovician strata, found in the interval stratigraphically below the Bigfort Chert, are dominantly hemipelagites with intercalated quartzose turbidite sandstones. These strata are interpreted as continental slope and rise deposits that accumulated along the southern flank of the rifted craton (Gleason et al., 1995) (Figure 6; blue). The Middle Ordovician to Lower Mississippian assemblage, which is bracketed by Bigfork Chert and Arkansas Novaculite, is composed of shales, cherts with interbedded argillites, and turbidites. The massive cherts and argillites are interpreted as pelagic and hemipelagic deep-marine deposits that accumulated south of the passive margin (Ethington et al., 1989) (Figure 6; green). The Lower to Upper Mississippian Stanley Group is a predominantly shaly turbidite succession deposited conformably on deep marine cherts and argillites of the Arkansas Novaculite (Morris, 1989) (Figure 6; yellow). Finally, Lower Pennsylvanian turbidite flysch was deposited on the Stanley Group as a complex series of overlapping deep-sea fans. Paleocurrents are generally westerly in these turbidites (Gleason et al., 1995) (Figure 6; red).

(Ma)	AGE	Appalachian/ ILLINOIS	OUACHITA
300	PENNSYLVANIAN	Pottsville/ TRADEWATER	ATOKA Johns Valley
320		CASEYVILLE	JACKFORK
340	MISSISSIPPIAN		STANLEY
360	DEVONIAN		ARKANSAS NOVACULITE
380			
400	SILURIAN		MISSOURI MOUNTAIN
420		Clinch	BLAYLOCK
440	ORDOVICIAN	Juniata	POLK CREEK
460		Martinsburg	BIGFORK
480		Tellico	WOMBLE
500			BLAKELY
			MAZARN
			CRYSTAL MT

Figure 6. Generalized stratigraphic column of the Appalachian/Illinois and the Ouachita basins (modified from Gleason et al., 1995).

CHAPTER 3: SANDSTONE PETROGRAPHY

3.0 INTRODUCTION

Sedimentary petrologists quantify relative abundance of mineralogic and textural constituents of a rock in order to determine the provenance history of the sediment. The abundances of these constituents can be determined by a direct extrapolation of the results from a two-dimensional analysis. This is performed by superimposing an orthogonal grid of points on a thin section surface and identifying components that fall at each grid point. Extensive work has been done on modal analysis of sandstones (i.e., Basu, 1976; McBride, 1985; Uddin and Lundberg, 1998) in order to delineate mineralogy of source rocks. Provenance of sandstones has cultivated a well-established relationship with petrography and tectonic setting (Dickinson and Suczek, 1979; Ingersoll and Suczek, 1979; Dickinson, 1985). Evolutionary trends in composition of sandstones within a sedimentary province often indicate variations in provenance and tectonic settings through time.

This chapter deals with the petrology and modal analysis of Lower Pennsylvanian sediments deposited in the Cahaba Basin in Alabama. This analysis focused on key aspects of detrital mineralogy in an attempt to evaluate lithologies and tectonic setting of source areas.

3.1 METHODS

Forty-eight mostly medium- to fine-grains sandstone samples were collected from drill cores provided by the Geological Survey of Alabama and CDX Gas Company. Thirty-two core samples were collected from the School of Mines and Energy Development (SOMED) drill core, made available by the Geological Survey of Alabama. An additional sixteen samples were collected from cores provided by CDX Gas Co. (Savage Creek, Mayberry Creek, Radio Tower, and Dogwood No. 1 cores). Samples were collected at various depths through each of Pashin and Carroll's (1999) magnafacies, with the objective of obtaining a representative collection of the entire formation. Figure 7 illustrates the cores and collection depths.

Modal analyses were conducted following the Gazzi-Dickinson method. This method counts sand-sized minerals within lithic fragments as the mineral phase rather than the host lithic fragment to account for grain-size variation (Dickinson, 1970; Dickinson and Suczek, 1979; Ingersoll et al., 1984). Careful attention was paid to the classification of lithic fragments and feldspars types (Pettijohn et al., 1987; Uddin and Lundberg, 1998). Thin sections were stained for plagioclase and potassium feldspars during preparation. A minimum of 300 points were counted per slide. Modal sandstone compositions were plotted on standard ternary diagrams (QtFL, QmFLt, QmPK, LsLvLm, etc.) and used to interpret temporal variations in provenance following the approach of Dickinson and others (Dickinson, 1970; Dickinson and Suczek, 1979).

Compositional parameters distinguished during point counting are in Table 1. These include: Qt = total quartz; Qm = monocrystalline quartz grains; Qp = polycrystalline quartz grains, including chert grains; F = total feldspar grains; P =

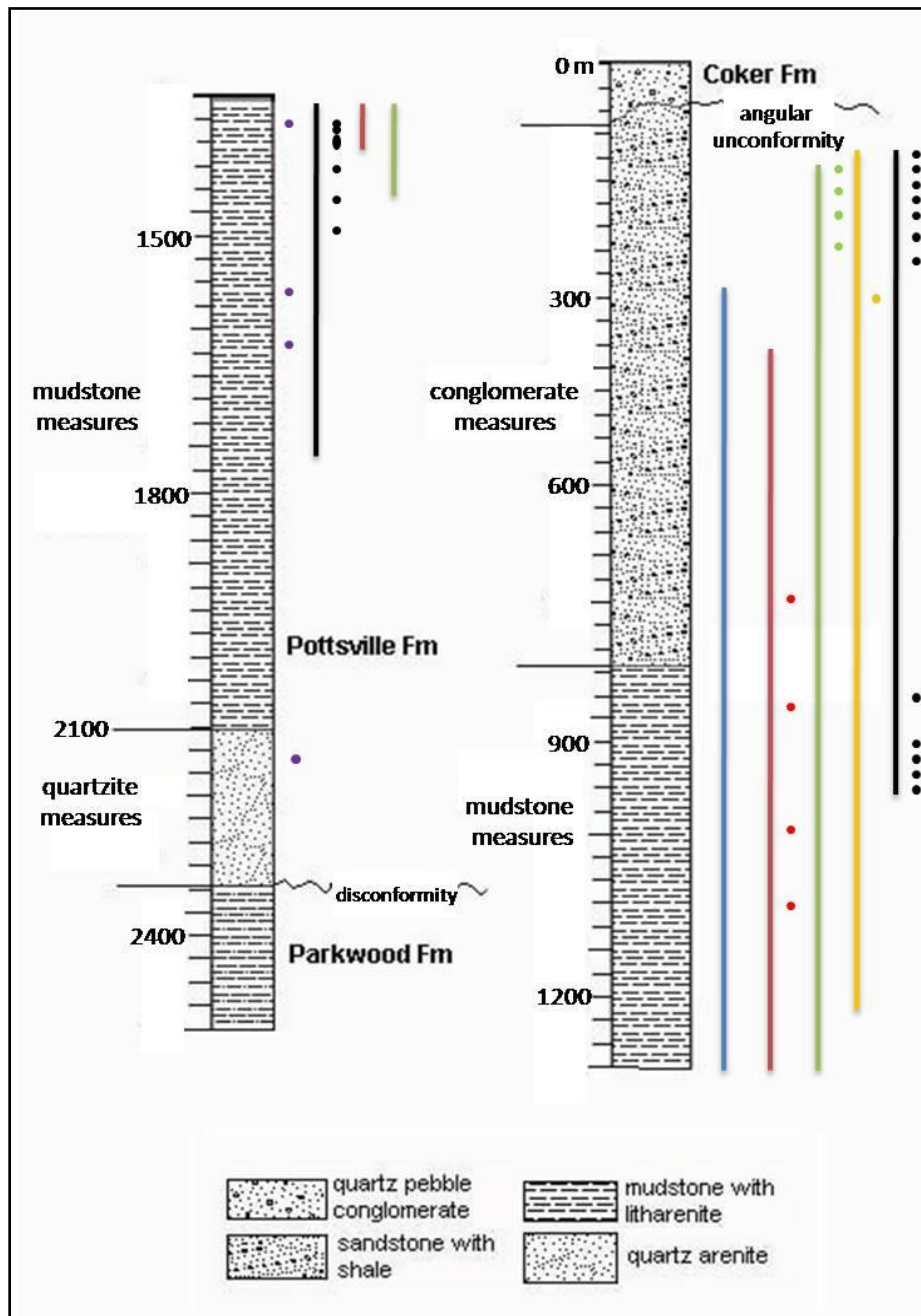


Figure 7. Generalized stratigraphic column of the Pottsville Formation in the Cahaba coalfield, Alabama (modified from Pashin and Carroll, 1999). Purple dots to the right of the column indicate depths at which outcrop samples were collected. Solid lines represent the depths that cores were drilled, while dots to the right show where samples were collected. Four cores were made available by CDX Gas Company (left to right: Mayberry Creek in blue; Dogwood No. 1 in red; Savage Creek in green; Radio Tower in orange). The fifth core, SOMED drill core (black), was provided by the Geological Survey of Alabama.

Table 1. Recalculated modal parameters of sand and sandstones.

1. Primary parameters

(Dickinson and Suczek, 1979; Dorsey, 1988)

$Q_t = Q_m + Q_p$, where

Q_t = total quartz grains

Q_m = monocrystalline quartz (>0.625 mm)

Q_p = polycrystalline quartz (or chalcedony)

Feldspar Grains ($F = P + K$)

F = total feldspar grains

P = plagioclase feldspar grains

K = potassium feldspar grains

Unstable Lithic Fragments ($L_t = L_s + L_v + L_m$)

L = total lithic fragments

L_t = total unstable lithic fragments

L_v = volcanic/metavolcanic lithic fragments

L_s = sedimentary/metasedimentary lithic fragments

L_m = metamorphic lithic fragments

2. Secondary parameters

(Dickinson, 1970; Uddin and Lundberg, 1998)

L_{m_1} = very low- to low-grade metamorphic lithic fragments

L_{m_2} = low- to intermediate-grade metamorphic lithic fragments

plagioclase feldspar grains; K = potassium feldspar grains; L = total lithic fragments; Lt = total unstable lithic fragments; Ls = sedimentary lithic fragments; Lv = volcanic lithic fragments; Lm = metamorphic lithic fragments; Lm₁ = low- to medium-grade metamorphic lithic fragments; and Lm₂ = high-grade metamorphic lithic fragments.

3.2 PETROGRAPHY

Twenty-six mostly medium-to fine-grained sandstone samples were selected for petrographic study. Sandstone modal analyses of the Pottsville Formation of Alabama are presented in Table 2. Derivative composition of these sandstones is quartzolithic. All of the samples analyzed consist predominantly of rounded to subangular monocrystalline grains (Figure 8a). Comparable abundances of detrital chert and poly-crystalline quartz grains are present (Figure 8b). Feldspars are uncommon, and plagioclase feldspar dominates over potassium feldspar. Many plagioclase grains are partially replaced by calcite. Among the lithic fragments, all three types are present. Volcanic fragments (Figure 9a) are scarce in stratigraphically lower samples, but become more common up-section. Metamorphic rock fragments (Figure 9b) are predominantly very low- to low-grade. Most sediments contain fine-grained sedimentary fragments (Figure 10). Chlorite grains are common. Summarily, sandstones from the Pottsville Formation of Cahaba Basin are mostly feldspar-poor lithic arenites.

Ternary diagrams of the major components (monocrystalline grains and the phaneritic lithic fragments) indicate sandstones were derived from a recycled orogen (Figures 11 and 12). The predominance of quartz and limited feldspars indicate relatively high sediment maturity (Figure 13). Sedimentary and metamorphic fragments occur in

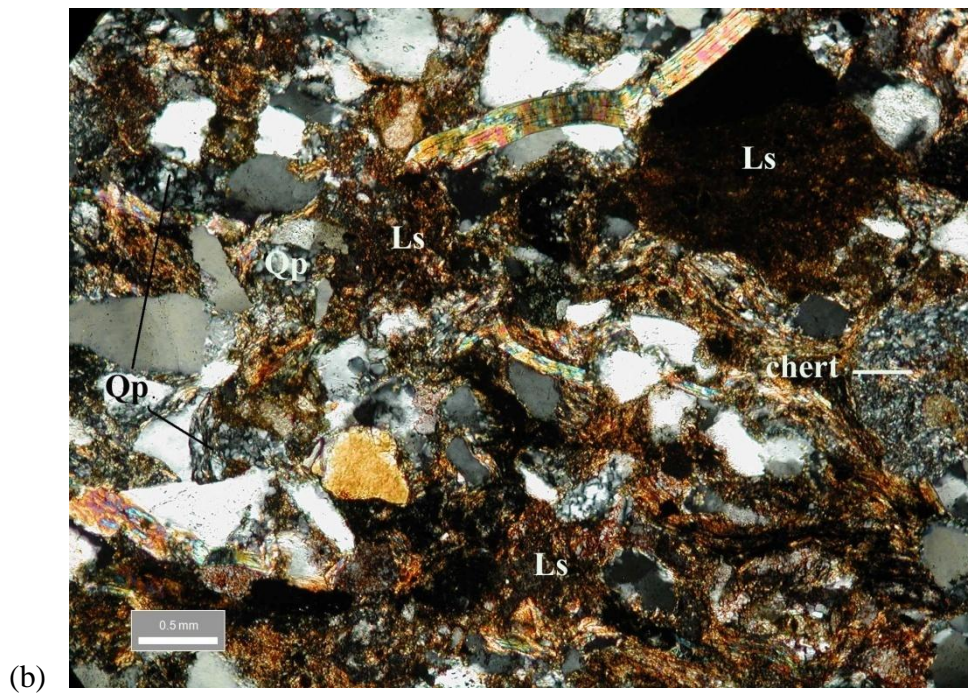
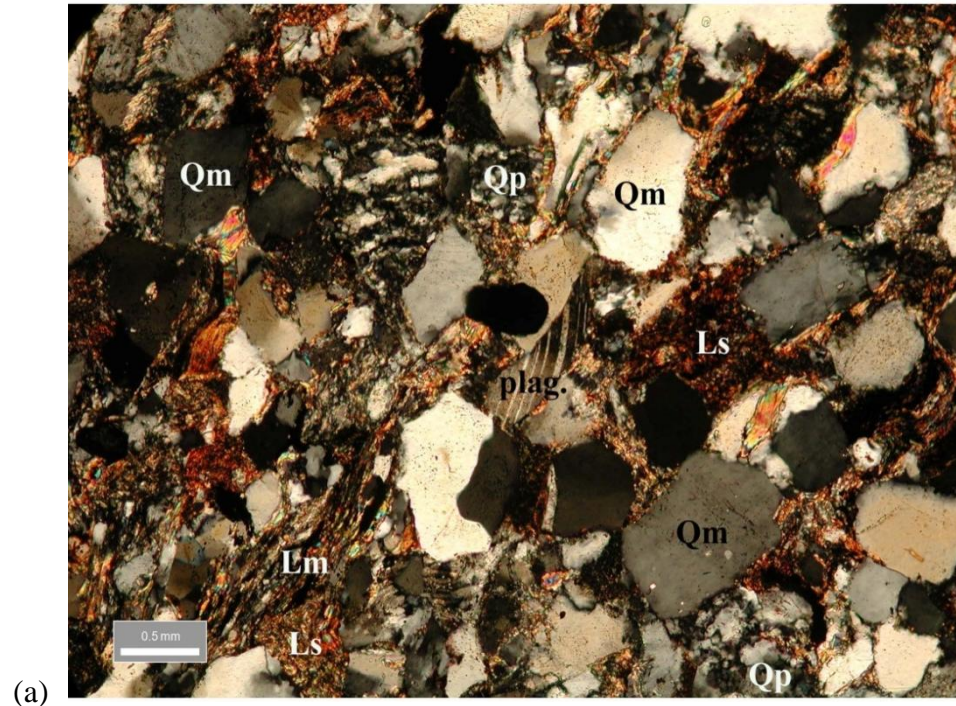
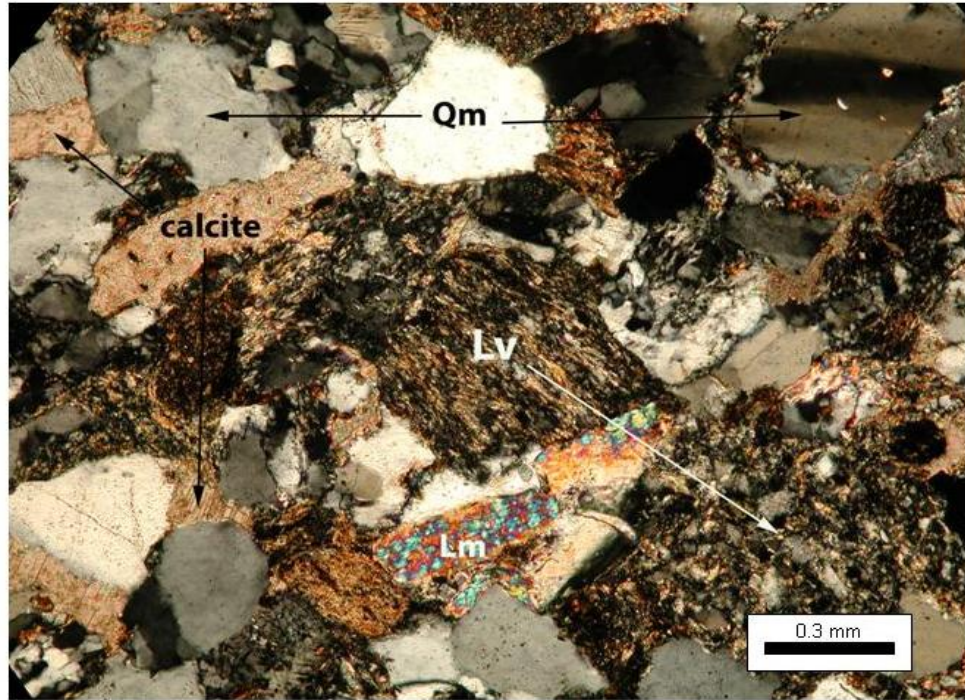
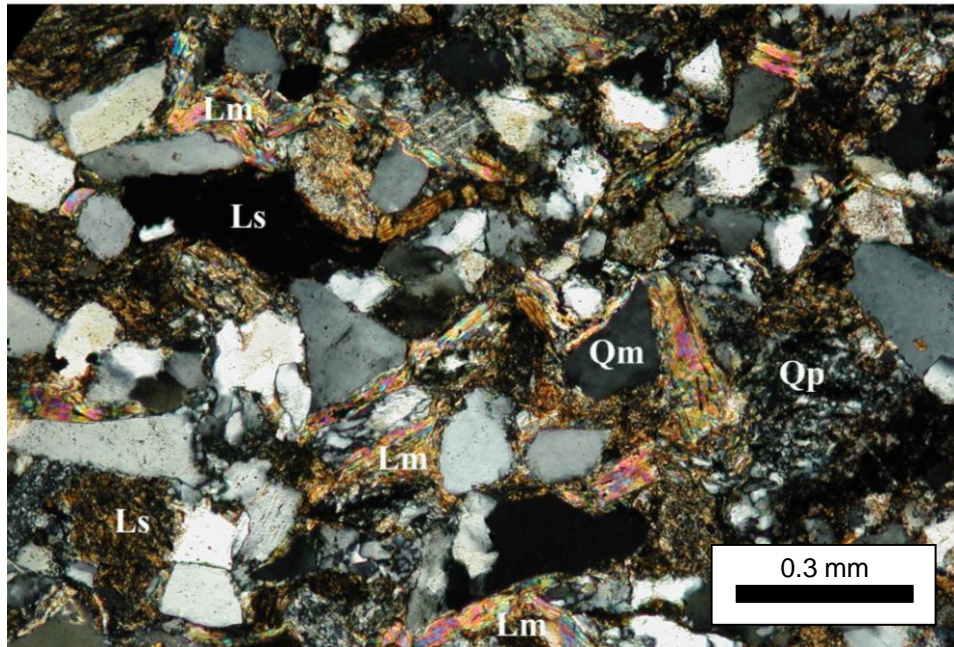


Figure 8. Representative photomicrographs of Pottsville sandstone. (a) Rounded to sub-angular monocrystalline grains (Qm) among polycrystalline quartz (Qp), sedimentary (Ls) and metamorphic lithic (Lm) fragments, and plagioclase (plag) (sample PSS-4, crossed polars). (b) Detrital chert and polycrystalline quartz grains (Qp) among lithic grains (Ls) (sample PSS-5, crossed polars).

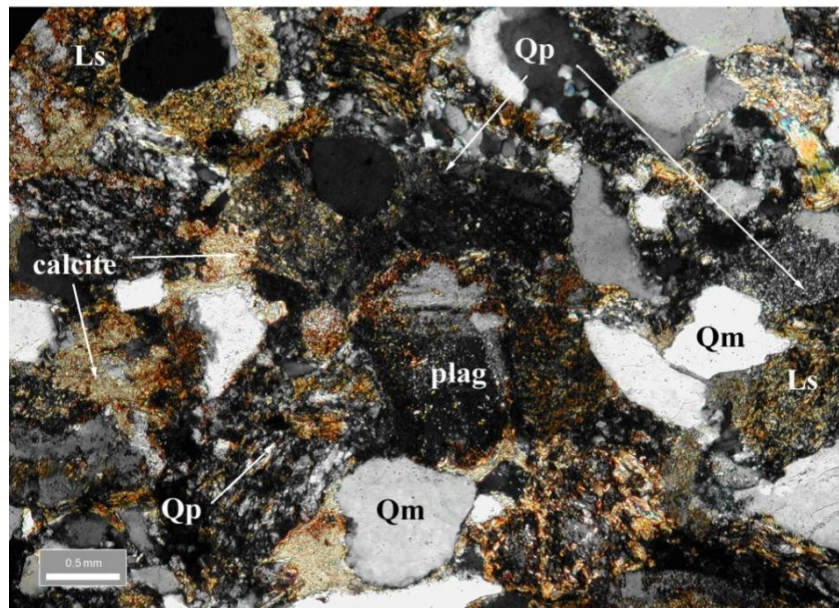
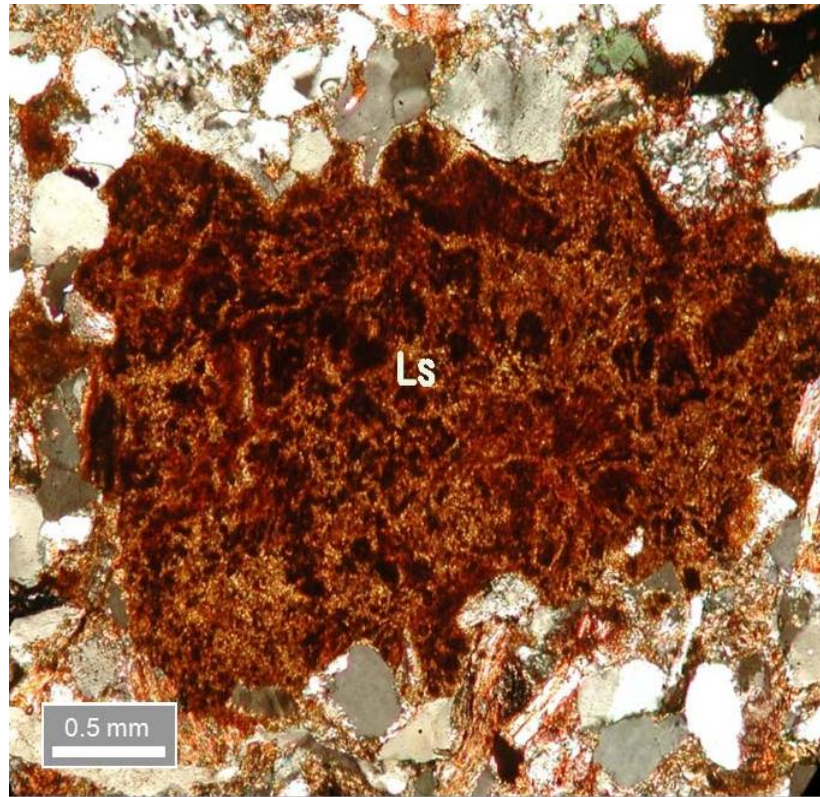


(a)



(b)

Figure 9. Representative photomicrographs of Pottsville sandstone. (a) Volcanic lithic fragments (Lv) with quartz (Qm) and calcite (sample PSS-5, crossed polars). (b) Very low- to low-grade metamorphic fragments (Lm) (sample PSS-3, crossed polars).



(a)

Figure 10. Representative photomicrographs of Pottsville sandstone. (a) Sedimentary rock fragment (Ls) (sample CHB-4, cross polars). (b) Plagioclase (plag) partially replaced by calcite, with monocrystalline (Qm) and polycrystalline quartz (Qp) grains (sample PSS-6, plane polar).

Table 2. Normalized modal compositions of sandstones from three magnafacies of the Lower Pennsylvanian Pottsville Formation.

	sample no.	Qt	F	L	Qm	F	Lt	Qm	P	K	Ls	Lv	Lm	Ls	Lm1	Lm2
Conglomerate measures	CHB-11	49	19	32	42	22	36	67	30	3	48	10	43	55	24	21
	CHB-9	49	21	30	47	22	31	96	4	0	51	17	32	61	27	12
	RTC-1	56	8	36	43	11	46	35	65	0	55	20	24	69	31	0
	CHB-8	36	27	37	27	31	42	55	44	1	34	10	56	37	42	21
	CHB-7	53	13	34	52	13	35	84	15	1	41	1	58	41	45	13
mudstone measures	PSS-1	53	8	39	46	9	44	84	9	7	53	8	39	58	38	4
	PSS-2	56	4	40	51	5	44	93	6	1	45	11	44	48	46	6
	PSS-3	47	9	44	44	9	47	83	11	6	30	16	54	36	48	15
	PSS-4	51	6	43	40	7	53	86	9	5	28	12	60	31	47	22
	PSS-5	57	7	36	52	8	40	88	12	0	38	16	46	45	45	10
	PSS-6	49	7	44	45	8	47	85	12	3	26	28	46	36	51	13
	PSS-7	63	6	31	54	7	39	88	10	2	37	33	30	55	45	0
	PSS-8	73	3	24	64	4	32	94	6	0	77	8	14	38	62	0
	PSS-9	65	5	30	56	6	38	91	8	1	35	33	32	51	45	4
	PSS-12	51	4	45	46	5	49	91	9	0	28	22	50	36	57	7
	PSS-13	55	5	40	50	5	45	90	9	1	36	38	26	59	39	2
	PSS-14	68	2	30	58	2	40	96	4	0	42	27	32	59	36	4
	PSS-15	57	4	39	52	4	44	92	5	3	36	27	37	50	44	6
	PSS-16	56	3	41	51	3	46	96	2	2	25	29	46	36	52	12
	DC-4	61	8	31	44	10	46	62	34	5	32	13	55	37	48	16
	CHB-6	50	4	46	42	4	54	93	6	1	12	10	78	14	48	38
	CHB-5	47	13	41	38	16	46	73	17	10	54	0	46	55	31	14
CHB-4	85	5	10	84	5	11	94	2	4	88	0	12	88	10	2	
CHB-3	82	5	13	80	6	14	92	4	4	62	23	15	81	14	5	
Quartz- arenite measures	CHB-1	75	8	17	72	9	19	89	4	7	75	11	14	86	9	5
	CHB-2	58	12	30	55	13	32	84	11	4	63	3	34	65	23	12
	mean:	58	8	34	51	9	39	84	13	3	44	16	39	51	39	10
	Std dev:	11	6	10	12	7	11	15	15	3	18	11	16	18	14	9

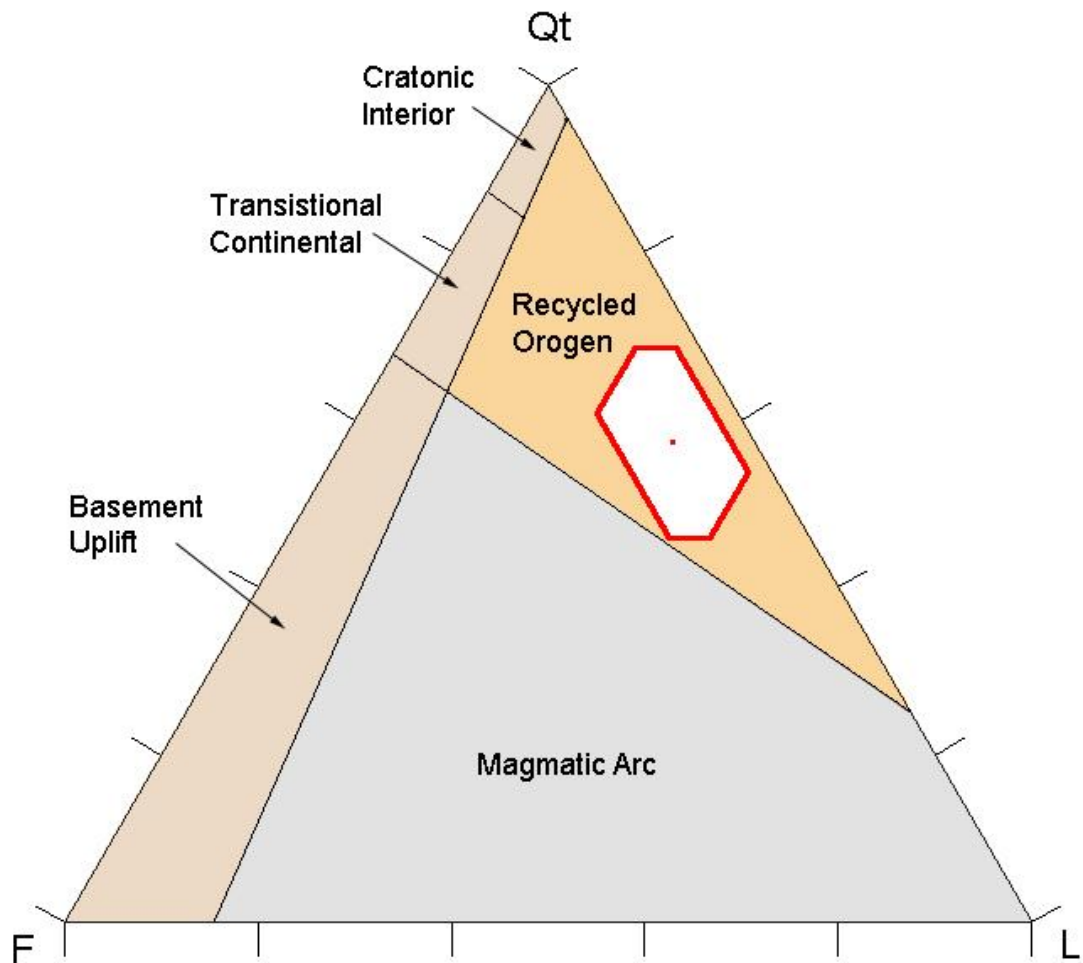


Figure 11. QtFL plot showing overall sandstone modes of Pottsville sandstones from the Cahaba Basin. Standard deviation polygon is drawn around the mean (shown as a red dot). Provenance fields are from Dickinson (1985). Qt=total quartz; F=feldspar; L=lithic grains. Most sands from the Pottsville Formation plot very close together within the “recycled orogenic” field.

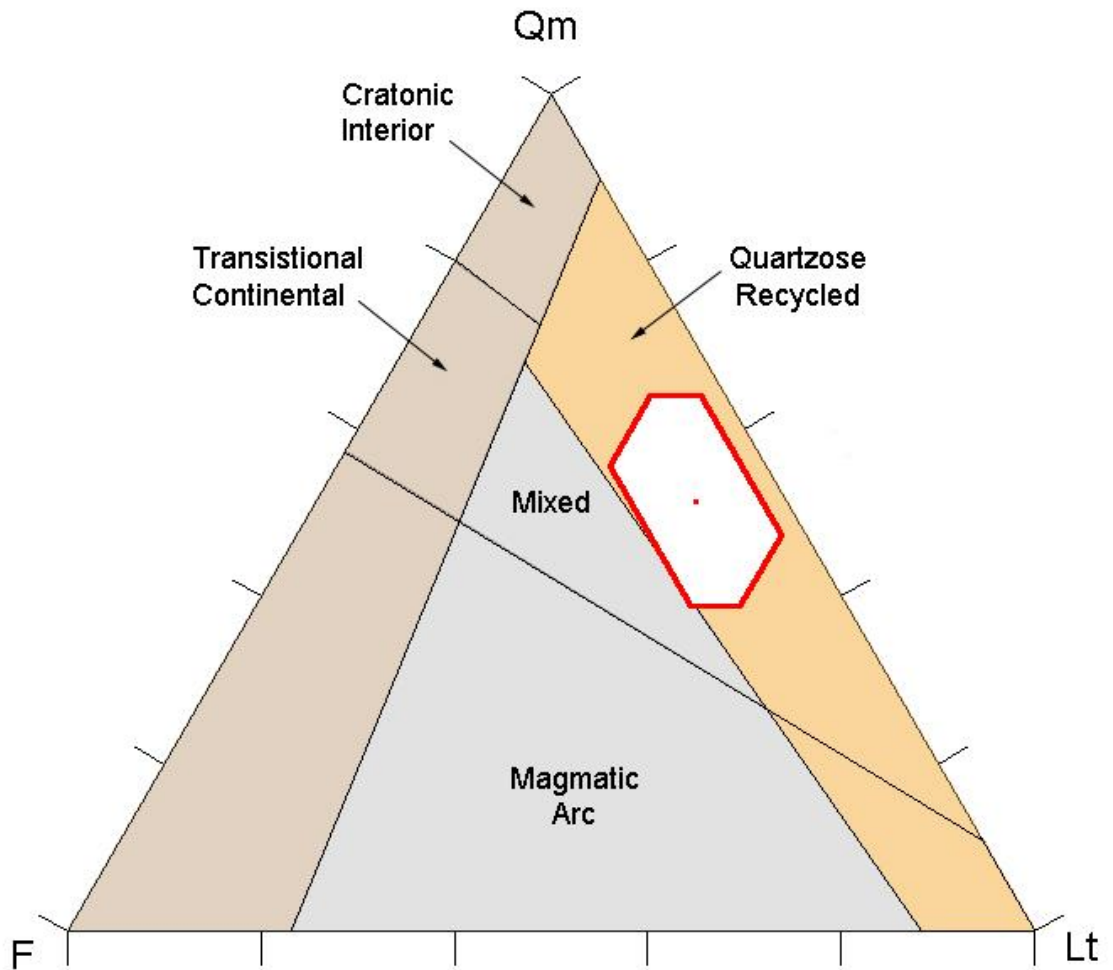


Figure 12. QmFLt plot of Pottsville sandstones from the Cahaba Basin, showing mean (red dot) and standard deviation polygon, with appropriate provenance fields from Dickinson (1985). Chert and other polycrystalline quartz are included in the total lithic counts (see Table 1). Qm=monocrystalline quartz; F=feldspar; Lt=total lithic fragments. Most sands from the Pottsville Formation plot very close together within the “quartzose recycled” field.

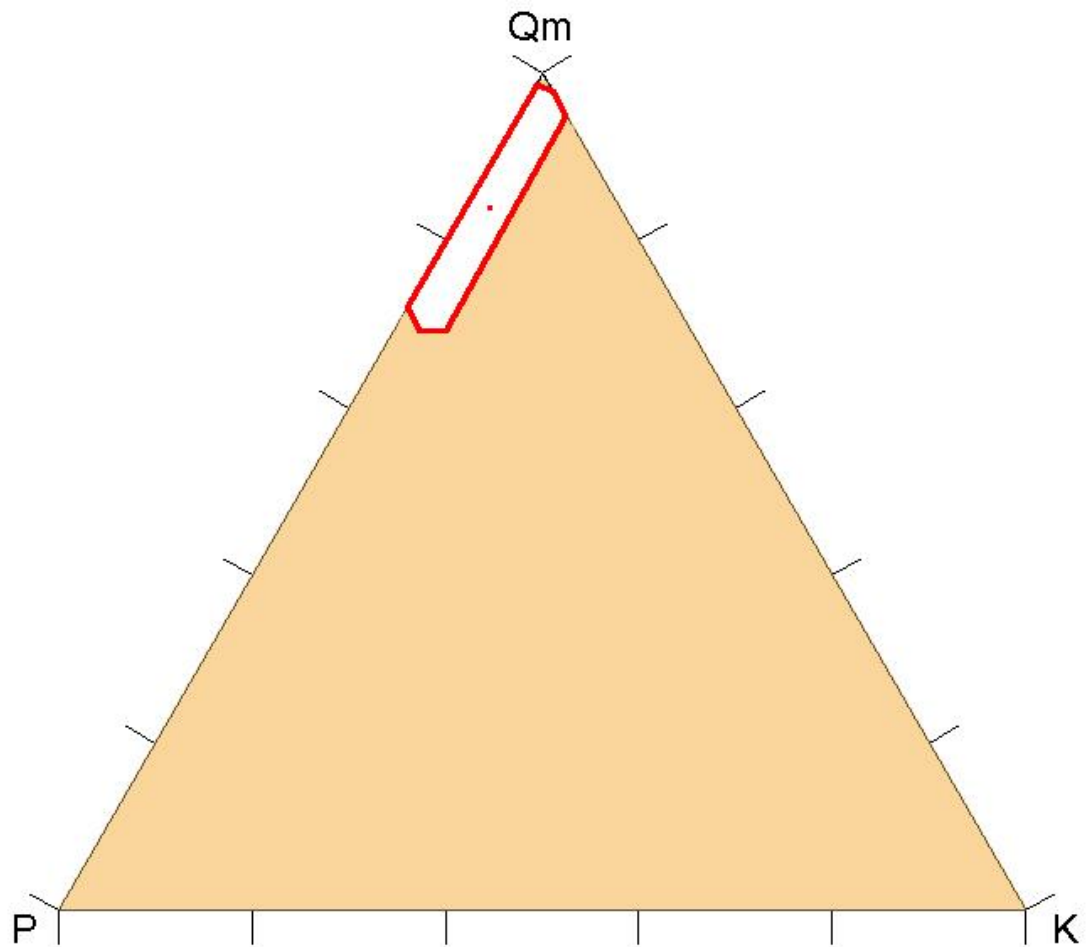


Figure 13. QmPK plot of Pottsville sandstones from the Cahaba Basin, showing mean (red dot) and standard deviation polygon. Qm=monocrystalline quartz; P=plagioclase feldspar; K=potassium feldspar. Most sands from the Pottsville Formation plot close to the Qm end member.

roughly equal amounts, while volcanic fragments are subordinate (less than 25%) (Figure 14). Among the metamorphic lithic fragments, very low- to low-grade metamorphic rock fragments are dominant (Figure 15).

Vertical changes in petrography through the Pottsville magnafacies are shown in Figures 16 through 20. Sediment composition is fairly consistent through most of the Pottsville. However, two patterns are recognized. First, the lowest part of the Pottsville is generally more quartzose (Figures 16 and 17); lithic fragments, particularly those of volcanic origin, are comparatively less abundant (Figures 16, 17, 19, 20). Second, the upper part of the Pottsville (conglomerate measures) is comparatively more feldspathic (Figures 16–18).

3.3 INTERPRETATIONS

Overall composition of the Pottsville sandstone in the Cahaba Basin indicates sediment was derived from a recycled orogenic source. The predominance of sedimentary and metamorphic lithics over volcanic lithics suggests principal origin from fold and thrust belts. The character of metamorphic lithic fragments indicates that metamorphic rocks in the source areas were predominantly of low grade.

Compared to the rest of the section, the base of the formation has higher quartz content. This likely reflects a more physically rigorous depositional environment and/or more intense chemical weathering.

The increase in feldspar content toward the top of the section could indicate a change in source terranes. Alternatively, higher feldspar contents could reflect increased relief and decreased weathering intensity in the source area.

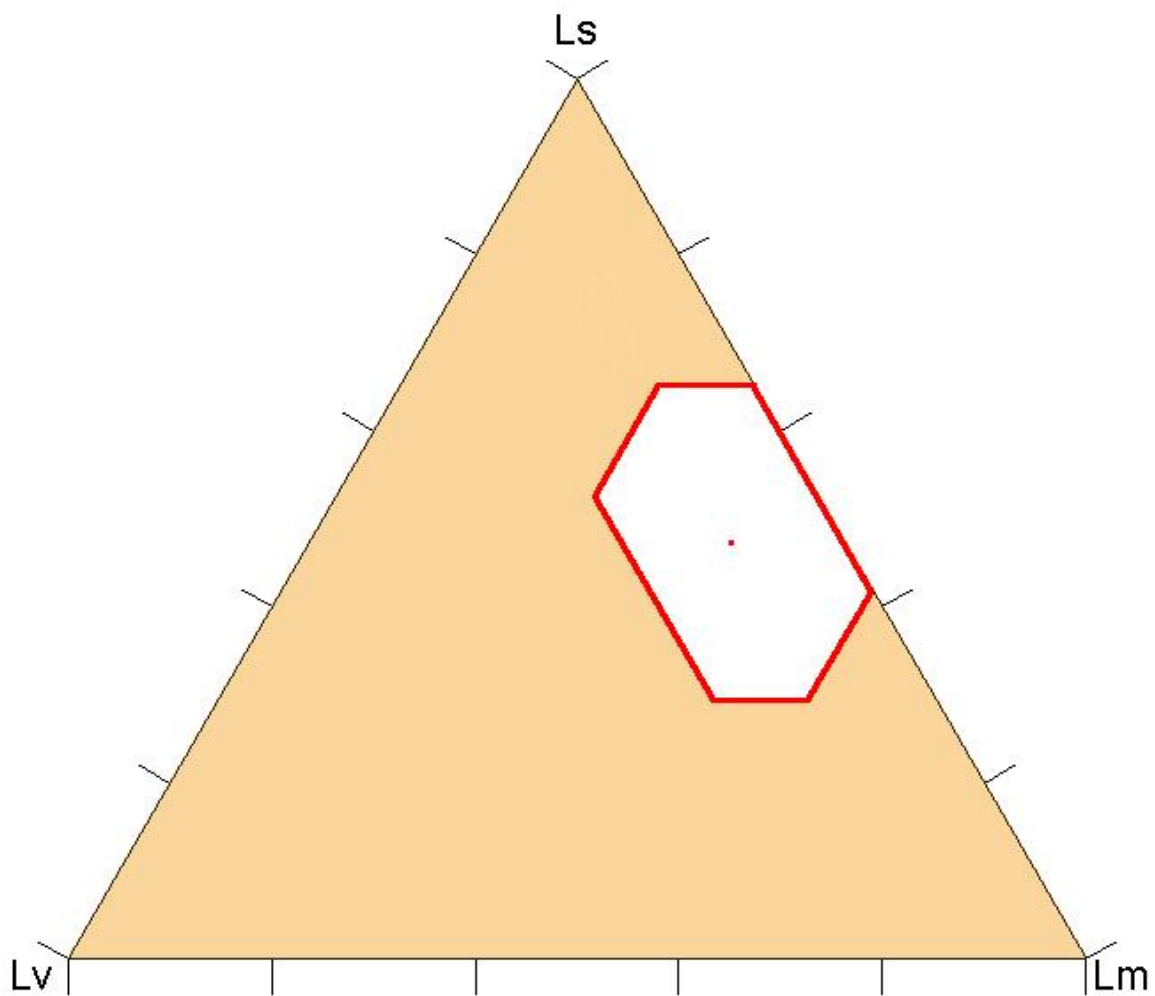


Figure 14. LsLvLm plot showing variations in the composition of lithic fragments in the Cahaba Basin. Ls = sedimentary lithic fragments, Lv = volcanic lithic fragments, and Lm = low- to intermediate-grade metamorphic rock fragments.

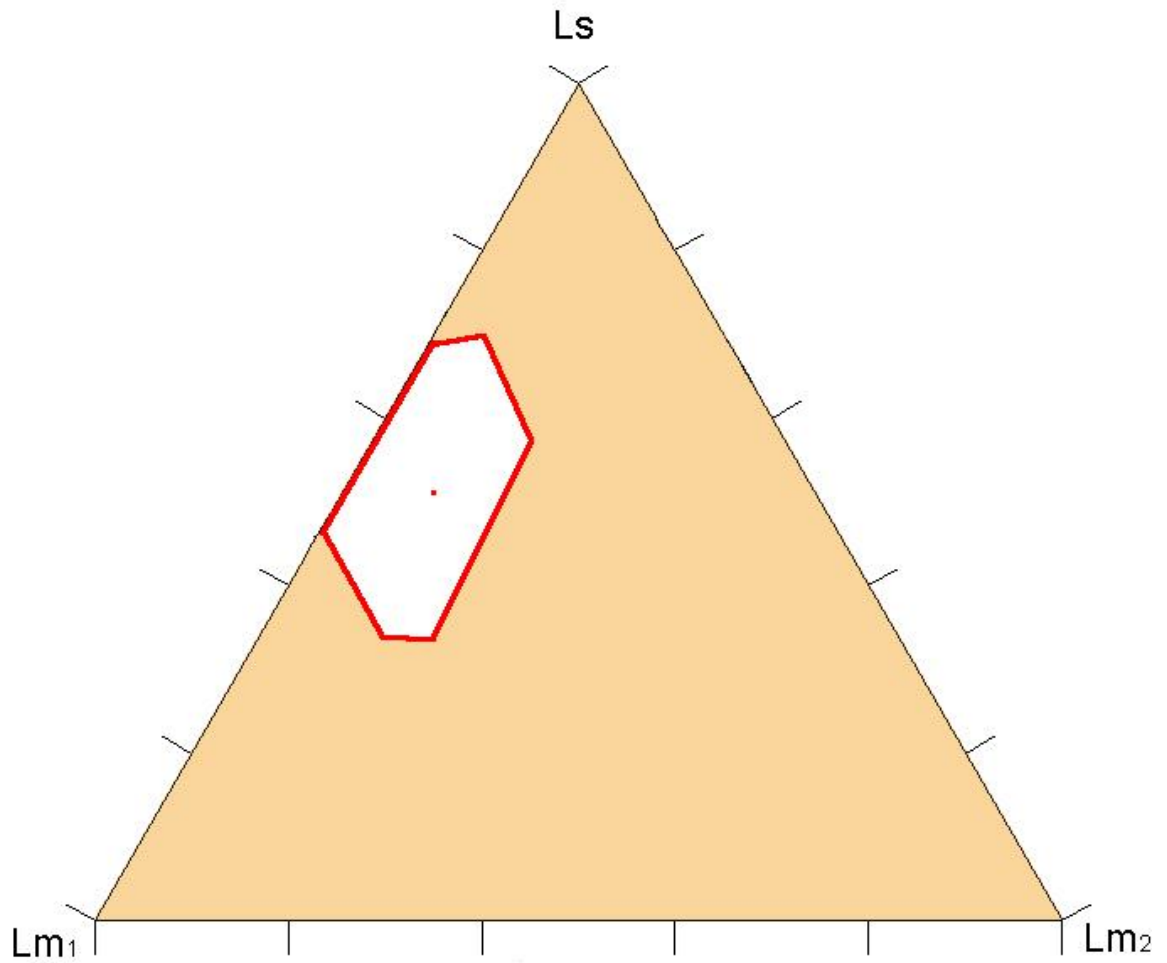


Figure 15. LsLm₁Lm₂ plot showing the mean (red dot) and standard deviation in composition of Pottsville sandstones in the Cahaba Basin. Ls = sedimentary lithic fragments, Lm₁ = very low- to low-grade metamorphic rock fragments, and Lm₂ = low- to intermediate-grade metamorphic rock fragments.

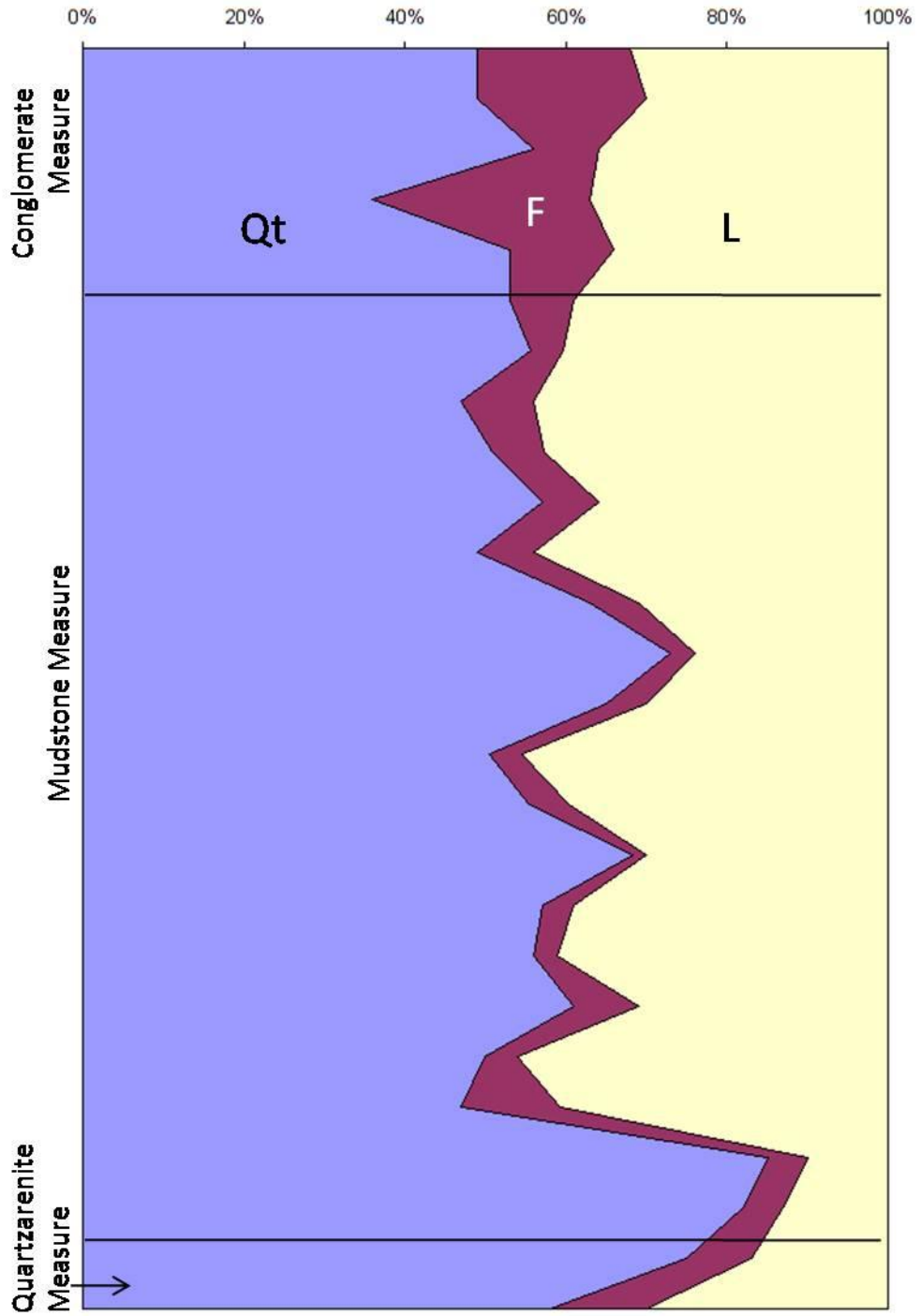


Figure 16. Profile plot of changes in percentages of total quartz (Qt), feldspars (F), and lithic fragments (L) through the Pottsville Formation in the Cahaba Basin.

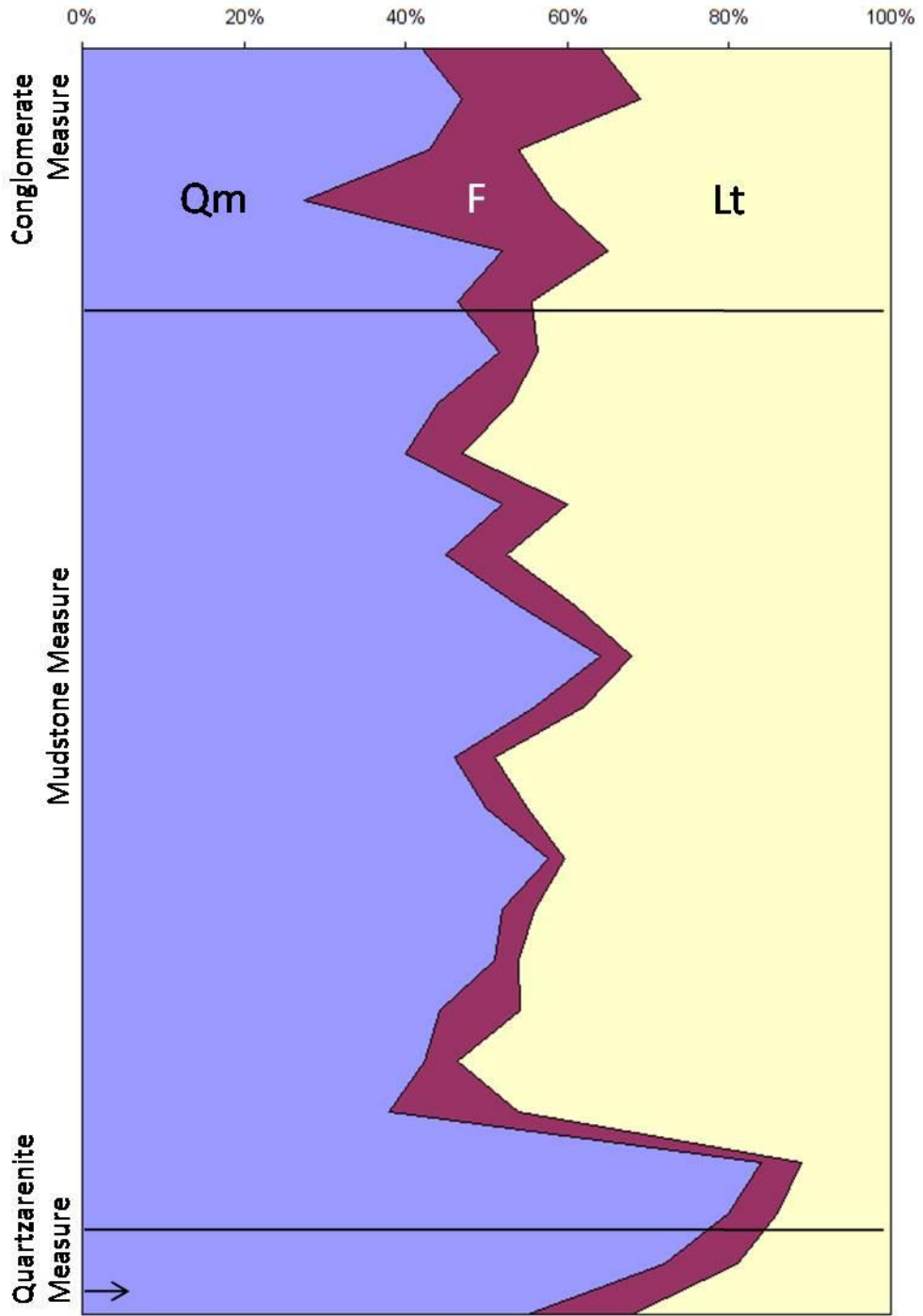


Figure 17. Profile plot of changes in percentages of monocrystalline quartz (Qm), feldspars (F), and total lithic fragments (Lt) through the Pottsville Formation in the Cahaba Basin. Chert and polycrystalline quartz are included in total lithic fragments.

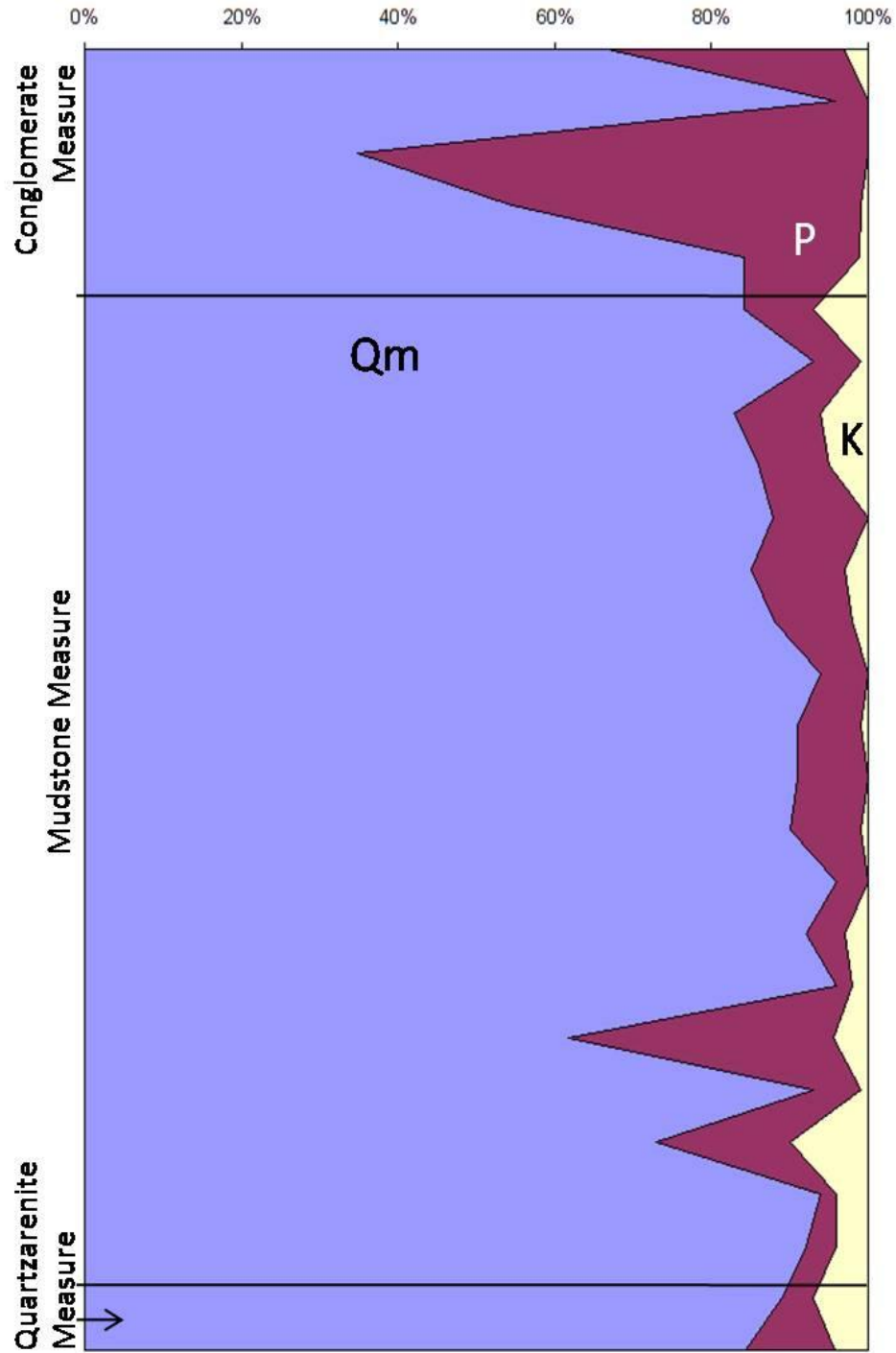


Figure 18. Profile plot of changes in percentages of monocrystalline quartz (Qm), plagioclase feldspars (P), and potassium feldspars (K) through the Pottsville Formation in the Cahaba Basin.

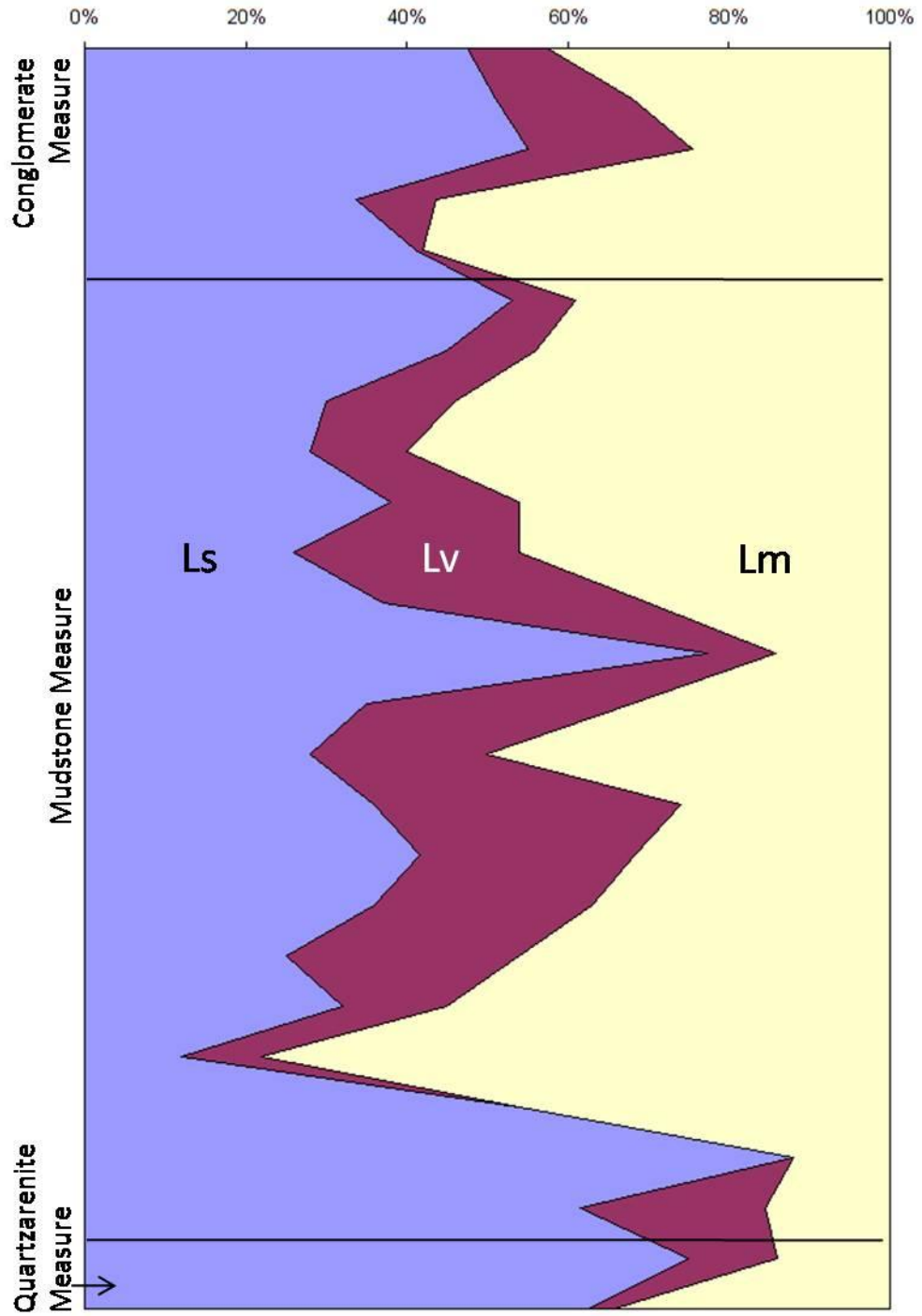


Figure 19. Profile plot of changes in percentages of sedimentary (Ls), volcanic (Lv), and metamorphic (Lm) lithic fragments through the Pottsville Formation in the Cahaba Basin.

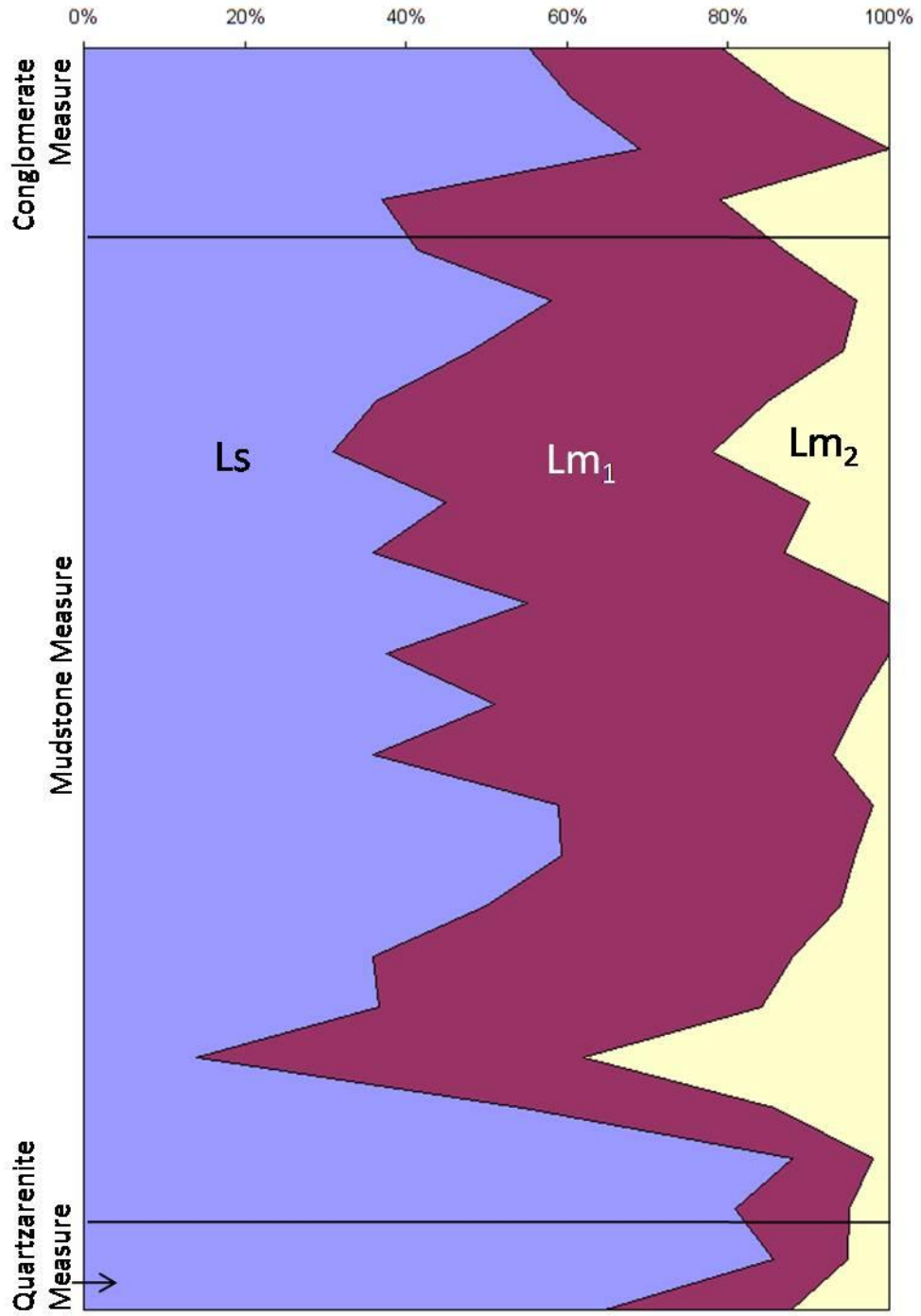


Figure 20. Profile plot of changes in percentages of sedimentary lithic fragments (Ls), very low- to low-grade metamorphic (Lm₁), and low- to intermediate-grade metamorphic (Lm₂) lithic fragments through the Pottsville Formation in the Cahaba Basin.

CHAPTER 4: HEAVY MINERALS

4.0 INTRODUCTION

Heavy mineral analysis is one of the most commonly used techniques in provenance studies, because many heavy minerals are indicative of particular source rocks. Heavy mineral analysis is also important in understanding extrabasinal (e.g., weathering of source area) and intrabasinal processes (e.g., hydraulic processes that influence formation of clastic rocks). Heavy minerals are defined as having a specific gravity of 2.9 or higher and generally have proportions of less than 1% in sandstones (Tucker, 1998). Over thirty common translucent detrital mineral species can be used as provenance indicators (Morton, 1985). Knowledge of the processes controlling the distribution of heavy minerals in sandstones has recently improved (Morton, 1985; Morton and Hallsworth, 1999; Uddin et al., 2007). While heavy mineral assemblages are greatly affected by provenance, they are also influenced by other factors (transport, weathering, deposition, and diagenesis) (Morton, 1985; Morton and Hallsworth, 1999). In this chapter, heavy mineral suites of Pottsville sandstones are characterized and interpreted in the context of source terranes.

4.1 METHODS

Nine samples were disaggregated to release individual detrital grains. To eliminate the effects of hydraulic sorting, disaggregated samples were sieved into whole-

phi fractions; the 0-4 phi fractions were used for the analysis. Heavy minerals were extracted using a gravity-settling method and the heavy liquid tetrabromoethane ($\text{Br}_2\text{CHCHBr}_2$, density 2.89 gm/cc). Dry and weighed samples were added to the tetrabromoethane in a separating funnel. The mixture was periodically stirred to ensure thorough saturation of the sample. Heavy minerals were then allowed to settle to the bottom of the funnel above a pinch clip. After settling of the heavy minerals ceased (about 12-15 hours), the stopcock was slowly opened and heavy fractions were collected in a filter paper in the lower funnel. The stopcock was closed immediately after the heavy minerals were poured to prevent lighter fraction minerals from escaping. The lighter fraction was then drained into a new paper funnel. Both fractions were thoroughly washed with acetone and dried in an oven.

A hand-held magnet was first used to separate highly magnetic fractions from the heavy-mineral separates. A Franz magnetic separator was then used to separate the remaining "heavy" fraction into four subfractions (Hess, 1966). These fractions are: Group-A: Strongly Magnetic (SM); Group-B: Moderately Magnetic (MM); Group-C: Weakly Magnetic (WM); and Group-D: Poorly Magnetic (PM). Strongly magnetic (Group-A) minerals include pyrrhotite, magnetite, garnet, olivine, hematite, chloritoid, chromite, and ilmenite. These were separated using a 0.4-ampere current, a side slope of 20° , and a forward slope of 25° . Group-B minerals, including actinolite, augite, biotite, chlorite, epidote, hornblende, hypersthene, staurolite, and tourmaline, were separated from weakly to poorly magnetic minerals using a 0.8-ampere current and a 20° side slope. Group-C minerals include diopside, enstatite, tremolite, spinel, staurolite (light), tourmaline (light), muscovite, clinozoisite, and zoisite. These were separated using a 1.2-

ampere current and a 20° side slope. Remaining heavy minerals were classified as Group-D (poorly magnetic). This group includes very weakly magnetic minerals, such as andalusite, apatite, leucoxene, monazite, sphene, and xenotime, and non-magnetic minerals, such as corundum, fluorite, beryl, kyanite, zircon, rutile, pyrite, and sillimanite (Hess, 1966).

Polished thin sections of heavy minerals were prepared for all nine samples. Magnetically separated fractions were segregated spatially on each section. A petrographic microscope, equipped with both reflected and transmitted light, was used to identify heavy minerals. Point counting was performed using a modified Fleet method (Fleet, 1926), in which nearly all grains on each microscope slide were counted. The sum of all identified grains from each magnetically separated fraction was used to calculate percentages of heavy minerals present in the 0–4 phi size fractions of all the slides. Heavy mineral suites were used to evaluate source areas.

4.2 RESULTS

Point-counting results for heavy minerals from lower Pennsylvanian Pottsville Formation of Cahaba Basin are presented in Table 3 and Figure 23. Heavy mineral assemblages include subangular to rounded zircon, tourmaline, rutile (Figure 21a), garnet (Figure 22a), chlorite/chloritoid (Figure 22b), biotite/muscovite, apatite, pyrite, magnetite, galena, hematite, limonite, and opaque minerals (Figure 22b). Opaque grains and stable minerals (ZTR) dominate the heavy mineral assemblages. Of the ultrastable minerals (ZTR), rutile is most abundant.

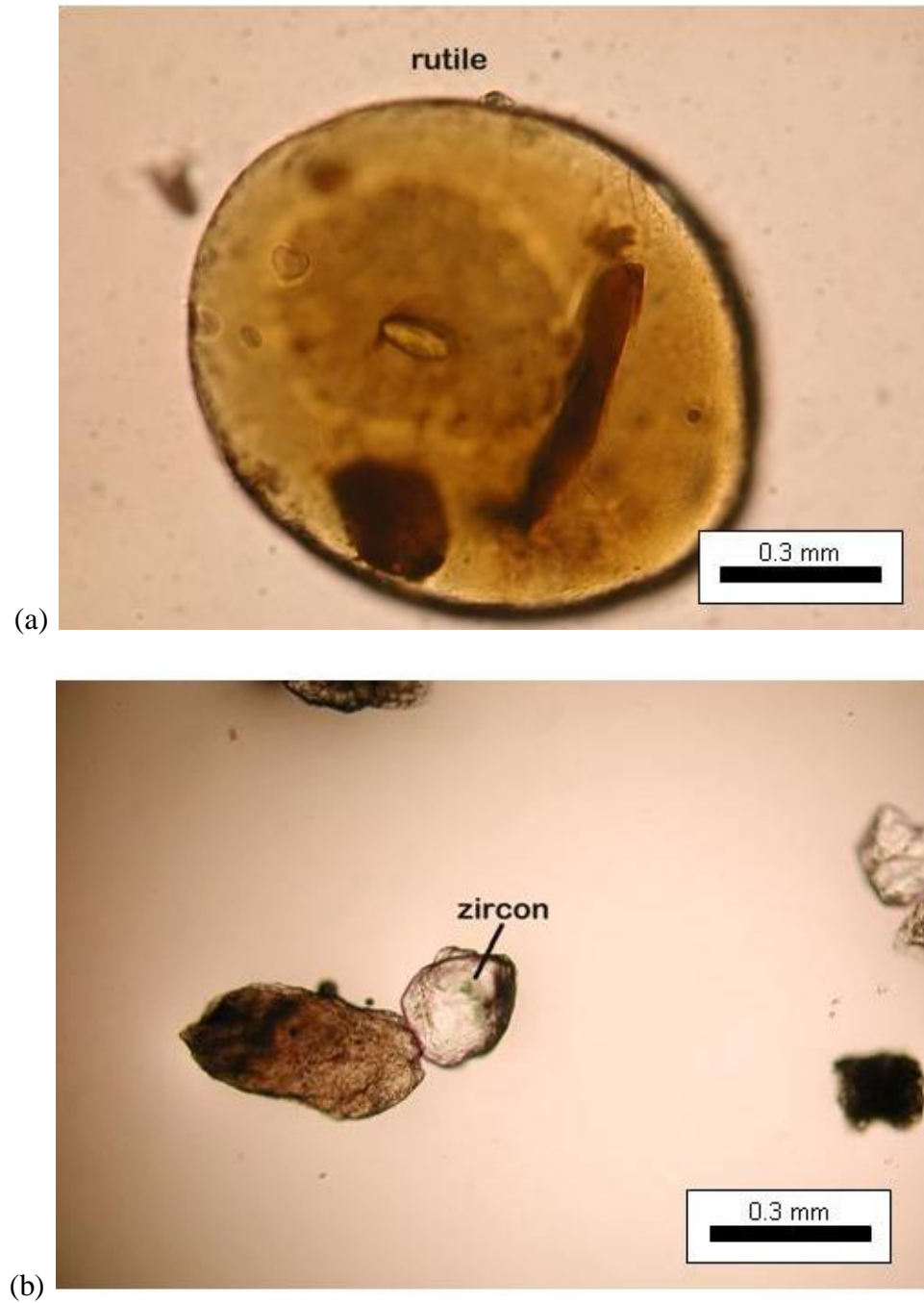
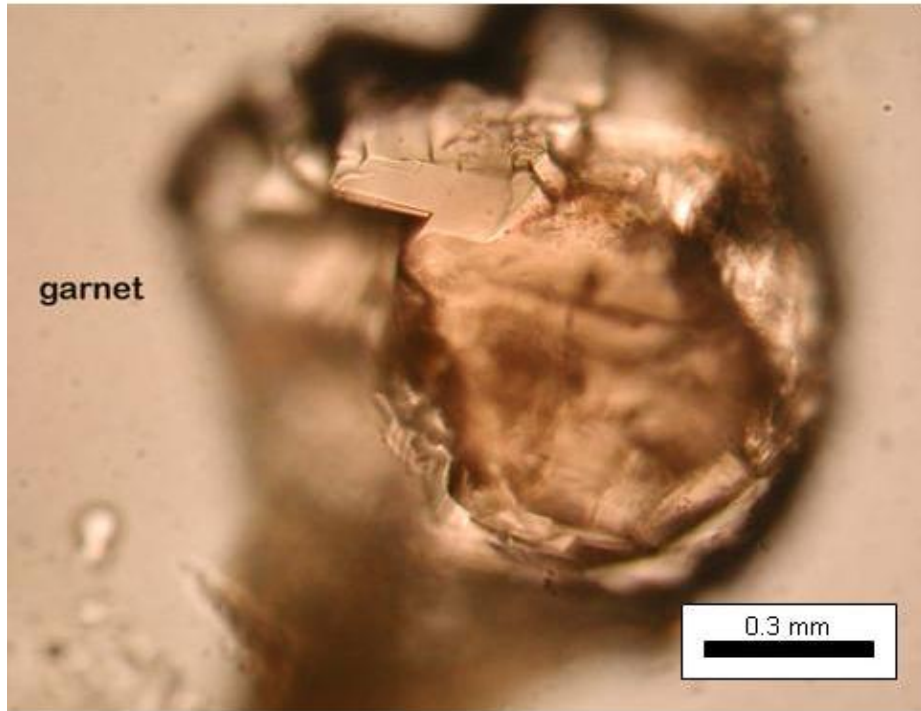
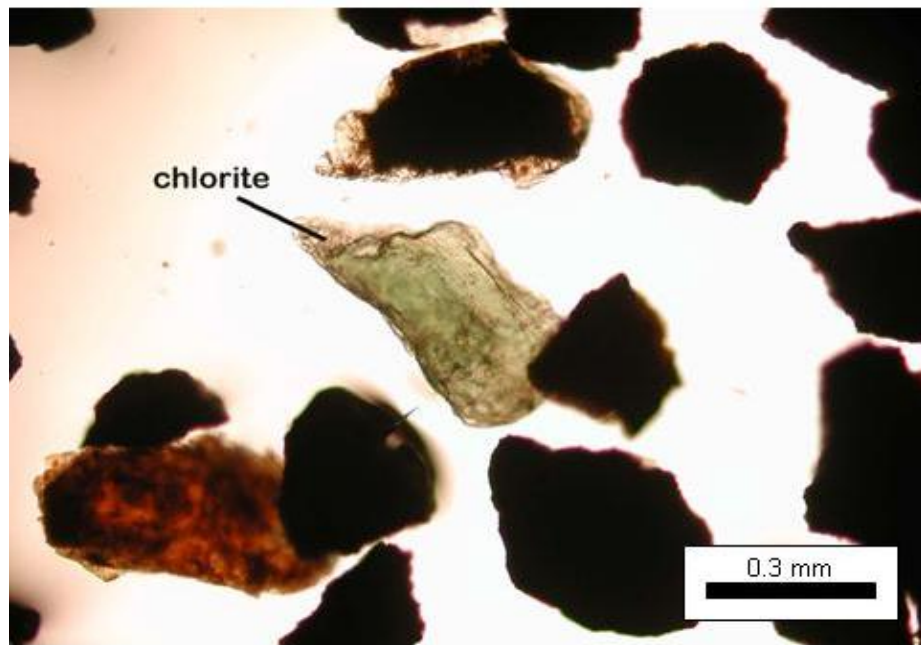


Figure 21. Photomicrographs of heavy minerals from Pottsville Formation. (a) Rutile grain in sample RTC-1 from the conglomerate measure. (b) Zircon grain in sample DC-4 also from the conglomerate measure. Both in plane transmitted light.



(a)



(b)

Figure 22. Photomicrographs of heavy minerals from Pottsville Formation, Cahaba Basin, Alabama. (a) Garnet grain in sample PSS-6 from the mudstone measure. (b) Chlorite surrounded by opaque minerals in sample PSS-12, also from the mudstone measure.

Table 3. Normalized abundances of heavy minerals of the Pottsville Formation, Cahaba Basin, Alabama. (ZTR – Zircon-Tourmaline-Rutile).

	Conglomerate Measure (n=3)				Quartzarenite Measure (n=3)			Total (n=9)	
	grain		grain		grain		grain		
	count	percentage	count	percentage	count	percentage	count	percentage	
Zircon	7	7%	3	3%	5	6%	15	5%	
Tourmaline	2	2%	1	1%	1	1%	4	1%	
Rutile	14	13%	17	15%	16	19%	47	16%	
ZTR %		22%		19%		27%		22%	
Garnet	4	4%	9	8%	11	13%	24	8%	
Chlorite/Chloritoid	6	6%	4	4%	3	4%	13	4%	
Biotite/Muscovite	6	6%	7	6%	5	6%	18	6%	
Apatite	1	1%	3	3%	4	5%	8	3%	
Pyrite	5	5%	6	5%	2	2%	13	4%	
Magnetite	1	1%	2	2%	1	1%	4	1%	
Galena	3	3%	0	0%	0	0%	3	1%	
Hematite	1	1%	2	2%	1	1%	4	1%	
Limonite	9	9%	5	4%	2	2%	16	5%	
Opakes	46	44%	54	48%	32	39%	132	44%	
total grains counted	105		113		83		301		

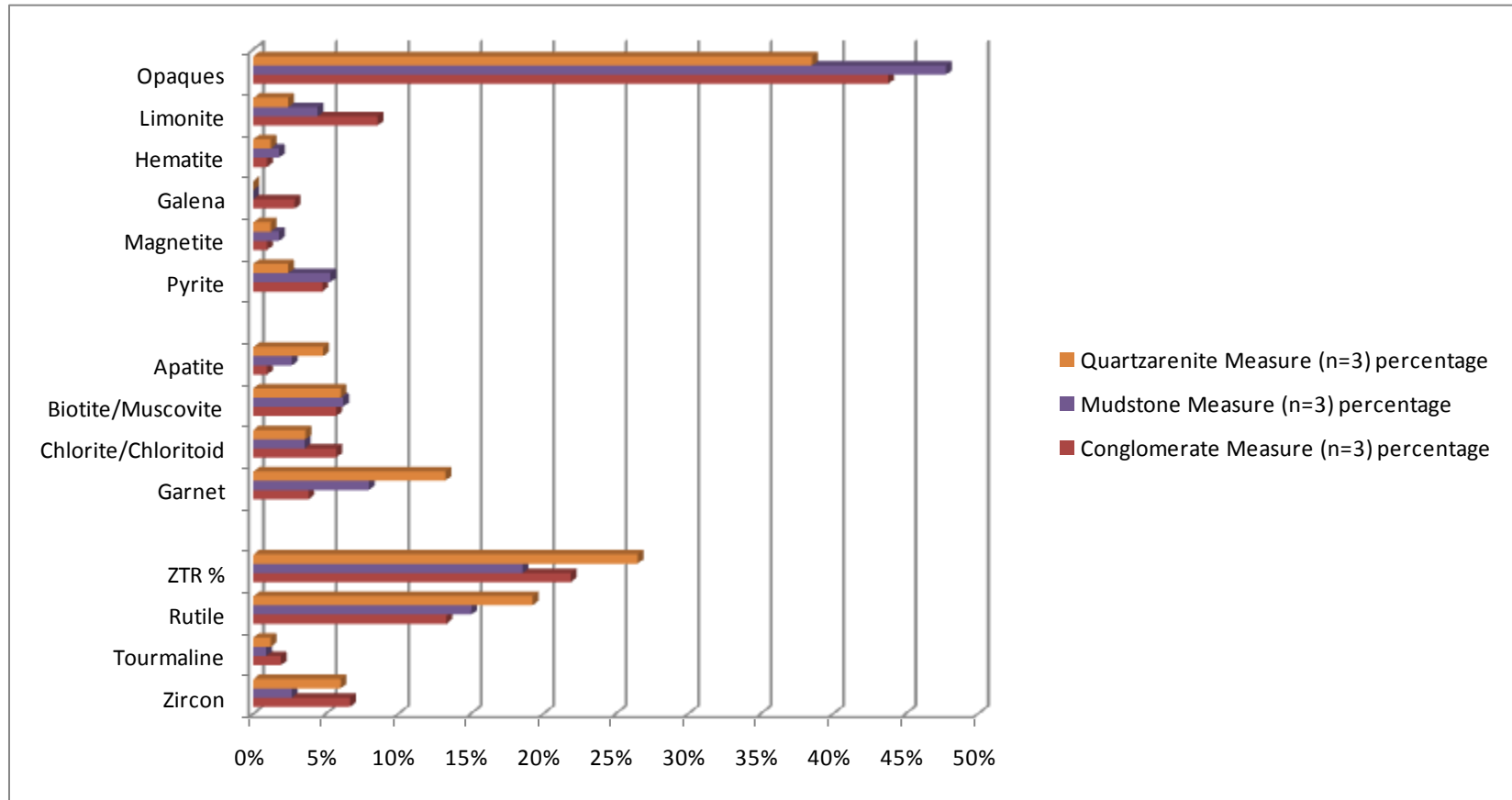


Figure 23. Heavy-mineral distribution in Pottsville sandstone showing distribution of all observed heavy minerals in conglomerate, mudstone, and quartzarenite measures.

4.3 INTERPRETATIONS

The low abundance of heavy minerals in the Pottsville sandstone and the abundance of ultrastable minerals reflect high sediment maturity, and indicate intense chemical weathering. This is consistent with the inferred location of the basin close to the equator during Pottsville time (Thomas et al., 2004).

The common occurrence of rutile suggests derivation from medium- to high-grade regionally metamorphosed terranes (Mange and Maurer, 1992; Zack et al., 2004). Garnets and chlorites/chloritoids also suggest a derivation from medium-grade metamorphic orogenic sources. Based on the relative shortage of zircon and tourmaline, compared to rutile, contributions from igneous source terranes were not substantial for the Pottsville Formation.

CHAPTER 5: MICROPROBE ANALYSIS OF GARNETS

5.0 INTRODUCTION

Electron–microprobe analysis of detrital garnet grains is perhaps one of the most powerful heavy mineral techniques currently applicable to provenance studies (Morton, 1986). Garnet $[X_3Y_2(SiO_4)_3]$ is commonly found in metamorphic rocks and certain igneous rocks. Garnet chemistry has been used to evaluate provenance in a number of regions (e.g., Morton, 1986; Morton and Taylor, 1991; Zang et al., 2003; Li et al., 2004). It provides an “index” of source-rock bulk composition, metamorphic grade, and, potentially, the pressure and temperature conditions of rock formation. In pelitic and mafic protoliths, the Mg content of garnet increases with respect to Fe^{+2} as metamorphic grade increases. Significant occupation of the octahedral site by cations other than Al^{3+} (i.e., Cr^{3+} , Fe^{3+}) also may be useful in constraining the chemical conditions of crystallization. In this chapter, the chemistry of garnets from Pottsville sandstone is used to assess provenance and pressure-temperature conditions of formation.

5.1 ELECTRON MICROPROBE

The electron microprobe provides a complete micron-scale quantitative chemical analysis of inorganic solids. The method is nondestructive and utilizes 63 characteristic x-rays excited by an electron beam incident on a flat surface of the sample.

In the electron microprobe, x-rays are emitted by the sample in response to a finely focused electron beam incident on the sample at a right angle. Some of the beam electrons are scattered backward. The backscattered electrons, as well as the characteristic x-rays of the elements, carry information about chemical composition. Secondary electrons, which are specimen electrons, mobilized by the beam through inelastic scattering, have energies in the range 0-50 eV with a most probable energy of 3-5 eV. Because of energy differences between backscattered electrons, characteristic x-rays, and secondary electrons, different detector setups are required for the detection of the three types of electron signal.

The electron microprobe serves two purposes: (1) it provides a complete micro-scale quantitative chemical analysis of microscopic volumes of solid materials through x-ray emission spectral analysis; and (2) it provides high-resolution scanning electron and scanning x-ray images. Backscattered electron (BSE) and scanning-cathodoluminescence images show compositional contrast in analyzed minerals.

5.2 METHODS

Six of the nine polished thin sections prepared for general heavy mineral analyses were used for microprobe analyses of garnet at the University of Georgia microprobe lab. A JEOL JXA 8600 microprobe using a 15 KeV accelerating voltage and 15 nA beam current was used for this study. Mineral grains were identified using a Noran Microtrace energy dispersive spectrometer (EDS) equipped with a SiLi detector and controlled by a PGT Avalon 4000 multichannel analyzer running eXcalibur software. The probe is automated by Geller Micro analytical laboratory dQANT automation. Both synthetic and

natural standards were used for calibration. A PRZ metric correction was used. Standard x-ray intensities of the elements to be measured were obtained on suitably chosen standards. Table 4 lists the standards that were used for the current study.

5.3 RESULTS

The garnets analyzed in the present study were associated with intergrown calcite (Figure 24). The calcite is most likely diagenetic. Ternary plots of chemical composition (Figures 25-28) indicate that garnets are predominantly of the almandine species and were derived from a medium-grade metamorphic source.

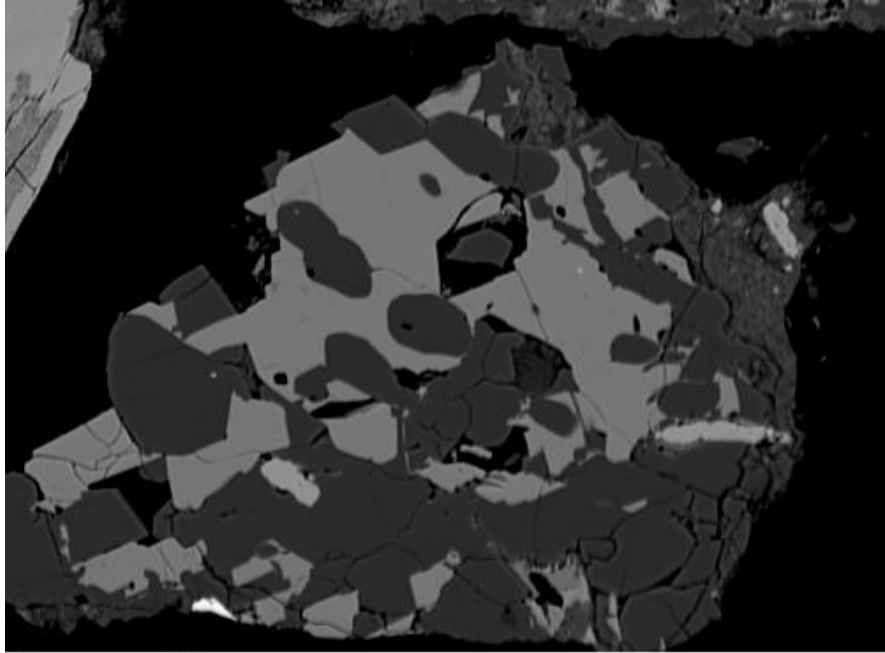
The Almandine + Spessartine, Grossular and Pyrope ternary plot (Figure 25) indicates garnets are predominately almandine/spessartine species. A plot of Pyrope + Almandine, Spessartine, and Grossular (Figure 26) indicates garnets are of the pyrope/almandine species. A plot of Spessartine + Grossular, Pyrope, and Almandine (Figure 27) shows that the garnets are exclusively of the almandine species.

Metamorphic grades of Pottsville garnets can be inferred from a plot of Spessartine, Almandine, and Pyrope (Figure 28). Most garnets fall within the low-grade amphibolite facies, although some grains do fall within the higher-grade granulite facies fields.

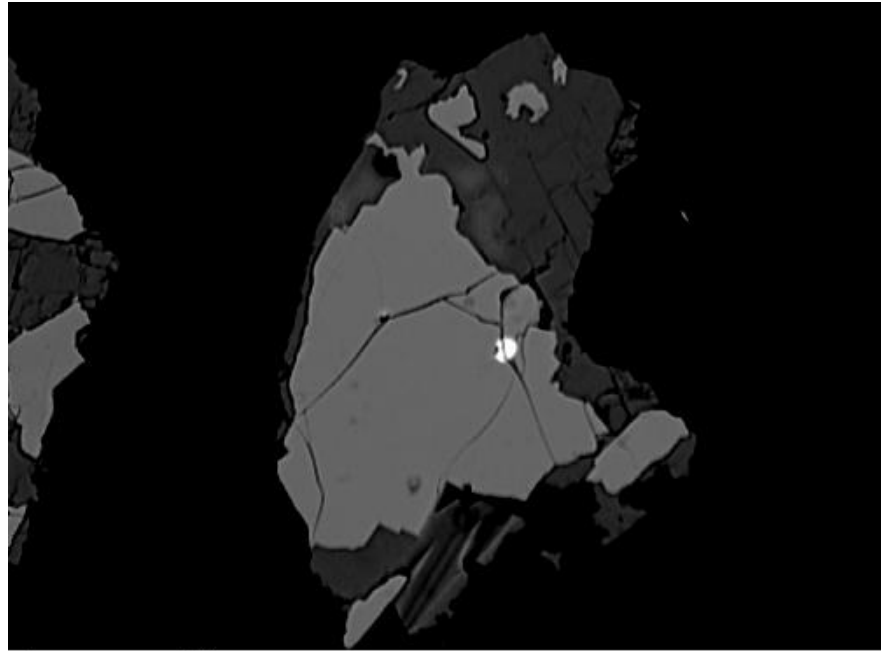
The chemistry of Pottsville garnets, specifically the Fe/(Fe+Mg) ratio, can be used to estimate temperature and pressure conditions (Figure 29). Assuming biotite in equilibrium with garnet for pelitic compositions and either Barrovian (medium-pressure,

Table 4. Electron microprobe standards used in this study.

Electron Microprobe Standards		
Element	Standard	Source
Cr	Chromite #5	C M Taylor Corp
Mg	Pyrope #39	C M Taylor Corp
Fe	Magnetite #9	Harvard Mineral Museum
Mn	Spessartine #4b	C M Taylor Corp
Al	Syn. Spinel	C M Taylor Corp
Si	Almandine	Harvard Mineral Museum



(a) 40 μ m



(b) 40 μ m

Figure 24. Backscatter images from microprobe analysis of garnet grains. (a) Garnet (lighter grain, high z; high average atomic number, common for iron-rich minerals) intergrown with calcite (darker grain, low z; typical of carbonates, quartz, etc.) (b) Garnet grain (lighter grain, high z) intergrown with large calcite (darker grain, low z) crystals.

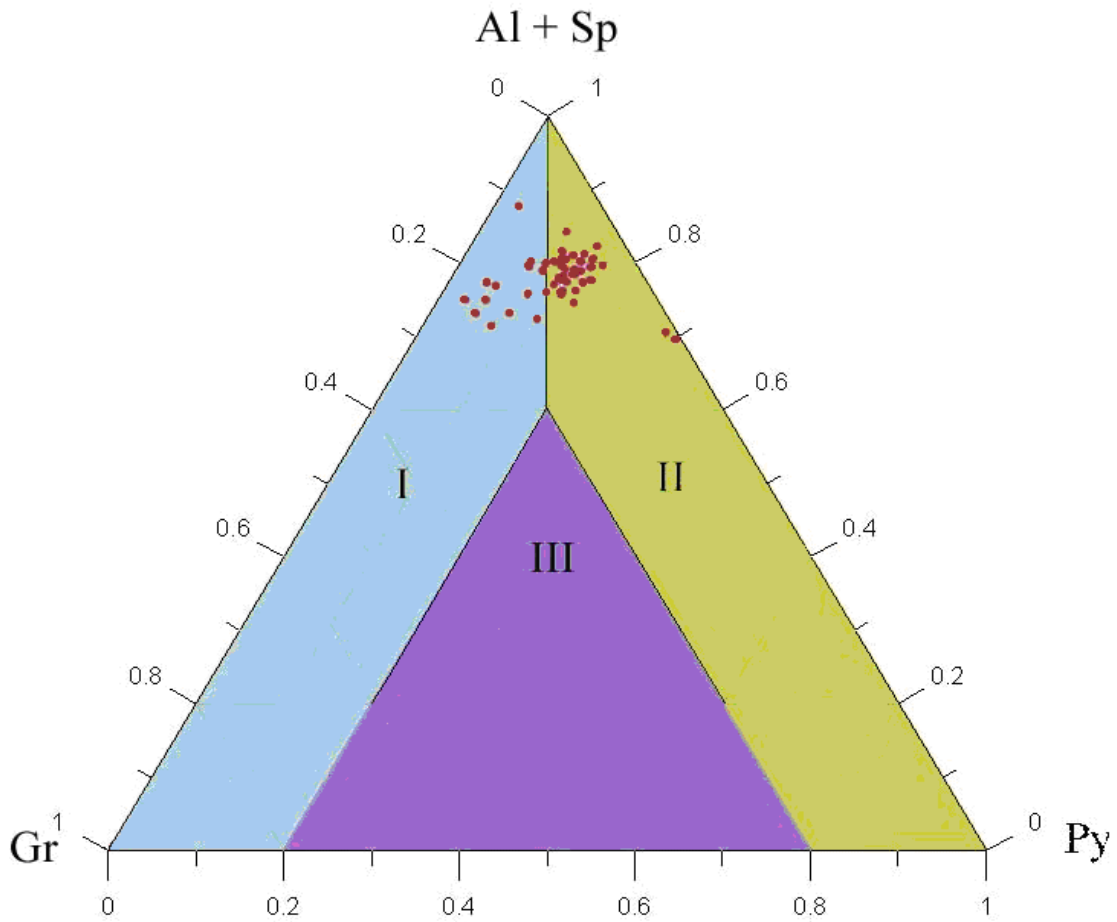


Figure 25. Ternary plot showing garnet chemistry; Al=almandine; Sp=spessartine; Gr=grossular; and Py=pyrope. I=garnets with almandine and grossular with <10% pyrope; II=garnets with almandine and pyrope with <10% grossular; and III=garnets with pyrope and grossular, both >10% (modified from Morton et al., 1992).

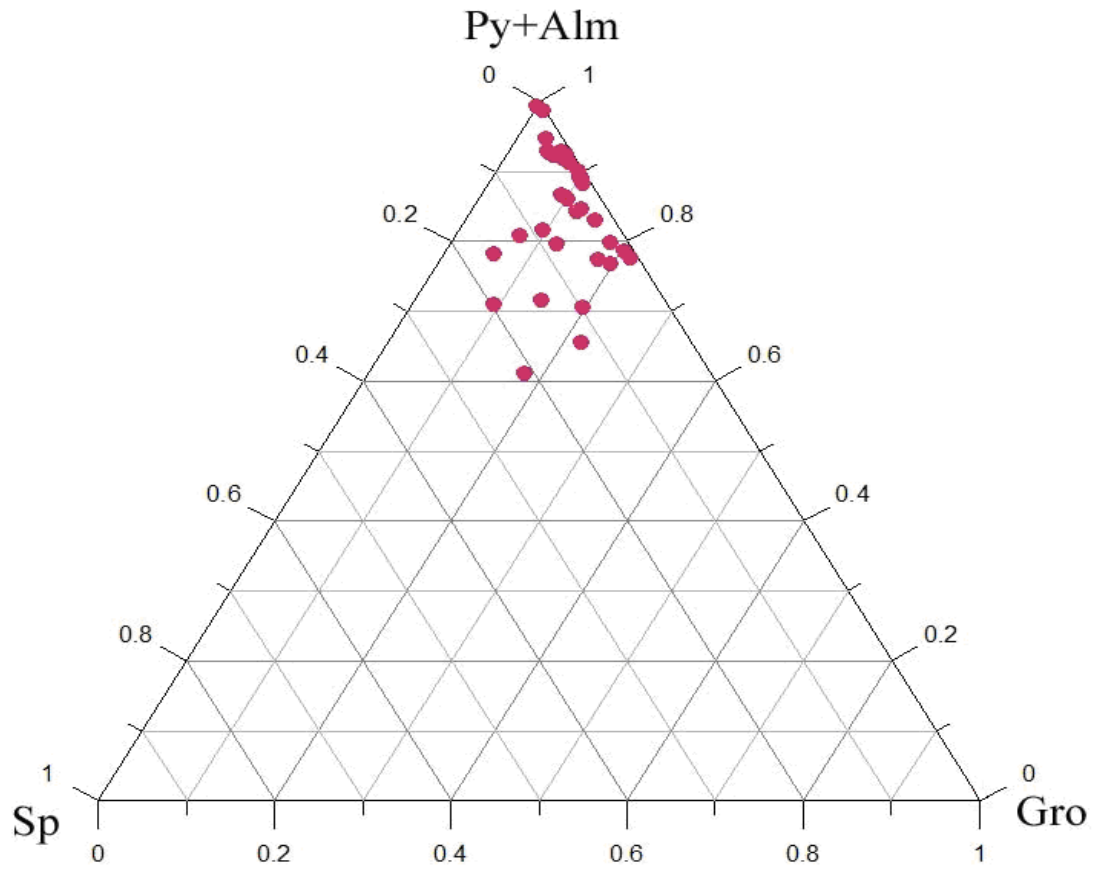


Figure 26. Ternary plot of garnet chemistry. Alm=almandine; Sp=spessartine; Gro=grossular; and Py=pyrope.

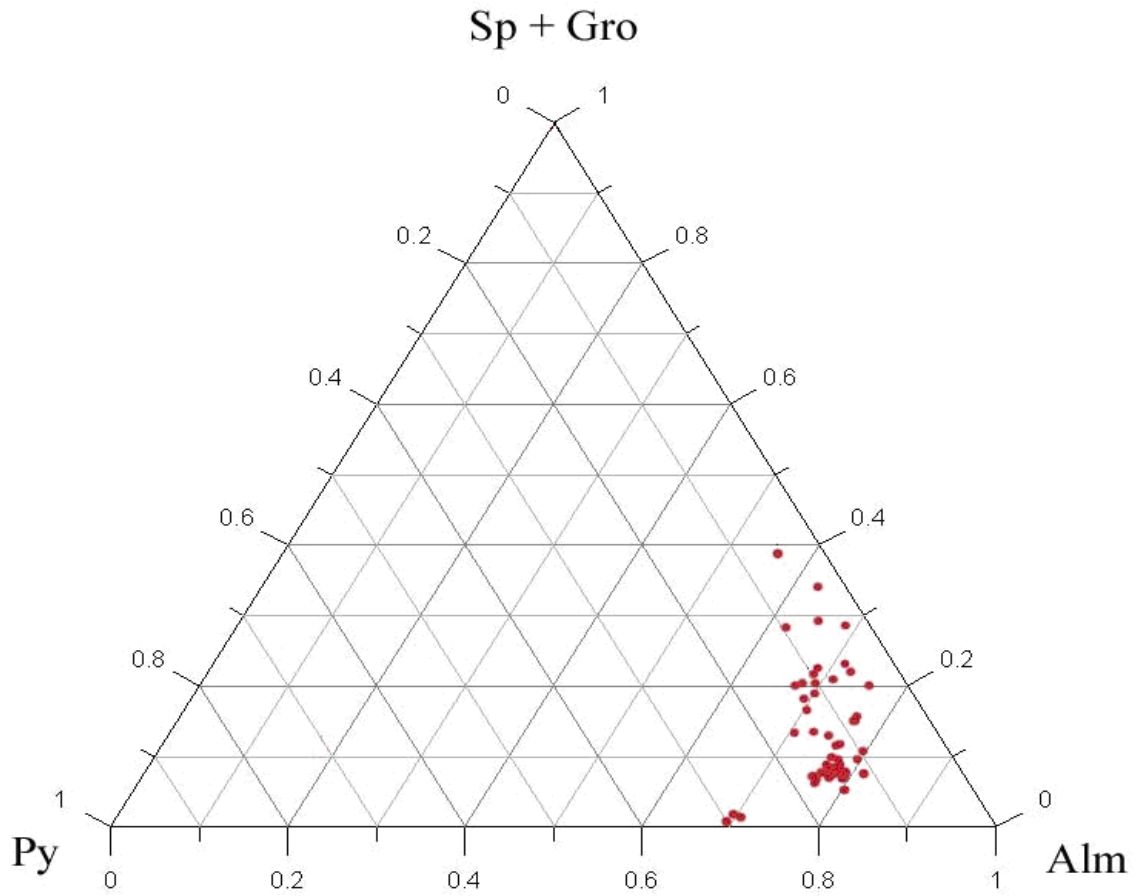


Figure 27. Ternary plot of garnet chemistry; Alm=almandine; Sp=spessartine; Py=pyrope; and Gro=grossular.

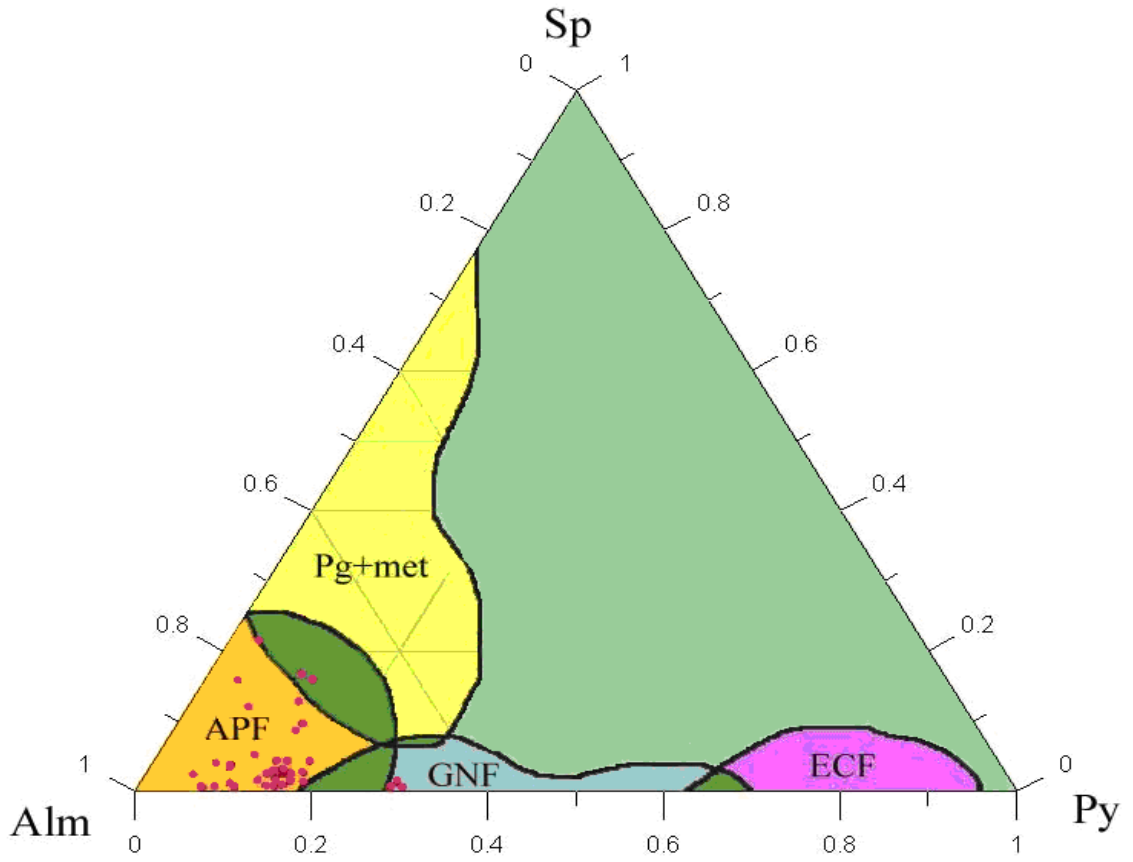


Figure 28. Ternary plot of garnet chemistry and its relation to metamorphic grade. Alm=almandine; Sp=spessartine; Py=pyrope. APF=amphibolites facies; GNF=granulite facies; ECF=eclogite facies; Pg=pegmatite; and met=metamorphic (after Nanayama, 1997).

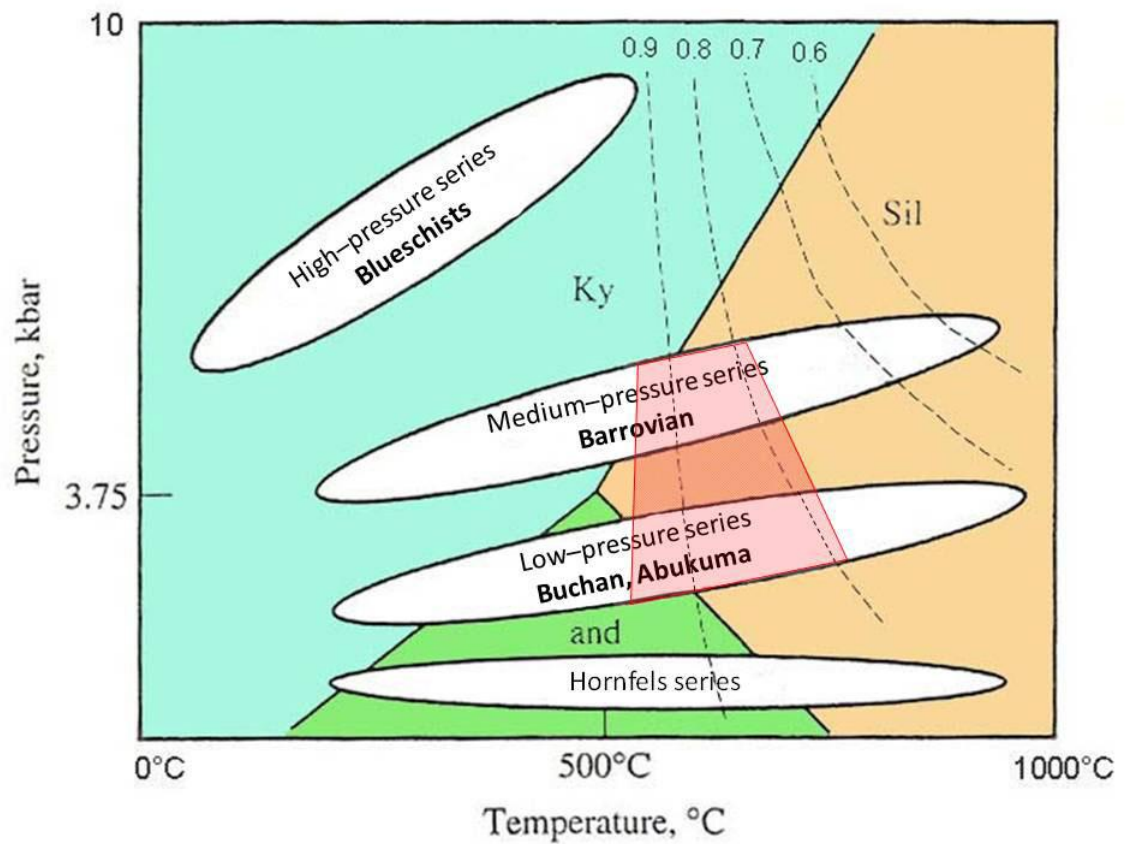


Figure 29. Relationship between Pottsville garnet chemistry and metamorphic pressures and temperatures. Dashed black lines are isopleths of constant $Fe/(Fe+Mg)$ calculated assuming garnet in equilibrium with biotite (from Spear and Cheney, 1989). Red shaded polygon indicates where Pottsville garnets would presumably plot if formed under Barrovian or Buchan/Abukuma.

high temperature) or Buchan (low-pressure) type facies, Pottsville garnets formed within a temperature–pressure range of 520–800°C and 2–6 kbar (550–700°C, 4–6 kbar for Barrovian; 520–800°C, 2–4 kbar for Buchan).

5.4 INTERPRETATIONS

Garnets analyzed were most likely derived from a medium-grade metamorphic source rock. Rocks in the Ouachita orogen consist primarily of intensely folded and deformed Paleozoic sandstones, shales, novaculites and cherts (Engel, 1952). Except for some localized contact metamorphism adjacent to igneous intrusions, only very low– to low–grade metamorphic rocks reaching the greenschist facies are present in the Ouachitas (Flawn et al., 1961; Richards et al., 2002). Hence, the Appalachians, specifically the Inner Piedmont and Western Blue Ridge terranes, presently to the northeast of the Cahaba Basin, are interpreted to be a more likely source for the garnet grains of the Pottsville Formation.

CHAPTER 6: $^{40}\text{Ar}/^{39}\text{Ar}$ DETRITAL MUSCOVITE AGES

6.0 INTRODUCTION

The $^{40}\text{Ar}/^{39}\text{Ar}$ age of a weathered grain of detrital muscovite should provide a time of cooling of the source rock through the closure temperature interval for muscovite (typically 300-400°C; e.g., Hames and Bowring, 1994). This concept is based on the assumption that no additional radiogenic ^{40}Ar is lost during transport or after deposition (Hodges et al., 2005). The interval of time between deposition of the sediment and isotopic cooling of the muscovite grain is inferred to be the amount of time required to erode 10-20 km of sediment (dependent upon geothermal gradient and error of uncertainty in the closure temperature).

For the current study, $^{40}\text{Ar}/^{39}\text{Ar}$ isotopic analyses were performed on selected detrital muscovites from three samples of the Pottsville Formation. Cooling ages derived from these analyses were used to infer possible source rocks in adjacent southern Appalachian Piedmont terranes.

6.1. PREVIOUS DETRITAL GEOCHRONOLOGY

Previous studies involving geochronology of detrital grains from the Pottsville Formation are limited. Meyer et al. (2005) employed K/Ar techniques to date muscovites in the Pottsville at various localities. Bulk analyses of detrital muscovites from the

northern Appalachian Basin were used to infer a single source with Acadian ages (360 ± 10 Ma) (Meyer et al., 2005). In contrast, comparable K/Ar analyses of muscovites from the southern Appalachian Basin yielded a broad range of ages, suggesting multiple sources (Meyer et al., 2005).

Becker et al. (2005) described U/Pb geochronology of detrital zircons from basal Pennsylvanian sandstones and conglomerates sampled through the Appalachian Basin (from Pennsylvania to Alabama). They noted a dominance of zircons that relate to the crustal-forming events of Laurentia. Detrital zircons from the Montevallo coal zone in the Cahaba Basin are predominantly Laurentian in nature, the ages fall within the Meso- and Paleoproterozoic (931–1817 Ma), but include one Archean grain (2880 ± 6 Ma). Based on these observations, Becker et al. (2005) concluded that the supply for Alleghenian clastic wedges in the Appalachian Basin was mostly from Laurentian sources.

6.2 $^{40}\text{Ar}/^{39}\text{Ar}$ DATING

Argon is a noble gas that naturally occurs in the atmosphere, while potassium is a common element in many minerals. A number of isotopes containing these elements relate to the K/Ar and $^{40}\text{Ar}/^{39}\text{Ar}$ dating techniques (Figure 30); see McDougall and Harrison (1999) for a complete discussion of the method.

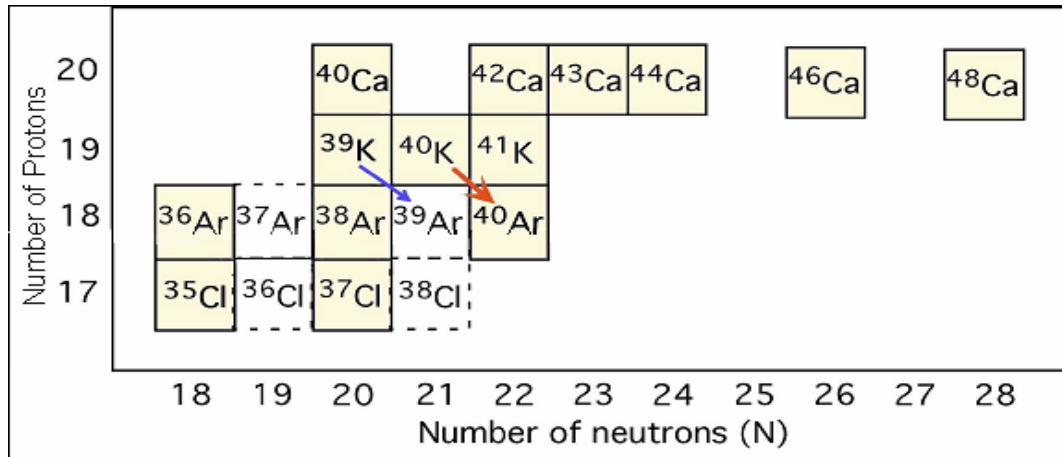


Figure 30. Decay scheme of relevant isotopes according to the $^{40}\text{Ar}/^{39}\text{Ar}$ technique. Filled boxes are naturally occurring isotopes; red arrow indicates $^{40}\text{K} \rightarrow ^{40}\text{Ar}$ decay, which is a naturally occurring reaction. The blue arrow indicates the $^{39}\text{K} (n,p) ^{39}\text{Ar}_K$ reaction, which is induced in a nuclear reactor, and makes $^{40}\text{Ar}/^{39}\text{Ar}$ dating possible.

6.3 METHODS

Muscovite grains were separated from three samples (D2S1, D2S2, and CHB-5) collected from outcrops of the lower half of the Pottsville Formation (Figure 31). Sample D2S1 is from the Pine Sandstone, which sharply overlies the Hardwick Tunnel Shale. Lenses of intraclastic conglomerate including shale, siderite, coal spars, and plant debris are irregularly dispersed at the base of the Pine Sandstone Member (sample collected at stop 1 of day 2 from Pashin and Carroll, 1999).

Sample D2S2 is from the Chestnut Sandstone, the oldest sandstone unit in the mudstone measures. The Chestnut sandstone forms a ridge that extends the length of the Cahaba Basin (Pashin and Carroll, 1999). The basal Chestnut Sandstone (~25 ft) is characterized by thinly interbedded shale and sandstone with wavy, lenticular, and pinstripe bedding. The middle part of the unit (~20 ft) is dominated by silty shale with siderite bands. The upper half of the unit is mostly fining-upward sequences of interbedded sandstone and shale (sample collected from stop 2 of day 2 from Pashin and Carroll, 1999).

Sample CHB-5 was collected from a sandstone unit within the Harkness Coal Zone. This zone includes, in ascending order, a thick, coarsening-upward succession of interbedded sandstone and mudstone, mudstone with siderite bands (~20 ft), and thickly interbedded sandstone and mudstone (Pashin and Carroll, 1999).

Seventy to ninety grains were picked from each sample (e.g., Figure 32) and sent to Hamilton, Ontario for neutron irradiation. Muscovites were analyzed at the Auburn Noble Isotope Mass Analysis Laboratory (ANIMAL) in the Department of Geology and Geography of Auburn University. The lab is set up for single-crystal isotopic analysis

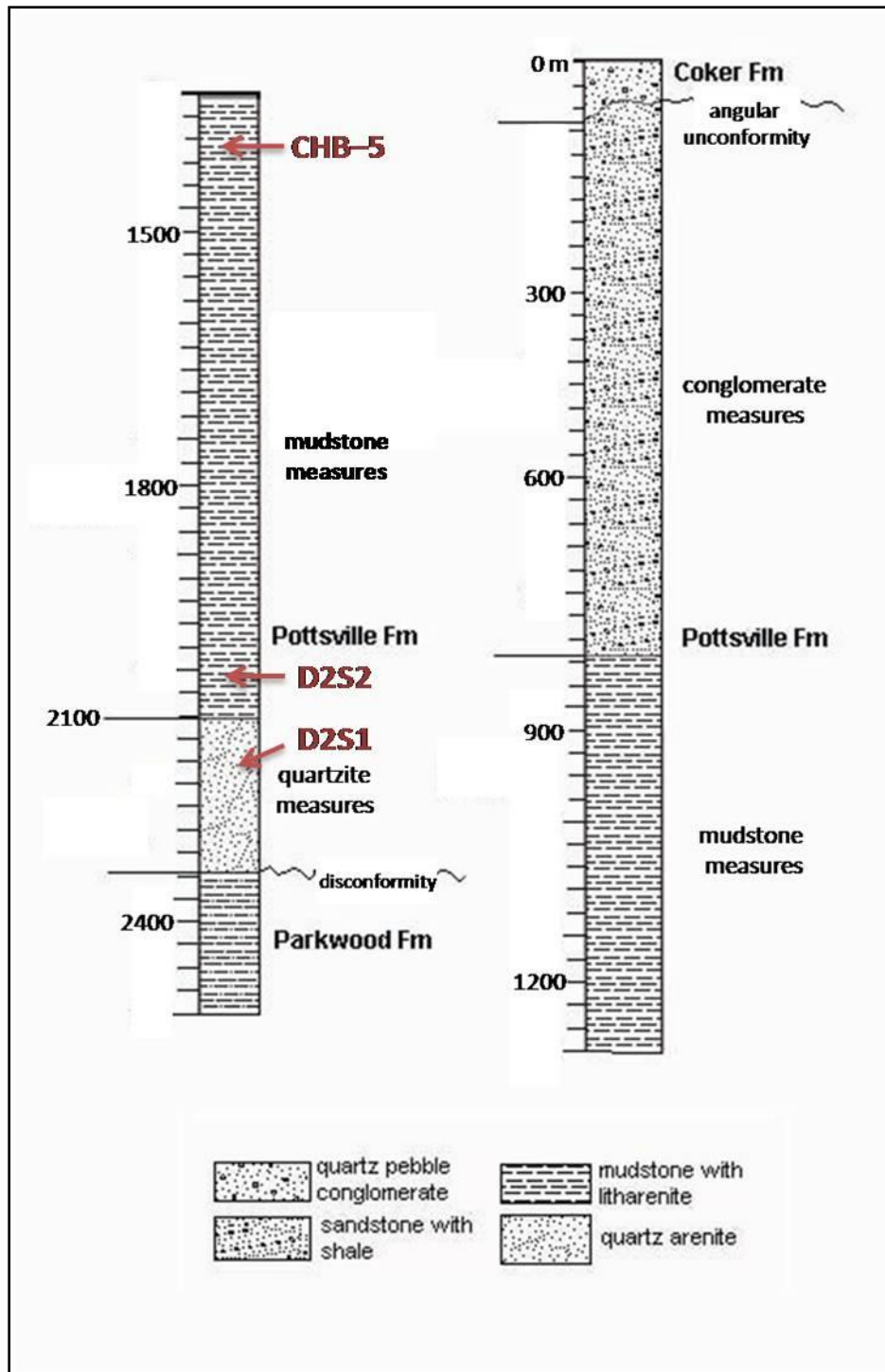


Figure 31. Generalized stratigraphic column of Pennsylvanian Pottsville Formation in the study area (modified from Pashin and Carroll, 1999). Stratigraphic positions of the three samples (D2S1, D2S2, and CHB-5), used to extract muscovite grains for $^{40}\text{Ar}/^{39}\text{Ar}$ dating are shown by arrows.

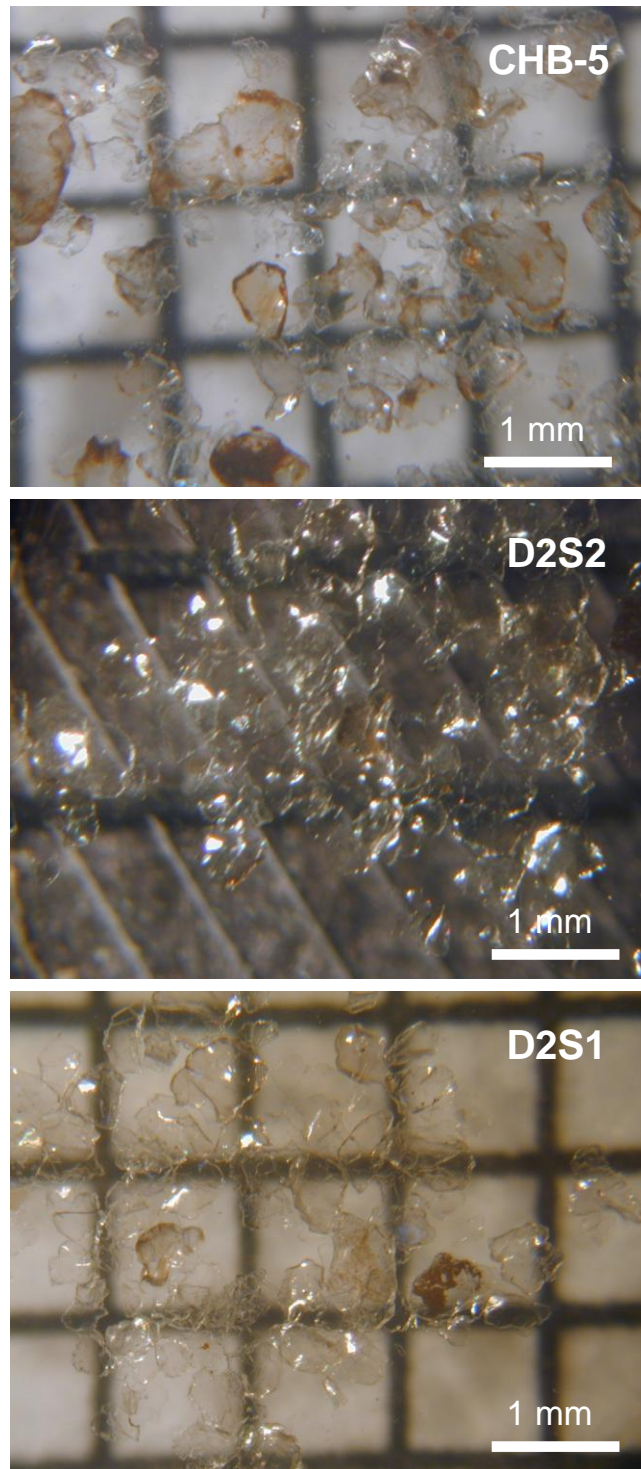


Figure 32. Photomicrographs of muscovite grains of samples D2S1, D2S2, and CHB-5.

using the $^{40}\text{Ar}/^{39}\text{Ar}$ technique. Single crystal analysis allows grain-scale evaluation of the effects of extraneous argon and heterogeneous-mineral assemblages, as well as inherent age variation among a population of crystals. The lab also provides increased sensitivity and resolution relative to other labs that use bulk sampling methods. Each analysis (Appendix C) corresponds to laser fusion and measurement of argon within a single crystal.

The Fish Canyon sanidine (28.02 ± 0.09 Ma; Renne et al., 1998) was used as a flux monitor for this study. Background interference was corrected by running blanks after three to five unknowns; mass discrimination was evaluated by analyzing 3–5 air aliquots daily. Approximately 65 irradiated muscovite grains from each sample were placed in a copper holding disc and analyzed by fusing single muscovite crystals with a CO_2 laser. The data were then reduced with an excel spreadsheet and analyzed with Isoplot (Ludwig, 2003).

Age-population distributions were constructed through probability plots for each sample, with corresponding error and relative probability of ages in million years (Figure 33). The Mean Square Weighted Deviate (MSWD) measures the scatter of the individual step ages, with their associated errors from the mean. Results are provided in Appendix C.

6.4 RESULTS

Variation in sample CHB–5 is greater than would be expected from the precision of single analyses, but the low standard error of the mean (0.4%) is consistent with a source terrane dominated by Devonian (~374 Ma) muscovite. Nine of the original 56

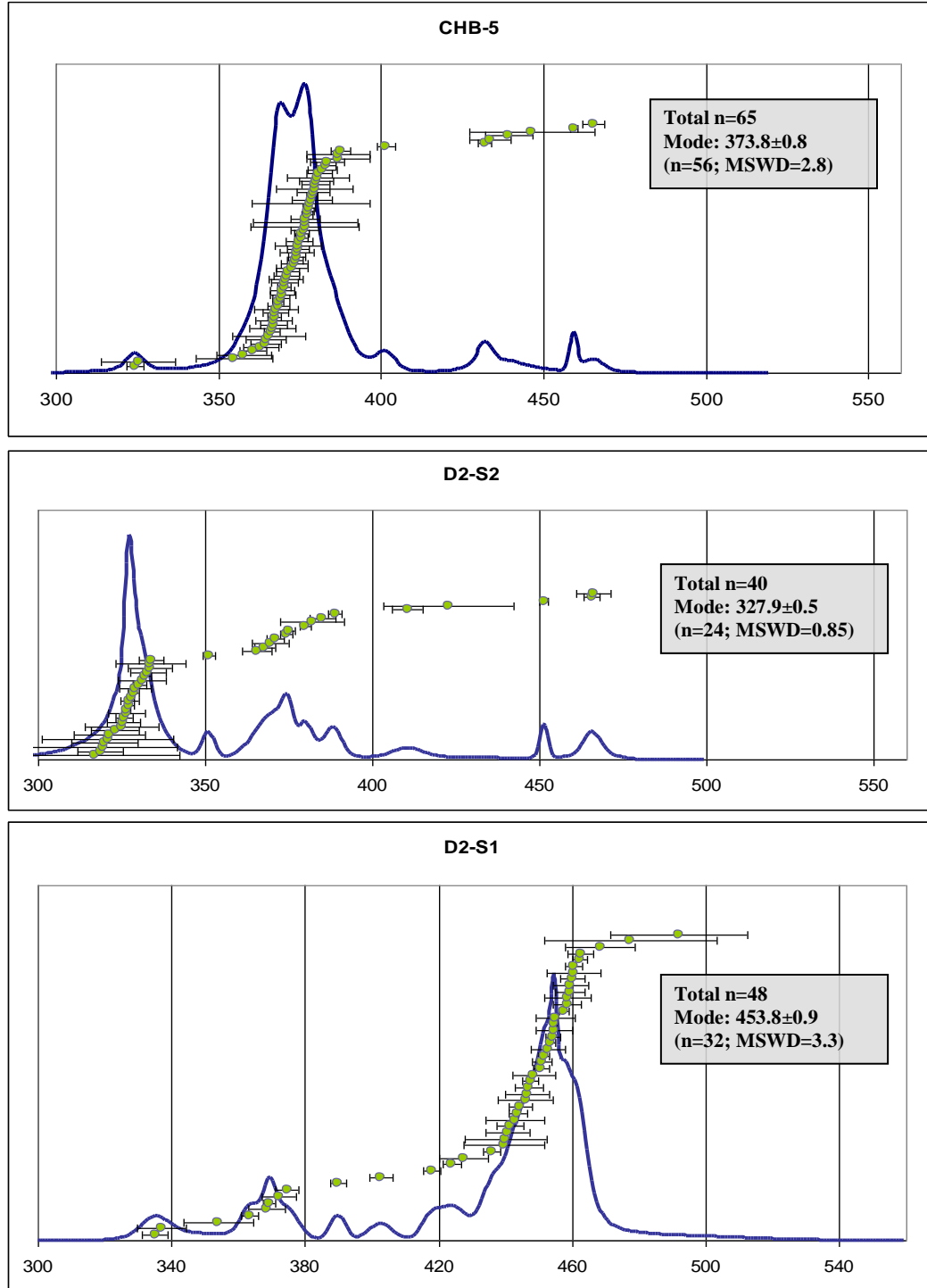


Figure 33. $^{40}\text{Ar}/^{39}\text{Ar}$ isotope ages for samples D2S1, D2S2, and CHB-5, in stratigraphic order. The curves show relative probability of ages. Error bars represent 1σ . Mode of CHB-5 was defined by analysis of all data using an algorithm for rejecting outliers in Isoplot (Ludwig, 2003). Modes of D2S2 and D2S1 were determined by inspection.

grains analyzed were automatically rejected (with values greater than 400 and less than 330) during MSWD calculations (with the standard rejection algorithm of Isoplot), resulting in a mean age of 373.8 ± 1.5 Ma, and an MSWD=2.8.

Sample D2S2 has a mode at approximately 330 Ma, with minor groups of analyses at ~380 Ma and ~450 Ma. Considering only points less than 350 Ma ($n=24$), a mean value associated with the mode is 327.94 ± 0.97 Ma, with an MSWD=0.85. Hence, the source of D2S2 is dominated by Early Carboniferous (Mississippian) muscovite.

Sample D2S1 has a mode at approximately 453 Ma. Considering only points less than 460 and greater than 430 ($n = 31$), a mean value associated with the mode is 453.0 ± 2 Ma, with an MSWD = 3.3. The source of D2S1 is dominated by a terrane rich in Middle Ordovician (Taconic) muscovite.

6.5 INTERPRETATIONS

Cooling ages for muscovites collected from the three horizons suggests temporal variations in source rocks. Detrital muscovite grains from sample D2S1, dated at 470-430 Ma, were logically derived from a Taconian source. Such a source may be associated with the Hillabee Greenstone of Alabama. McClellan et al. (2007) published U/Pb zircon ages of 470 ± 4 Ma for the Hillabee Greenstone.

The Alleghenian age for sample D2S2, (330–320 Ma) may reflect derivation from the Talladega Slate belt or the Western Blue Ridge. Single crystal $^{40}\text{Ar}/^{39}\text{Ar}$ analyses of muscovites from phyllites and schists of the frontal zone of the Talladega Belt and Mineral Bluff Group of the Western Blue Ridge yield ages in the range of 335–320 Ma (McDonald, 2008).

Finally, sample CHB-5 is most likely derived from a source rock of Acadian age. Acadian rocks are intermittently exposed in the Appalachian Mountains (Osberg et al., 1989). Muscovite cooling ages of 390-360 Ma may link this detritus to the Tugaloo and Cat Square terranes of the Inner Piedmont. The Tugaloo terrane is made up of migmatic metasediments, amphibolite, granitic intrusives, and minor ultramafic rocks (Hatcher et al., 2005). The Cat Square terrane is predominantly aluminous schists and metagraywacke, intruded by Devonian-Carboniferous granitoids (Merschhat and Hatcher, 2007).

CHAPTER 7: MUDROCK CHEMISTRY

7.0 INTRODUCTION

A generalization is commonly made that mudrock composition should be representative of the average composition of the continental crust (e.g., Allegre and Rousseau, 1984; Taylor and McLennan, 1985). This should be true of mudrocks in marine settings, the components of which have been transported great distances (Taylor and McLennan, 1985). However, many mudrocks form in more confined basins and from more restricted source rocks and, therefore, are not representative of global crustal compositions. Bhatia and Taylor (1981) and Bhatia (1985) have shown that the compositions of mudrocks from volcanic arc settings are related to the compositions of their source rocks and bear little resemblance to average shale compositions.

In studies of global variation in mudrock chemistry (Garrels and Mackenzie, 1971; Ronov and Migdisov, 1971; Taylor and McLennan, 1985; Uddin et al., 2005), the average composition for any given time is ordinarily computed from a database of individual mudrock samples, all of which are from a known source-rock type in unambiguous tectonic settings. Information on the controls of mudrock composition on a small scale is impertinent to an understanding of variations in mudrock composition on a global scale (Cox et al., 1995). With the exception of a few works (i.e., Bhatia and Taylor, 1981; Bhatia, 1985; and Roser and Korsch, 1988), little information is available

on the effects of provenance and tectonic setting on the composition of mudrocks (Cox et al., 1995).

In addition to the sandstones described in previous chapters, the Pottsville Formation also contains thick mudrock/shales that may potentially hold significant information on source rocks and their depositional environments. The objective of this chapter is to describe whole rock analyses of Pottsville mudrocks and their implications for sedimentary provenance.

7.1 METHODS

Five mudrock samples were collected from drill cores from the Cahaba Basin in order to perform whole-rock chemical analyses. Samples were collected from both the conglomerate measure and the mudstone measure (Figure 34). After cutting core in half, samples were shipped to ACME Analytical Laboratories (Vancouver), Ltd. At ACME, a sample of up to 1 kg was crushed to 70% passing at 10-mesh. A 250-g split was then pulverized to 95% passing at 150 mesh. A multi-element assay for 11 oxides (SiO_2 , Al_2O_3 , Fe_2O_3 , MgO , CaO , Na_2O , K_2O , TiO_2 , P_2O_5 , MnO , and Cr_2O_3) and 7 trace elements (Ba, Ni, Sr, Zr, Y, Nb, and Sc) was performed by digestion of a 1-g sample split followed by inductively coupled plasma–mass spectrometry (ICP–MS) methods.

7.2 RESULTS

Table 5 provides the results of mudrock chemical analyses. As expected, both silica and aluminum contents are very high, ranging from 54-64% and 15–20%,

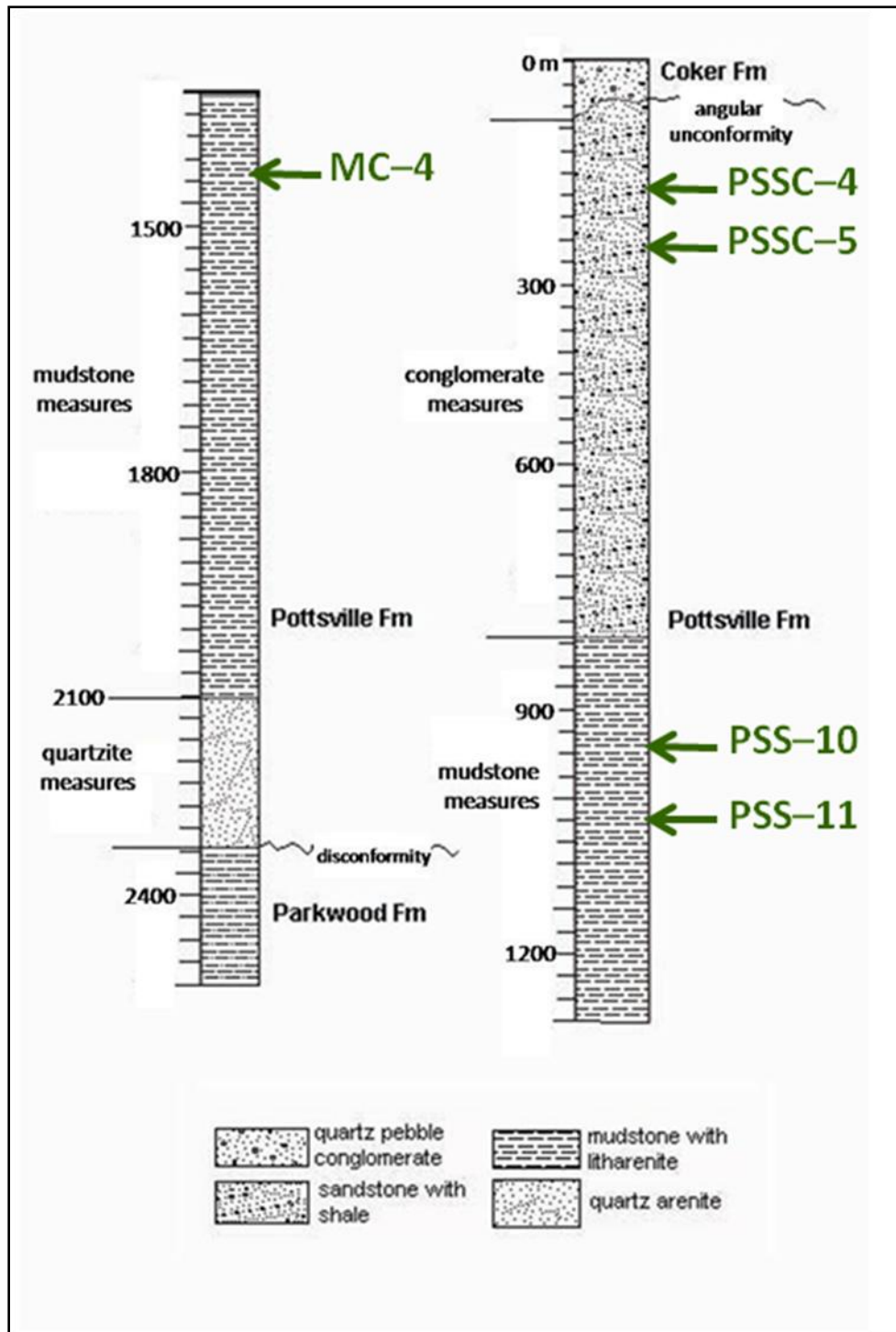


Figure 34. Generalized stratigraphic column of Pottsville Formation in the study area (modified from Pashin and Carroll, 1999) showing depths at which samples (MC-4, PSS-11, PSS-10, PSSC-5, PSSC-4) were collected for whole-rock chemical analysis.

Table 5. Results of whole-rock chemical analyses of Pottsville samples PSS-10, PSS-11, PSSC-4, PSSC-5, and MC-4.

		PSS-10	PSS-11	PSSC-4	PSSC-5	MC-4
SiO ₂	%	62.07	57.33	54.43	64.99	58.06
Al ₂ O ₃	%	18.07	21.14	20.67	15.21	19.68
Fe ₂ O ₃	%	5.54	6.81	8.25	6.54	6.32
MgO	%	1.66	1.9	2.43	1.95	2.04
CaO	%	0.33	0.1	0.3	0.49	0.38
Na ₂ O	%	1.01	0.35	0.62	1.58	1.09
K ₂ O	%	4.13	5.05	4.48	2.85	3.98
TiO ₂	%	1.1	0.96	0.97	0.88	1.01
P ₂ O ₅	%	0.151	0.068	0.186	0.156	0.142
MnO	%	0.05	0.03	0.06	0.07	0.06
Cr ₂ O ₃	%	0.013	0.014	0.014	0.009	0.014
Ba	ppm	1016	1175	1135	717	878
Ni	ppm	42	53	57	32	49
Sr	ppm	138.2	104.3	128.2	98.4	111.2
Zr	ppm	310	158	153	199	176
Y	ppm	46	41	42	37	41
Nb	ppm	25	16	21	19	17
Sc	ppm	18	23	24	18	21
LOI	%	5.1	5.5	6.7	4.7	6.6
Sum	%	99.4	99.48	99.28	99.61	99.55
total C	%	0.87	0.27	1.03	0.69	1.39
total S	%	0.08	0.02	0.03	0.06	0.09

respectively (Figure 35). Iron and potassium are of secondary importance, while concentrations of all other major elements are low. Barium is the dominant trace element (Figure 36) followed by zircon and strontium.

Based on the relative concentrations of SiO_2 , K_2O , and Na_2O Pottsville mudrocks fall in the “active continental margin” and “island arc” provenance fields of the Roser and Korsch (1988) discriminatory plot (Figure 37). When plotted on a Si–Ca+Mg–Na+K ternary plot (Taylor and McLennan, 1985; Rieu et al., 2007), Pottsville mudrocks fall close to the granite provenance field, indicating that basaltic and ultramafic rocks were not important in source areas (Figure 38). In the A–CN–K (Al_2O_3 –CaO+ Na_2O – K_2O) compositional space triangle (Nesbit and Young, 1984), Pottsville samples plot close to the Al_2O_3 end member, possibly indicating intense chemical weathering (Figure 39). The chemical index of alteration; (CIA; $\text{Al}_2\text{O}_3/(\text{Al}_2\text{O}_3+\text{K}_2\text{O}+\text{Na}_2\text{O}+\text{CaO})*100$) value Pottsville mudrock samples is high (CIA=77.85).

7.3 INTERPRETATIONS

Mudrock geochemical data are generally consistent with interpretations drawn from sandstone petrology in that they reflect the importance of source rocks formed in active continental margins and of intense chemical weathering. The relative lack of certain constituents, such as chromium and nickel, reflect the absence or insignificance of ophiolites and other ultra mafic rocks in source areas.

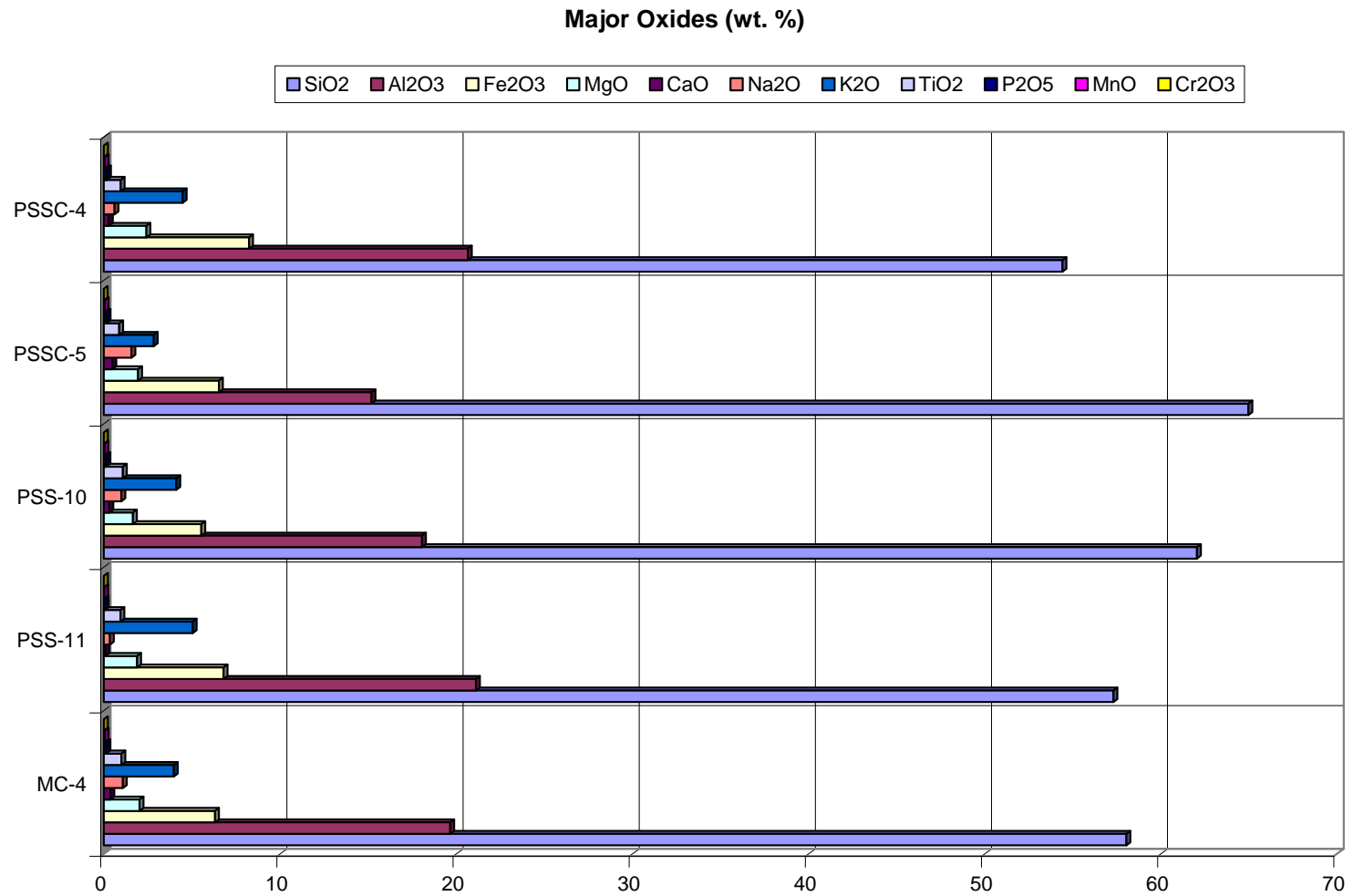


Figure 35. Weight percentages of major oxides present in the Pottsville samples.

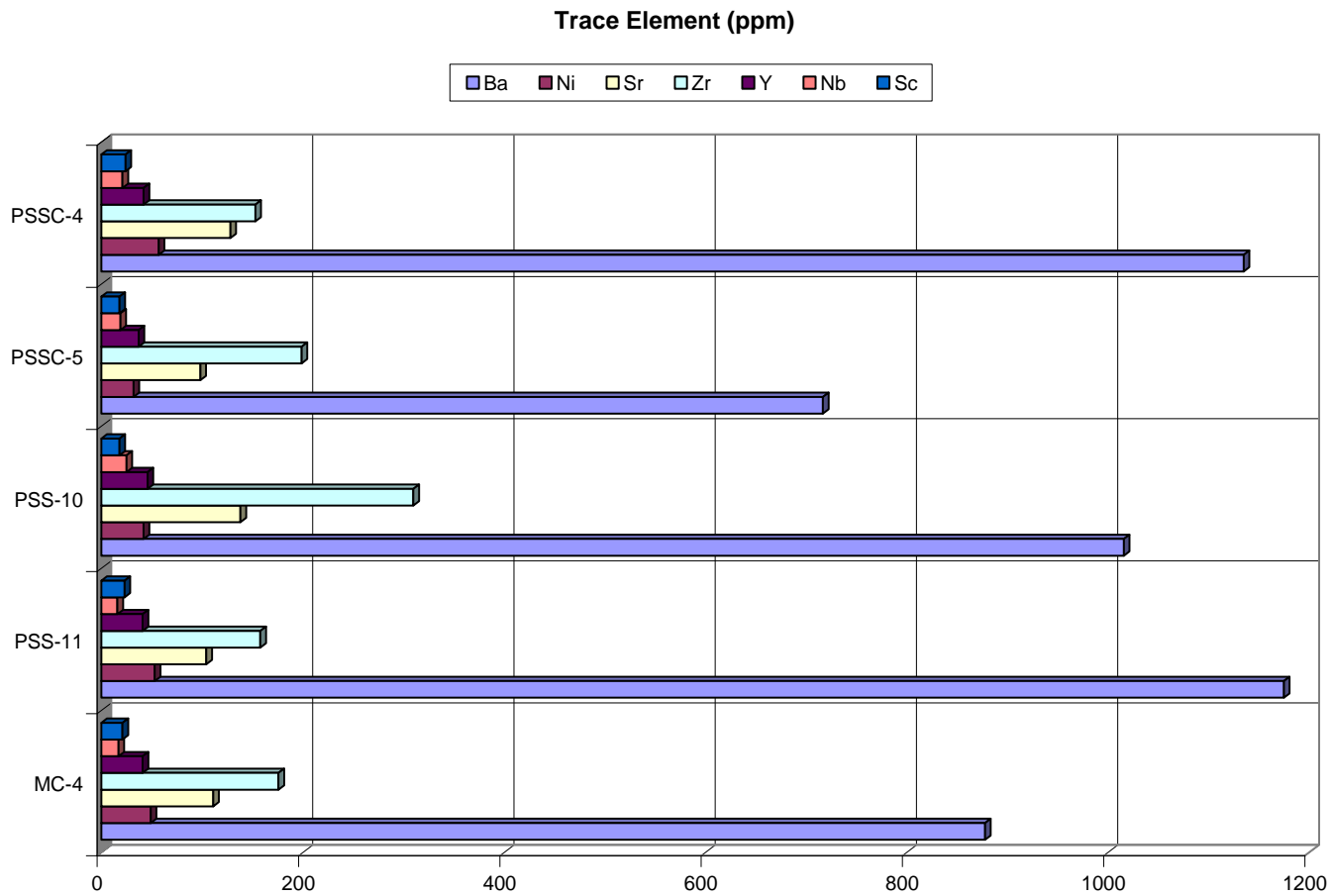


Figure 36. Trace elements of Pottsville samples, given in parts per million.

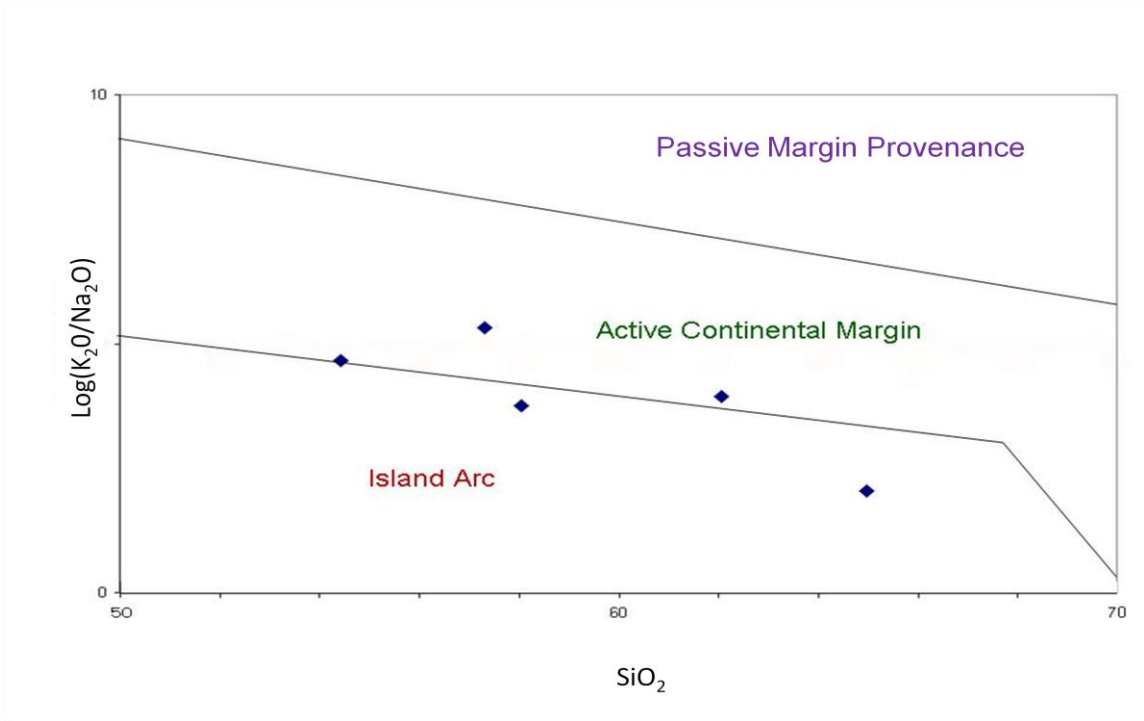


Figure 37. Plot of the log of K_2O/Na_2O versus SiO_2 for Pottsville mudrock samples (modified from Roser and Korsch, 1988). Samples fall in both active continental margin and island-arc provenances. The two samples that plot in the island arc provenance are PSSC-5 and MC-4.

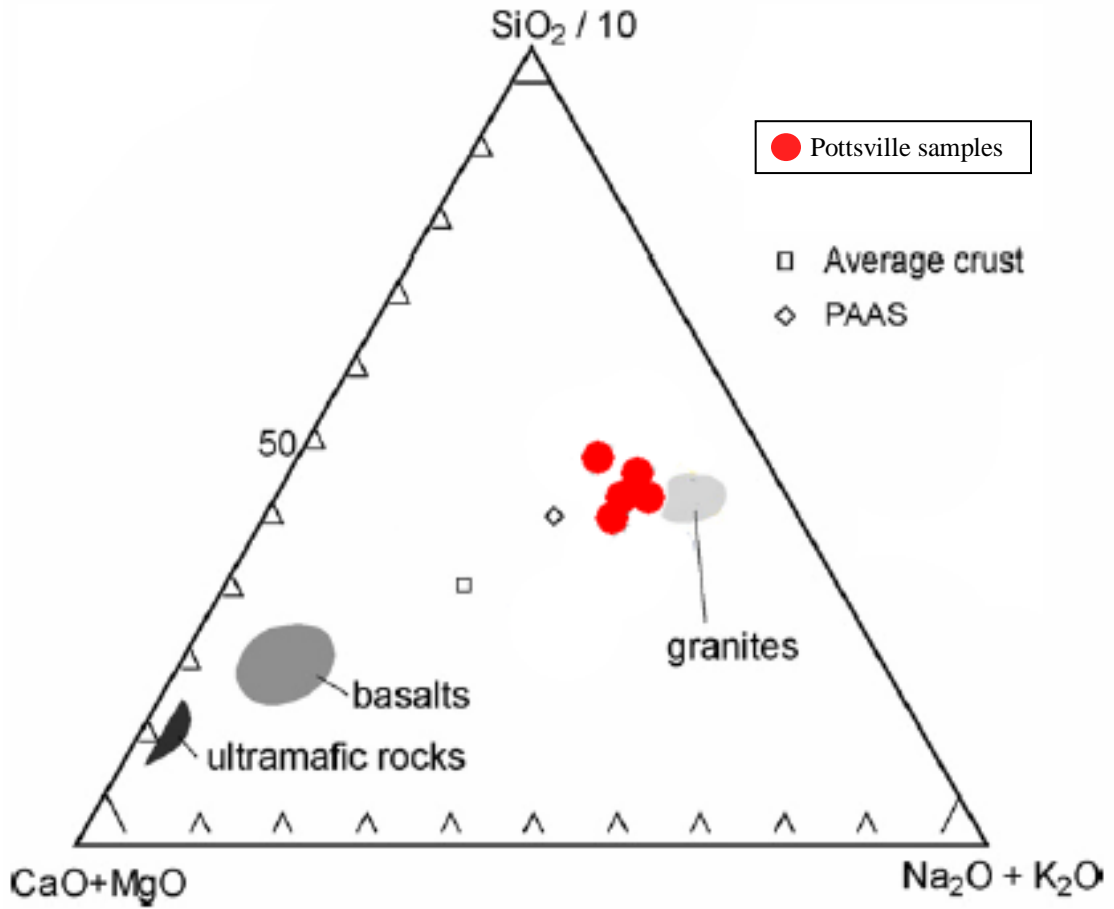


Figure 38. Possible source rock affinities of Pottsville mudrock samples illustrated in Si–Ca+Mg–Na+K ternary plot (after Taylor and McLennan, 1985). Post Archean average shale (PAAS) and average crustal composition are taken.

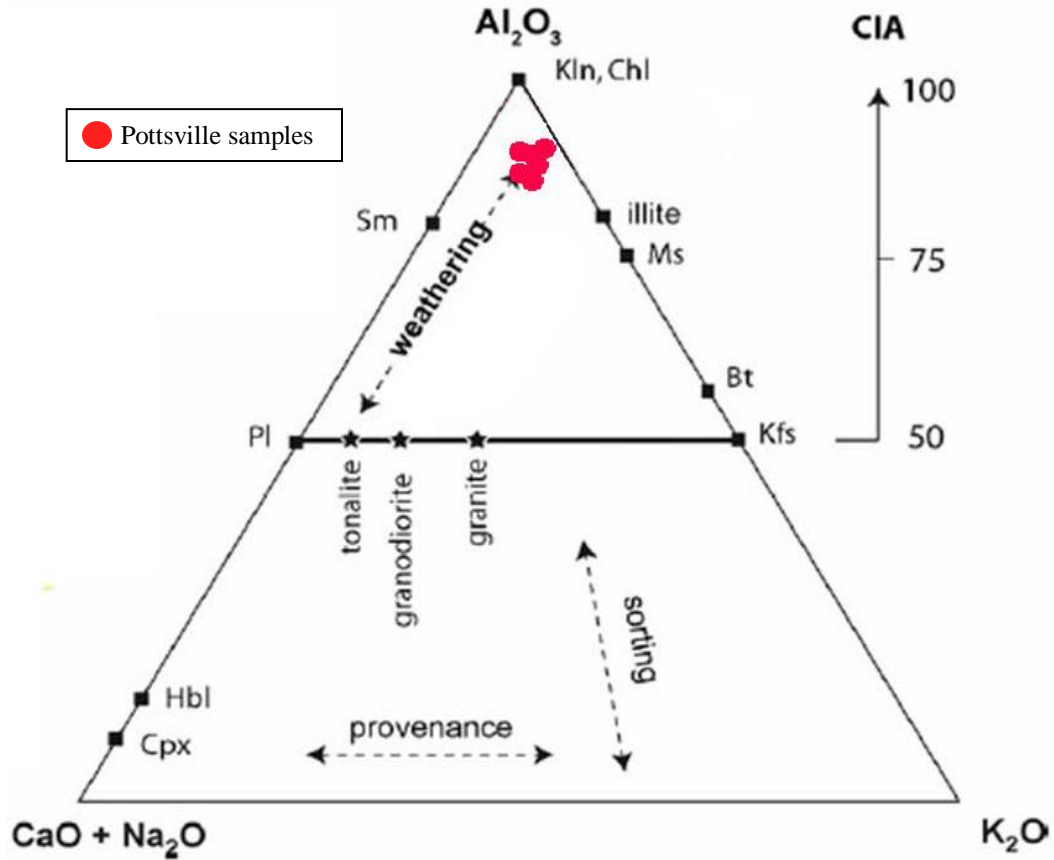


Figure 39. Compositional variations of mudrock samples of Cahaba Basin illustrated in A–CN–K (Al_2O_3 – $\text{CaO}+\text{Na}_2\text{O}$ – K_2O) compositional space triangle (after Nesbit and Young, 1984). CIA is the chemical index of alteration $[(\text{Al}_2\text{O}_3/(\text{Al}_2\text{O}_3+\text{K}_2\text{O}+\text{Na}_2\text{O}+\text{CaO}))\times 100]$. Pottsville samples plot close to the Al_2O_3 apex, indicating intense chemical weathering. Kln=kaolinite; Chl=chlorite; Ms=muscovite; Bt=biotite; Kfs=potassium-feldspar; Cpx=clinopyroxene; Hbl=hornblende; Pl=plagioclase; Sm=smectite.

CHAPTER 8: DISCUSSION

Deposition of the Pottsville occurred during the Alleghenian orogeny, when both the Appalachian and Ouachita Mountains were experiencing uplift. Some previous workers have suggested most of the Pottsville sediments in the Cahaba Basin were derived from the Ouachita Mountains (Mack et al., 1983). However, the current study supports alternative Appalachian source, at least for the Cahaba Basin.

It has been inferred that the Ouachita orogeny was caused by an arc-continent collision due to a relatively brief duration of thrusting and a general lack of precursor effects along the southern continental margin (Graham et al., 1976). Mack et al. (1983) found andesitic \pm basaltic and dacitic volcanic rock fragments in the upper and lower Pottsville sandstone (up to 50%). A general paucity of detrital feldspars and volcanic lithic fragments in the Pottsville sandstone indicates that these were not derived predominantly from an arc orogen.

Data from modal analysis suggest that the Pottsville sandstones of the Black Warrior Basin are less quartzose (more lithics) than the sandstones of the Ouachitas (Fig. 8a; Graham et al., 1976). Composite modal analysis data from this study agree with that of Graham et al. (1976).

Highly weathered, recycled orogenic, quartzose sandstones make up the basal Pottsville Formation of the Cahaba Basin, reflecting intense chemical weathering in an

equatorial region. Various sources were responsible for deposition into the basin, which can be seen by the fluctuations in sandstone composition throughout the section (Figure 40). During the transition from the quartzarenite measure to the mudstone measure quartz and sedimentary lithic fragments were predominant, suggesting sedimentary and metasedimentary provenances from a collision orogen.

Rutile is indicative of a medium- to high-grade metamorphic source rock, and not stable at greenschist facies conditions (Zack et al, 2004). The dominance of rutile suggests there was a prevailing medium- to high-grade metamorphic source supplying sediment to the Cahaba Basin. Rocks of the Ouachitas were metamorphosed from zeolite to lower greenschist facies (Goldstein and Reno, 1952; Flawn et al., 1961). Therefore, the Ouachitas could not be the source of the rutile present in the Cahaba Basin. The prevalence of almandine species garnets and their Fe/(Fe+Mg) ratios further emphasizes a predominance of a medium-grade metamorphic source.

Basalt-rich material was not a significant source to the basin, based on both the lack of chromium and titanium oxides in the sediment. Majority of the source was felsic crustal material. The Cenozoic Assam and Bengal basins of the Himalayan system are active foreland basins that have been extensively studied for provenance data (Uddin and Lundberg, 1998; Uddin et al., 2005). Whole-rock mudstone chemical data from the Pottsville Formation were compared with existing data from these two basins from the eastern Himalayas (the proximal Assam basin; and the distal Bengal basin) (Uddin et al., 2005). Pottsville mudrocks more closely resemble those from the Bengal basin, which is distal to the Himalayan orogen front, in the Ni-Fe₂O₃+MgO plot (Figure 41).

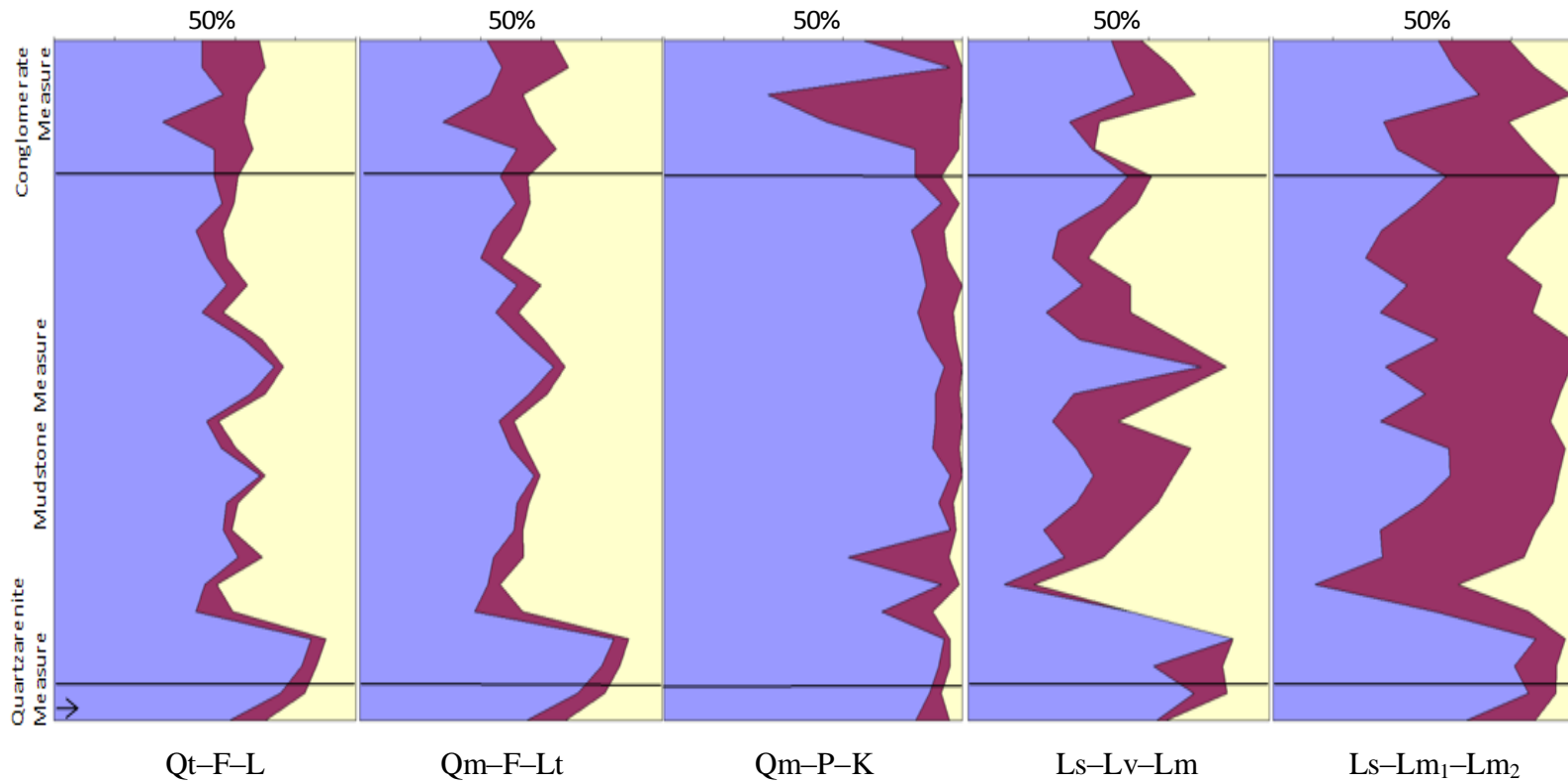


Figure 40. Composite profile of petrographic data of the Pottsville Formation. In Qt-F-L: Qt=blue, F=dark red, L=yellow. In Qm-F-Lt, Q: Blue, F: Dark red, Lt: yellow. In Qm-P-K, Qm: Blue, P: Dark red, K: yellow. In Ls-Lv-Lm, Ls: Blue, Lv: Dark red, Lm: yellow. In Ls-Lm₁-Lm₂, Ls: Blue, Lm₁: Dark red, Lm₂: yellow.

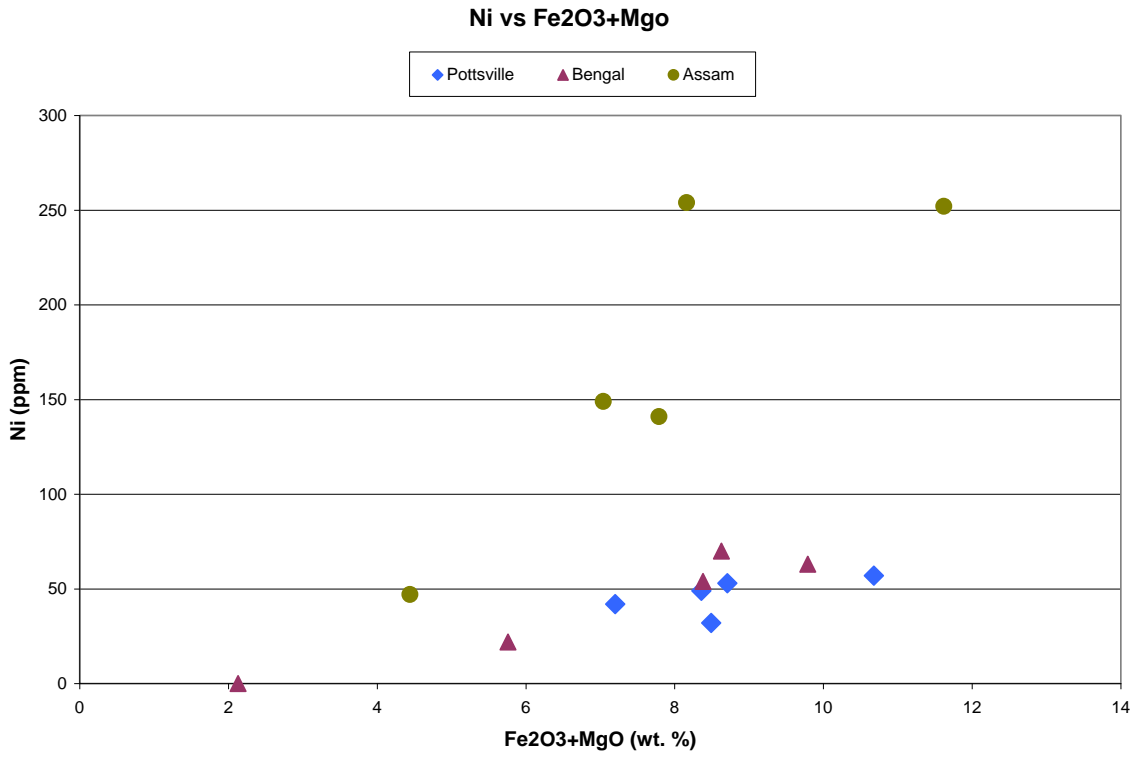


Figure 41. Nickel versus ferric oxide + magnesium oxide. Pottsville samples are plotted along with samples from two basins in the Himalayan orogen; the Assam basin, proximal to the orogen, and the Bengal basin, more distal the orogen. Pottsville samples are more closely related to the Bengal basin with respect to Ni content.

While nickel is indicative of igneous, oceanic, or suture sources, only the Assam Basin had those types of input, because of its proximity to Himalayan suture belts. Thus, the Pottsville Formation most likely deposited farther from the orogenic front. A second plot ($\text{TiO}_2 - \text{Fe}_2\text{O}_3 + \text{MgO}$) comparing the three basins suggests there is little difference in the concentrations of titanium oxides (Figure 42). Titanium oxide (TiO_2) is indicative of presence of rutile, which is commonly sourced from medium- to high-grade metamorphic terranes. All three basins are relatively high in titanium suggesting significant metamorphic sources.

Muscovite crystals extracted for $^{40}\text{Ar}/^{39}\text{Ar}$ analysis reveal temporal variations in source material. The source rocks most likely responsible for filling the Cahaba Basin during the early Pennsylvanian were the Talladega Slate Belt, the Blue Ridge, and possibly the Tugaloo and Cat Square terranes of the Inner Piedmont. Sample D2S1 contains Middle Ordovician to Early Silurian muscovites (ca. 460–430 Ma), which correlates with a Taconian age source, perhaps related to the the Hillabee Greenstone of Alabama. Source rocks of these ages have not been reported from the Ouachitas (Gleason et al., 1994). Mississippian muscovites in sample D2S2 (330–320 Ma) provide a predominant Alleghenian age suggesting derivation from the Talladega Slate belt or the Western Blue Ridge. Source rocks of this age may be available in the Ouachitas, but based on other data in this research, they are unlikely. The youngest sample analyzed (CHB-5; 390-360 Ma) strongly indicates a source terrane of Acadian age. Acadian terranes are not well represented in the southern Appalachians because impact of the Acadian orogeny was weaker in this area (Naylor, 1971; Osberg et al., 1989). However, the Tugaloo and Cat Square terranes of the Inner Piedmont may serve as sources for this

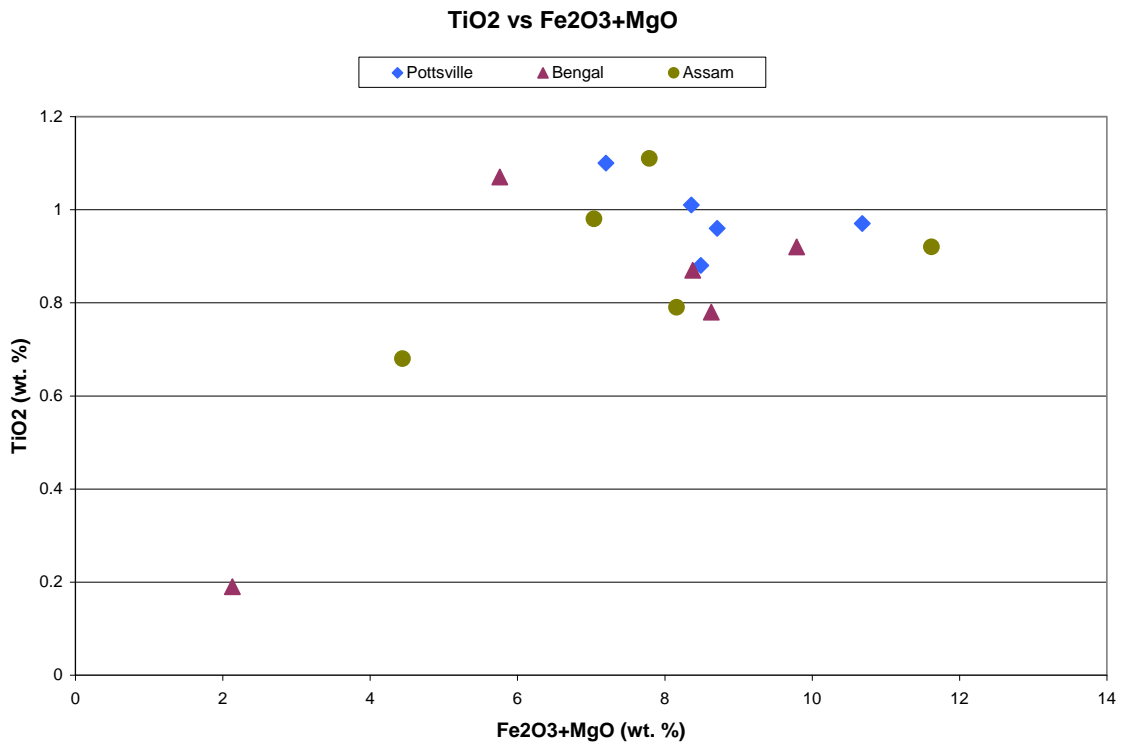


Figure 42. Plot of titanium oxide versus ferric oxide + magnesium oxide. Pottsville samples are plotted along with samples from two separate basins in the Himalayan orogen; the Assam basin, proximal to the orogen, and the Bengal basin, distal to the orogen. Himalayan and Appalachian samples plot relatively close.

sample. Source rocks of this age are not known in the Ouachitas.

Based on compositional and geochronologic data acquired, a paleogeographic map has been constructed, suggesting probable provenance terranes and transport direction for the deposition of the Pottsville sediments. Detritus was delivered to the basin from the east-northeast direction (Figure 43), and was not inhibited by the bounding structural features of the basin (Figure 1).

The Helena Thrust Fault presently separates Cahaba and Coosa basins to the east-southeast. The Helena fault today is a large-displacement thrust fault that cuts across the preserved Paleozoic section. Pottsville sediment extends more than a mile southeastward below the Helena Thrust fault along much of the Cahaba Basin (Pashin and Carroll, 1999). Thus, major movement of the fault post-dates the Pottsville deposition (Pashin et al., 1995; Pashin, 1998).

The Black Warrior, Cahaba, and Coosa basins were originally part of a single foreland basin, which was referred to as the "Greater Black Warrior Basin" (Thomas, 1997). Thus, there was an easy dispersal of sediments across the basin. This has been disputed by Pashin et al. (1995) and Pashin (1998), suggesting incipient growth of Appalachian structures during the Pottsville sedimentation. Part of this growth was the uplift of the Birmingham Anticlinorium which isolated the Cahaba Basin from the Black Warrior Basin.

Mack et al. (1983) worked mostly in the Black Warrior Basin on the Pennsylvanian Pottsville and the Mississippian Parkwood formations. That study revealed predominant sediment source from the southwest. This study is focused only in

the Cahaba Basin on the Pennsylvanian Pottsville Formation. Results from this research suggest source terranes in the Appalachians to the east and northeast.

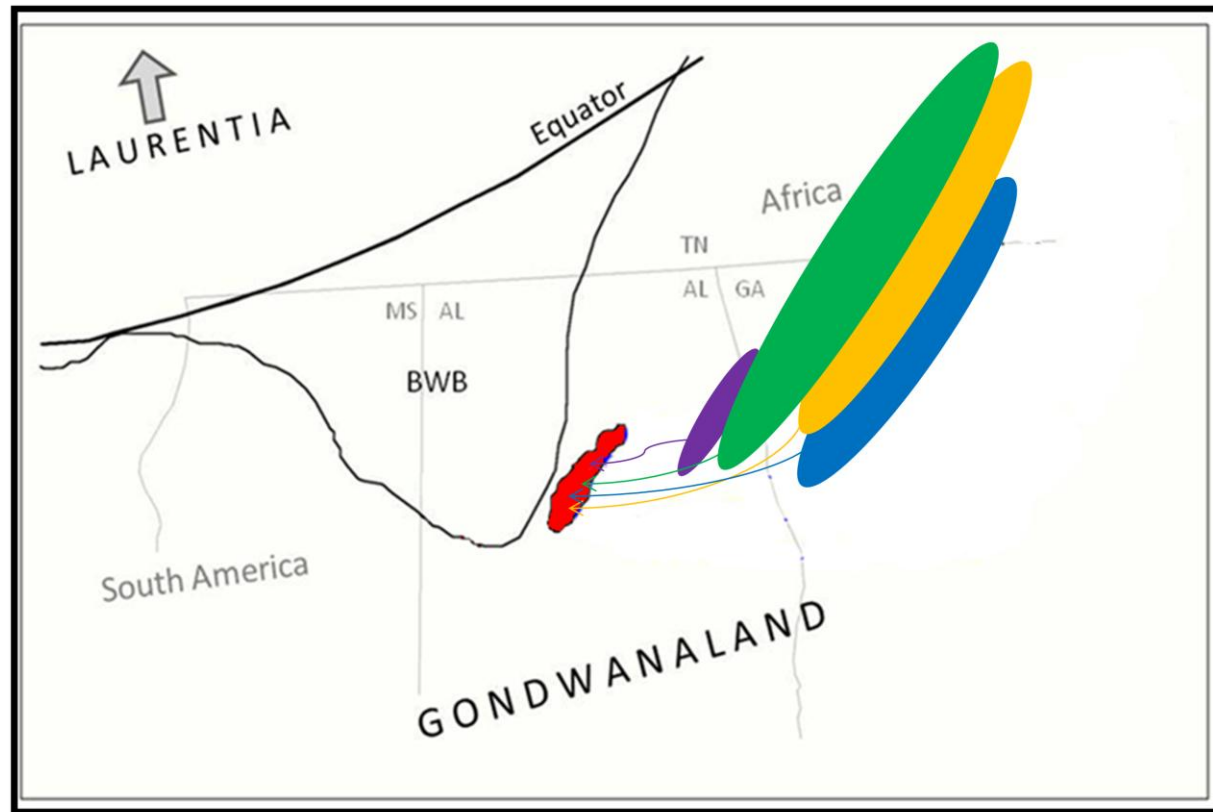


Figure 43. Lower Pennsylvanian paleogeographic map of the Cahaba Basin region of Alabama and regional surroundings. Note the proximity of the region to the equator. Purple represents the Hillabee Greenstone of Alabama (Mersch and Hatcher, 2007). Green represents the Talladega Slate belt and Western Blue Ridge of the Appalachians (McDonald, 2008). Yellow represents the Tugaloo terrane and blue represents the Cat Square terrane of the Appalachians (McClellan et al., 2007). Uplifted terranes were located further to the east of Cahaba than they are today and are the primary sources of sediment (BWB: Black Warrior Basin).

CONCLUSIONS

Based on sandstone modal analysis, heavy-mineral assemblages, garnet chemistry, argon isotopic analysis, and mudrock geochemistry, the following conclusions can be drawn:

- Sandstones from the Pottsville Formation, Cahaba Basin, are mostly lithic arenites, with few feldspars, derived from a recycled orogenic provenance.
- Heavy mineral assemblages in the Pottsville Formation are dominated by stable minerals (ZTR) and opaques. Predominance of rutiles and garnets suggests mostly medium-grade metamorphic terranes as the source rocks.
- Garnet chemistry reveals a prevalence of almandine species, indicating the importance of medium-grade metamorphic sources.
- Muscovite cooling dates indicate three distinct age peaks at 470-430 Ma, 345-315 Ma, and 390-360 Ma, these ages are compatible with source rocks in the Inner Piedmont and Western Blue Ridge of the Appalachian Mountain belts.
- This study adds to previous studies (Schlee, 1963; Graham et al., 1976; Demirpolat, 1989; Liu and Gastlido, 1992; Pashin et al., 1995; Pashin and Carroll, 1999, Pashin, 2004) in the Pottsville Formation that sediment source was from the uplifted Appalachians located to the east and northeast.
- Future work on the provenance of the Pottsville Formation, of the Cahaba Basin should include more detailed microprobe analyses and more detailed isotopic analysis, such as more samples throughout the entirety of the formation.

REFERENCES

- Allegre C. J., and Rousseau D., 1984, The growth of the continents through time studied by Nd isotopic analysis of shales: *Earth and Planetary Science Letters*, v. 67, p. 19-34.
- Arbenz, J.K., 1989, The Ouachita system. *in*: Bally, A.W., Palmer, A.R. (eds.), *The Geology of North America, Volume A—An Overview*. Geological Society of America, Boulder, CO, p. 371–396.
- Bally, A. W., and Palmer, A. R., editors, 1989, *The Geology of North America: An Overview*: Geological Society of America, Boulder, CO., 619 p.
- Basu, A., 1976, Petrology of Holocene alluvial sand derived from plutonic source rocks; Implication to paleoclimate interpretation: *Journal of Sedimentary Petrology*, v. 4, p. 694-709.
- Becker, T., Thomas, W., Samson, S., and Gehrels, G., 2005, Detrital zircon evidence of Laurentian crustal dominance in the lower Pennsylvanian deposits of the Alleghenian clastic wedge in eastern North America: *Sedimentary Geology*: v. 182, p. 59-86.
- Bhatia M. R., 1985, Rare earth element geochemistry of Australian Paleozoic graywackes and mudrocks: provenance and tectonic control. *Sedimentary Geology*, v. 45, p. 97-113.
- Bhatia M. R. and Taylor S. R., 1981, Trace element geochemistry and sedimentary provinces: A study from the Tasman Geosyncline, Australia: *Chemical Geology* v. 33, p. 115- 125.
- Bradley, D.C., 1989, Taconic plate kinematics as revealed by foredeep stratigraphy, Appalachian orogen: *Tectonics*, v. 8, p. 1037-1049.
- Coleman, J.L., Jr., 2000, Carboniferous submarine basin development of the Ouachita Mountains of Arkansas and Oklahoma, *in* Bouma, A.H., and Stone, C.G., editors, *Fine-Grained Turbidite Systems: American Association of Petroleum Geologists (AAPG) Memoir 72 and Society of Sedimentary Geology (SEPM) Special Publication 68*, p. 21–32.

- Cox, R., Lowe, D., and Culler, R., 1995, The influence of sediment recycling and basement composition on evolution of mudrock chemistry in the southwestern United States: *Geochimica et Cosmochimica Acta*, v. 59, p. 2919-2940.
- Demirpolat, S., 1989, Environment of deposition of selected sandstones and conglomerates in southern part of Cahaba Basin, Alabama [Ph.D. Thesis]: Tallahassee, Florida, Florida State University, 121 p.
- Dickinson, W.R., 1970. Interpreting detrital modes of greywacke and arkose. *Journal of Sedimentary Petrology*, v. 40, p. 695–707.
- Dickinson, W.R., and Suczek, C., 1979, Plate tectonics and sandstone compositions: *American Association of Petroleum Geologists Bulletin*, v. 63, p. 2164-2182.
- Dickinson, W.R., 1985, Interpreting provenance relations from detrital modes of sandstones: *in* G.G. Zuffa (ed.), *Provenance of Arenites*, D. Reidel Publishing, Boston, p. 333-361.
- Dorsey, R.J., 1988, Provenance evolution and unroofing history of a modern arc-continent collision; Evidence from petrography of Plio-Pleistocene sandstones, eastern Taiwan, *Journal of Sedimentary Petrology*, v. 58, p. 208–218.
- Drake, A., Sinha, A., Laird, J., and Guy, R., 1989, The Taconic orogen: The Geology of North America, v. F-2, *The Appalachian-Ouachita Orogen in the United States*, Geological Society of America, p. 101-178.
- Engel, A.E., 1952, Quartz crystal deposits of western Arkansas: *United States Geological Survey Bulletin* 973-E, p. 173-260.
- Ethington, R.L., Finny, S.C., and Repetski, J.E., 1989, Biostratigraphy of the Paleozoic rocks of the Ouachita orogen, Arkansas, Oklahoma, west Texas, *in* Hatcher, R.D., Jr., Thomas, W.A., and Viele, G.W., editors, *The Appalachian-Ouachita orogen in the United States: Boulder, Colorado*, Geological Society of America, *Geology of North America*, v. F-2, p. 563-574.
- Flawn, P.T., Goldstein, A., Jr., King, P.B., and Weaver, C.E., 1961, *The Ouachita System*: Austin, University of Texas Bureau of Economic Geology Publication 6120, 401 p.
- Fleet, W.F., 1926, Petrological notes on the Old Red Sandstones of the West Midlands: *Geological Magazine*, v. 65, p. 505-516.
- Garrels, R. M. and Mackenzie, F. T., 1971, *Evolution of Sedimentary Rocks*, W.W. Norton Inc. 397 p.
- Gleason, J.D., Patchett, P.J., Dickinson, W.R., and Ruiz, J., 1995, Nd isotopic constraints

- on sediment sources of the Ouachita-Marathon fold belt, *Geological Society of America Bulletin*, v. 107, no. 10, p. 1192-1210.
- Goldstein, A., and Reno, D.H., 1952, Petrography and metamorphism of sediments of Ouachita facies: *American Association of Petroleum Geologists Bulletin*, v. 36, p. 2275–2290.
- Graham, S.A., Ingersoll, R.V., and Dickinson, W.R., 1976, Common provenance for lithic grains in Carboniferous sandstones from Ouachita Mountains and Black Warrior Basin: *Journal of Sedimentary Petrology*, v. 46, p. 620-632.
- Hames, W.E., and Bowring, S.A., 1994, An empirical evaluation of the argon diffusion geometry in muscovite: *Earth and Planetary Science Letters*, v. 124, p. 161-167.
- Hatcher, R.D., Thomas, W.A., Geiser, P.A., Snoke, A.W., Mosher, S., Wiltschko, D.V., 1989, Alleghenian orogen: The Geology of North America, v. F-2, The Appalachian-Ouachita Orogen in the United States: *The Geological Society of America*, p. 233-318.
- Hatcher, R.D., Jr., 2002, Alleghenian (Appalachian) orogeny, a product of zipper tectonics: Rotational transpressive continent-continent collision and closing of ancient oceans along irregular margins, *in* Martinez Catalan, J.R., Hatcher, R.D., Jr., Arenas, R., and Diaz Garcia, F., eds., *Variscan-Appalachian dynamics: The building of the late Paleozoic basement: Geological Society of America Special Paper 364*, p. 199-208.
- Hess, H.H., 1966, Notes on operation of Frantz isodynamic magnetic separator, Princeton University: User manual guide, p. 1-6.
- Hodges, K.V., Ruhl, K.W., Wobus, C.W., and Pringle, M.S., 2005, $^{40}\text{Ar}/^{39}\text{Ar}$ thermochronology of detrital minerals: *Reviews in Mineralogy and Geochemistry*, v. 58, p. 239-257.
- Horton, J.W., Jr., Drake, A.A., and Rankin, D.W., 1989, Tectonostratigraphic terranes and their boundaries in the central and southern Appalachians: *Geological Society of America Special Paper 230*, p. 213-245.
- Ingersoll, R.V., and Suczek, C.A., 1979, Petrology and provenance of Neogene sand from Nicobar and Bengal Fans, DSDP sites 211 and 218: *Journal of Sediment. Petrology*, v. 54, p. 1217-1228.
- Ingersoll, R.V., Bullard, T. F., Ford, R. L., Grimm, J. P., Pickle, J. D., and Sares, S.W., 1984, The effect of grain size on detrital modes: A test of the Gazzi-Dickinson point counting method: *Journal of Sedimentary Petrology*, v. 54, p. 103–116.

- Li, R., Lib, S., Jin, F., Wan, Y., Zhang, S., 2004, Provenance of Carboniferous sedimentary rocks in the northern margin of Dabie Mountains, central China and the tectonic significance: constraints from trace elements, mineral chemistry and SHRIMP dating of zircons: *Sedimentary Geology*, v. 166, p. 245–264.
- Liu, Y., and Gastaldo, R.A., 1992, Characteristics and provenance of log-transported gravels in a Carboniferous channel deposit: *Journal of Sedimentary Petrology*, v. 62, p. 1072-1083.
- Ludwig, K.R., 2003, User's manual for ISOPLOT, version 3, A geochronological toolkit for Microsoft Excel: Berkeley Geochronological Center, Special Publication, n. 4, 70 p.
- Mack, G.H., Thomas, W.A., and Horsey, C.A., 1983, Composition of Carboniferous sandstone and tectonic framework of southern Appalachian-Ouachita Orogen: *Journal of Sedimentary Petrology*, v. 53, p. 931-946.
- Mange, M.A., and Maurer, H.F.W., 1992, *Heavy Minerals in Color*: Chapman & Hall, London, 147 p.
- McBride, E.F., 1985, Diagenetic processes that affect provenance determinations in sandstone: NATO ASI Series. Series C: Mathematical and Physical Sciences, v. 148, p. 95-113.
- McClellan, E.A., and Miller, C.F., 2000, Ordovician age confirmed for the Hillabee Greenstone, Talladega belt, southernmost Appalachians: *Geological Society of America Abstract with Program*, v. 32, p. 117.
- McClellan, E.A., Steltenpohl, M.G., Thomas, C., and Miller, C.F., 2007, Isotopic age constraints and metamorphic history of the Talladega belt: New evidence for timing of arc metamorphism and terrane emplacement along the southern Laurentian margin: *Journal of Geology*, v. 115, p. 541-561.
- McDonald, W., 2008, $^{40}\text{Ar}/^{39}\text{Ar}$ ages of muscovite from the Western Blue Ridge and Talladega Belt, Georgia and North Carolina, [MS Thesis], Auburn University, Auburn, Alabama, 114 p.
- McDougall, I., and Harrison, M.T., 1999, Geochronology and thermochronology by the $^{40}\text{Ar}/^{39}\text{Ar}$ method: New York, Oxford University Press, 269 p.
- Merschat, A.J., and Hatcher, R.D, Jr., 2007, The Cat Square terrane: Possible Siluro-Devonian remnant ocean basin in the Inner Piedmont, southern Appalachians, USA, in Hatcher, R.D., Jr., Carlson, M.P., McBride, J.H., and Martinez Catalan, J.R., editors, *4-D Framework of Continental Crust*: Geological Society of America Memoir p. 553–566.

- Meyer, E., Aronson, J., and Haynes, J., 2005, K/Ar dating of Blue Ridge thrusting and its influence on sediment input to two Pennsylvanian-age depocenters in the Appalachian Basin: poster presentation, 40th Annual Meeting Northeastern Section GSA, paper v. 26, p. 8.
- Morris, R.C., 1989, Stratigraphy and sedimentary history of post-Arkansas Novaculite Carboniferous rocks of the Ouachita Mountains, *in* Hatcher, R.D., Jr., Thomas, W.A., and Viele, G.W., editors., The Appalachian-Ouachita orogen in the United States: Boulder, Colorado, Geological Society of America, Geology of North America, v. F-2, p. 591-602.
- Morton, A.C., 1985, Heavy minerals in provenance studies: *in* G.G. Zuffa (editor), Provenance of Arenites, D. Reidel Publishing, Boston, p. 249-277.
- Morton, A.C., 1986, Influences of provenance and diagenesis on detrital garnet suites in the Paleocene Forties sandstones, central North Sea: *Journal of Sedimentary Petrology*, v. 57, p. 1027-1032.
- Morton, A.C., and Taylor, P.N., 1991. Geochemical and isotopic constraints on the nature and age of basement rocks from Rockall Bank, NE Atlantic: *Journal of Geological Society of London*, v. 148, p. 631–634.
- Morton, A.C., Davies, J.R., and Waters, R.A., 1992, Heavy minerals as a guide to turbidity provenance in the lower Paleozoic southern Welsh Basin; a pilot study, *Geological Magazine*, v. 129, p. 573-580.
- Morton, A.C., and Hallsworth, C.R., 1999, Processes controlling the composition of heavy mineral assemblages in sandstones: *Sedimentary Geology*, v. 124, p. 3-30.
- Nanayama, F., 1997, An electron microprobe study of the Amazon Fan: *Proceedings the Ocean Drilling Program, Scientific Results*, v. 155, p. 147-168.
- Naylor, R.S., 1971, Acadian Orogeny: an abrupt and brief event: *Science*, v. 172, p. 558-560.
- Nesbit, H.W., and Young, G.M., 1984, Predictions of some weathering trends of plutonic and volcanic rocks based on thermodynamics and kinetic considerations: *Geochimica et Cosmochimica Acta*, v. 48, p. 1523–1534.
- Osberg, P.H., Tull, J.F., Robinson, P., Hon, R., Butler, J.R., 1989, The Acadian orogen, *in* Hatcher, R.D., Jr., Thomas, W.A., Viele, G.W., (editors), The Appalachian–Ouachita orogen in the United States, The geology of North America, v. F-2. Geological Society of America, Boulder, p. 179–232.

- Pashin, J., Carroll, R.E., Barnett, R.L., and Beg, M.A., 1995, Geology and coal resources of the Cahaba coal field: Bulletin Geological Survey of Alabama, v. 163, p. 1-49.
- Pashin, J., and Carroll, R.E., 1999, Geology of the Cahaba Coalfield: Guidebook for the 36th Annual Field Trip of the Alabama Geological Society, 98 p.
- Pashin, J., 2004, Cyclothems of the Black Warrior Basin, Alabama, USA.: Eustatic snapshots of foreland basin tectonism, in Pashin, J. C. and Gastaldo, R. A., editors, Sequence stratigraphy, paleoclimate, and tectonics of coal-bearing strata: American Association of Petroleum Geologists Studies in Geology 51, p. 199–218.
- Pashin, J., 2006, Stratigraphy and depositional environments of the Pottsville Formation at the Union Chapel track site: Abstracts with Programs - Geological Society of America, v. 38, no.3, p. 71.
- Pettijohn, F.J., Potter, P.E., and Siever, R., 1987, Sand and Sandstone: New York, Springer-Verlag, 553 p.
- Rast, N., 1984, The Alleghenian orogeny in eastern North America: Geological Society, London: Special Publications, v. 14, p. 197-217.
- Renne, P.R., Swisher, C.C., Deino, A.L. Karner, D.B., Owens, T.L., DePaolo, D.J., 1998, Intercalibration of standards, absolute ages and uncertainties in ⁴⁰Ar/³⁹Ar dating: Chemical Geology, v. 145, p.117-152.
- Richards, I.J., Connelly, J.B., Gregory, R.T., and Gray, D.R., 2002, The importance of diffusion, affection, and host-rock lithology on vein formation: A stable isotope study from the Paleozoic Ouachita orogenic belt, Arkansas and Oklahoma: Geological Society of America Bulletin, v. 114, p. 1343-1355.
- Rieu, R., Allen, P.A., Plotze, M., and Pettka, T., 2007, Compositional and mineralogical variations in a Neoproterozoic glacially influenced succession, Mirbat area, south Oman: Implications for paleo-weathering conditions: Precambrian Research, v. 154, p. 248–265.
- Ronov A.B., and Migdisov A. A., 1971, Evolution of the chemical composition of the rocks in the shields and sediment cover of the Russian and North American platforms: Sedimentology, v. 16, p. 137-185.
- Roser, B.P., and Korsch, R.J., 1988, Provenance signatures of sandstone –mudstone suites determined using discriminate function analysis of major-element data: Chemical Geology, v. 67, p. 119-139.
- Rowley, D. B., and Kidd, W. S. F., 1981, Stratigraphic relationships and detrital

composition of the Middle Ordovician flysch of western New England: Implications for the tectonic evolution of the Taconic orogeny: *Journal of Geology*, v. 89, p. 199–218.

Schlee, J., 1963, Early Pennsylvanian currents in the southern Appalachian Mountains: *Geological Society of America Bulletin*, v. 74, p. 1439-1452.

Secor, D.T., Jr., Snoke, A.W. and Dallmeyer, R.D., 1986, Character of the Alleghenian orogeny in the southern Appalachians: Part III. Regional tectonic relations: *Geological Society of America Bulletin*, v. 97, p. 1345-1353.

Spear, F.S., and Cheney, J.T., 1989, A petrogenetic grid for pelitic schists in the system $\text{SiO}_2\text{-Al}_2\text{O}_3\text{-FeO-MgO-K}_2\text{O-H}_2\text{O}$: *Contributions to Mineralogy and Petrology*, v. 101, p.149-164.

Stevens, G.C. and Wright, T.O., 1981, Stratigraphy of the Martinsburg Formation, West of Harrisburg in the Great Valley of Pennsylvania: *American Journal of Science*, v. 281, p. 1009-1020.

Suttner, L.J., 1974, Sedimentary petrographic provinces: An evaluation: *in* Ross, C.A., (ed.), *Paleogeographic Provinces and Provinciality*: *Society of Economic Paleontologists and Mineralogists Special Publication*, v. 21, p. 75-84.

Taylor, S.R., and McLennan, S.M., 1985, *The Continental Crust: It's Composition and Evolution*, Blackwell Scientific Publishing, Oxford, 312 p.

Thomas, W.A., 1977, Evolution of Appalachian-Ouachita salients and recesses from reentrants and promontories in the continental margin: *American Journal of Science*, v. 277, p. 1233-78.

Thomas, W.A., 1991, The Appalachian-Ouachita rifted margin of southeastern North America: *Geological Society of America Bulletin*, v. 103, p. 415-431.

Thomas, W.A., Becker, T.P., Samson, S.D., Hamilton, M.A., 2004, Detrital zircon evidence of a recycled orogenic foreland provenance for Alleghenian clastic-wedge sandstones: *Journal of Geology*, v. 112, p. 23-37.

Thomas, W.A., 2006, Tectonic inheritance at continental margin: *GSA Today*, v. 16, p. 4-11.

Tucker, M., 1998, *Techniques in Sedimentology*: Blackwell Scientific Publications, London, 395 p.

Uddin, A., and Lundberg, N., 1998, Cenozoic history of the Himalayan-Bengal system:

Sand composition in the Bengal basin, Bangladesh: Geological Society of America Bulletin, v.110, p. 497-511.

Uddin, A., Kish, S. Hames, W., Zahid, K.M., Kumar, P., and Akhter, S.H., 2005, Geochemical constraints on provenance of Tertiary sediments in Assam, India, and the Bengal basin: Abstracts with Programs - Geological Society of America, v. 37, p. 480.

Uddin, A., Kumar, P., Sarma, J.N., and Akhter, S.H., 2007, Heavy-mineral constraints on provenance of Cenozoic sediments from the foreland basins of Assam, India and Bangladesh: Erosional history of the eastern Himalayas and the Indo-Burman ranges, *in* Mange, M.A., and Wright, D.T., eds., Heavy minerals in use, Developments in Sedimentology, Elsevier, Amsterdam, v. 58, p. 823-847.

Zack, T., von Eynatten, H., and Kronz, A., 2004, Rutile geochemistry and its potential use in quantitative provenance studies: Sedimentary Geology, v. 171, p. 37–58.

Zahid, K.M., 2005, Provenance history of Paleogene and Paleogene-Neogene transitional sediments from Bengal Basin, Bangladesh: [M.S. Thesis]: Auburn, Alabama, Auburn University, 142 p.

Zhang, H.F., Menzies, M.A., and Matthey, D., 2003, Mixed mantle provenance: diverse garnet compositions in polymict peridotites, Kaapvaal craton, South Africa, Earth Planet Science Letters, v. 216, p. 329–346.

APPENDICES

Appendix-A:

Garnet data from Cahaba Basin (MC-Mayberry Creek No. 1 core; PSSC-SOMED core)

	Garnet Standard	MC-3-1	MC-3-2	MC-3-3	PSSC-10-1	PSSC-10-2	PSSC-10-3	PSSC-10-4	PSSC-10-5	PSSC-10-6
SiO2	40.88	36.46	36.68	36.89	36.48	36.93	61.83	25.29	36.81	36.58
TiO2	0.68	0.04	0	0.07	0.11	0.08	0.01	3.71	0.12	0.26
Al2O3	22.22	21.44	21.24	21.75	21.46	21.5	22.77	17.37	21.55	21.01
FeO	9.86	35.44	37.02	33.56	34.52	35.27	0.02	31.73	35.46	33.93
MnO	0.52	0.45	0.68	1.69	0.44	0.45	0	0.09	0.29	1.59
MgO	20.79	3.7	3.37	3.51	3.13	3.72	0	7.13	3.76	1.99
CaO	4.27	2.77	2.45	3.66	3.81	2.15	4.4	0.4	2.44	4.18
TOTAL	99.22	100.3	101.44	101.13	99.95	100.1	89.03	85.72	100.43	99.54
Si	5.97	2.93	2.93	2.93	2.94	2.96	4.4	2.44	2.94	2.97
Ti	0.09	0	0	0	0.01	0	0	0.27	0.01	0.02
Al	3.77	2.03	2	2.04	2.04	2.03	1.91	1.97	2.03	2.01
Fe	1.14	2.38	2.48	2.23	2.32	2.36	0	2.56	2.37	2.3
Mn	0.03	0.03	0.05	0.11	0.03	0.03	0	0.01	0.02	0.11
Mg	4.42	0.44	0.4	0.42	0.38	0.44	0	1.02	0.45	0.24
Ca	0.68	0.24	0.21	0.31	0.33	0.18	0.34	0.04	0.21	0.36
TOTAL	16.1	8.05	8.07	8.04	8.05	8	6.65	8.31	8.03	8.01
End members										
Alm	70.9	76.98	79.01	72.61	76	78.2	0.4	70.44	77.79	76.33
Sp	17.98	0.98	1.46	3.7	0.98	1	0	0.21	0.66	3.63
Pyr	10.6	14.33	12.82	13.54	12.28	14.7	0.05	28.21	14.7	7.99
Gr	0.52	7.71	6.71	10.15	10.74	6.1	99.55	1.14	6.85	12.05
TOTAL	100	100	100	100	100	100	100	100	100	100

Appendix-A continued:

Garnet data from Cahaba Basin (MC-Mayberry Creek No. 1 core; PSSC-SOMED core)

	Garnet Standard	PSSC-10- 6	PSSC-10- 7	PSSC-10- 8	MC-3-4	PSSC-6-1	PSSC-6-2	PSSC-6-3	PSSC-6-4	PSSC-6-5
SiO2	40.88	36.44	36.28	36.22	35.19	35.91	36.25	24.3	41.18	35.6
TiO2	0.68	0.19	0.14	0.08	0.1	0.2	0.1	0.05	0.62	0.09
Al2O3	22.22	21.45	21.03	20.69	21.04	21.19	21.02	21.59	21.8	20.68
FeO	9.86	32.25	28.63	25.25	32.6	29.57	34.36	33.84	9.6	31.78
MnO	0.52	0.44	5.55	9.4	1.61	4.34	0.91	0.28	0.32	9.01
MgO	20.79	2.02	0.76	1.32	1.38	1.36	1.09	8.22	20.77	0.71
CaO	4.27	7.27	7.85	6.27	6.97	6.92	6.47	0.04	4.22	3.38
TOTAL	99.22	100.06	100.24	99.23	98.89	99.49	100.2	88.32	98.51	101.25
Si	5.97	2.93	2.94	2.96	2.89	2.92	2.94	2.28	2.98	2.91
Ti	0.09	0.01	0.01	0.01	0.01	0.01	0.01	0	0.03	0.01
Al	3.77	2.03	2.01	1.99	2.04	2.03	2.01	2.39	1.86	1.99
Fe	1.14	2.17	1.94	1.72	2.24	2.01	2.33	2.66	0.58	2.17
Mn	0.03	0.03	0.38	0.65	0.11	0.3	0.06	0.02	0.02	0.62
Mg	4.42	0.24	0.09	0.16	0.17	0.17	0.13	1.15	2.24	0.09
Ca	0.68	0.63	0.68	0.55	0.61	0.6	0.56	0	0.33	0.3
TOTAL	16.1	8.04	8.05	8.04	8.07	8.04	8.04	8.5	8.04	8.09
End members										
Alm	70.9	70.71	62.7	55.92	71.45	65.34	75.49	69.3	18.34	68.33
Sp	17.98	0.97	12.31	21.08	3.58	9.71	2.03	0.58	0.62	19.62
Pyr	10.6	7.9	2.96	5.21	5.4	5.36	4.27	30	70.71	2.74
Gr	0.52	20.42	22.03	17.79	19.57	19.59	18.21	0.12	10.33	9.31
TOTAL	100	100	100	100	100	100	100	100	100	100

Appendix-A continued:

Garnet data from Cahaba Basin (MC-Mayberry Creek No. 1 core; PSSC-SOMED core)

	Garnet Standard	PSSC-10- 6	PSSC-10- 7	PSSC-10- 8	MC-3-4	PSSC-6-1	PSSC-6-2	PSSC-6-3	PSSC-6-4	PSSC-6-5
SiO2	40.88	36.44	36.28	36.22	35.19	35.91	36.25	24.3	41.18	35.6
TiO2	0.68	0.19	0.14	0.08	0.1	0.2	0.1	0.05	0.62	0.09
Al2O3	22.22	21.45	21.03	20.69	21.04	21.19	21.02	21.59	21.8	20.68
FeO	9.86	32.25	28.63	25.25	32.6	29.57	34.36	33.84	9.6	31.78
MnO	0.52	0.44	5.55	9.4	1.61	4.34	0.91	0.28	0.32	9.01
MgO	20.79	2.02	0.76	1.32	1.38	1.36	1.09	8.22	20.77	0.71
CaO	4.27	7.27	7.85	6.27	6.97	6.92	6.47	0.04	4.22	3.38
TOTAL	99.22	100.06	100.24	99.23	98.89	99.49	100.2	88.32	98.51	101.25
Si	5.97	2.93	2.94	2.96	2.89	2.92	2.94	2.28	2.98	2.91
Ti	0.09	0.01	0.01	0.01	0.01	0.01	0.01	0	0.03	0.01
Al	3.77	2.03	2.01	1.99	2.04	2.03	2.01	2.39	1.86	1.99
Fe	1.14	2.17	1.94	1.72	2.24	2.01	2.33	2.66	0.58	2.17
Mn	0.03	0.03	0.38	0.65	0.11	0.3	0.06	0.02	0.02	0.62
Mg	4.42	0.24	0.09	0.16	0.17	0.17	0.13	1.15	2.24	0.09
Ca	0.68	0.63	0.68	0.55	0.61	0.6	0.56	0	0.33	0.3
TOTAL	16.1	8.04	8.05	8.04	8.07	8.04	8.04	8.5	8.04	8.09
End members										
Alm	70.9	70.71	62.7	55.92	71.45	65.34	75.49	69.3	18.34	68.33
Sp	17.98	0.97	12.31	21.08	3.58	9.71	2.03	0.58	0.62	19.62
Pyr	10.6	7.9	2.96	5.21	5.4	5.36	4.27	30	70.71	2.74
Gr	0.52	20.42	22.03	17.79	19.57	19.59	18.21	0.12	10.33	9.31
TOTAL	100	100	100	100	100	100	100	100	100	100

Appendix-A continued:

Garnet data from Cahaba Basin (MC-Mayberry Creek No. 1 core; PSSC-SOMED core)

	Garnet Standard	PSSC-6- 15	PSSC-6- 16	PSSC-6- 17	PSSC-6- 18	PSSC-6- 19	MC-4-1	MC-4-2	MC-4-3
SiO2	40.88	36.6	36.27	36.62	36.22	36.03	36.51	36.34	35.8
TiO2	0.68	0.02	0.06	0.03	0.26	0.11	0.09	0.06	0.01
Al2O3	22.22	21.16	19.94	19.7	20.38	19.79	20.22	20.45	20.47
FeO	9.86	32.43	32.35	30.56	34.43	30.75	31.08	31.44	34.59
MnO	0.52	1.02	1.77	3.68	1.28	5.15	2.04	3.92	1.13
MgO	20.79	3.37	4.05	3.03	2.03	2.78	2.26	3.2	3.94
CaO	4.27	5.38	3.44	4.26	4.4	2.53	6.34	3.38	1.66
TOTAL	99.22	99.98	97.88	97.88	99	97.14	98.54	98.79	97.6
Si	5.97	2.93	2.98	3.01	2.97	3	2.98	2.97	2.96
Ti	0.09	0	0	0	0.02	0.01	0.01	0	0
Al	3.77	2	1.93	1.91	1.97	1.94	1.95	1.97	1.99
Fe	1.14	2.2	2.22	2.1	2.36	2.14	2.13	2.15	2.39
Mn	0.03	0.07	0.12	0.26	0.09	0.36	0.14	0.27	0.08
Mg	4.42	0.4	0.5	0.37	0.25	0.34	0.28	0.39	0.48
Ca	0.68	0.46	0.3	0.38	0.39	0.23	0.56	0.3	0.15
TOTAL	16.1	8.06	8.05	8.03	8.05	8.02	8.05	8.05	8.05
End members									
Alm	70.9	70.15	70.69	67.69	76.54	69.63	68.62	69.18	77.07
Sp	17.98	2.21	3.91	8.26	2.87	11.81	4.56	8.74	2.54
Pyr	10.6	12.87	15.77	11.96	8.06	11.22	8.89	12.55	15.65
Gr	0.52	14.77	9.63	12.09	12.53	7.34	17.93	9.53	4.74
TOTAL	100	100	100	100	100	100	100	100	100

Appendix–A: continued

Garnet data from Cahaba Basin (MC-Mayberry Creek No. 1 core; PSSC-SOMED core)

	Fe(Fe+Mg)		Fe(Fe+Mg)
MC-3-2	0.925017283	PSSC-6-1	0.982877
MC-3-3	0.93409308	PSSC-6-1	0.942405
PSSC-10-1	0.92500968	PSSC-6-1	0.917204
PSSC-10-2	0.93418259	PSSC-6-1	0.968215
PSSC-10-3	0.924425904	PSSC-6-1	0.931981
PSSC-10-4	0.696864111	PSSC-6-1	0.912546
PSSC-10-5	0.851643471	PSSC-6-1	0.927791
PSSC-10-6	0.924011503	PSSC-6-1	0.936256
PSSC-10-7	0.956410914	PSSC-6-1	0.94419
PSSC-10-8	0.953631795	PSSC-6-1	0.932298
PSSC-10-9	0.979872413	PSSC-6-1	0.950034
PSSC-10-10	0.961024315	PSSC-6-1	0.926034
PSSC-10-11	0.968155177	PSSC-6-1	0.911487
PSSC-10-12	0.965520703	PSSC-6-1	0.928579
MC-3-4	0.975960024	PSSC-6-1	0.956179
PSSC-6-1	0.841480644	PSSC-6-1	0.934459
PSSC-6-2	0.373059589	PSSC-6-1	0.946623

Appendix-B:

Whole rock data from Cahaba Basin (PSS-SOMED core; MC-Mayberry Creek No.1 core).

Major Elements (%)	PSS-10	PSS-11	PSSC-4	PSSC-5	MC-4
SiO ₂	62.07	57.33	54.43	64.99	58.06
Al ₂ O ₃	18.07	21.14	20.67	15.21	19.68
Fe ₂ O ₃	5.54	6.81	8.25	6.54	6.32
MgO	1.66	1.90	2.43	1.95	2.04
CaO	0.33	0.10	0.30	0.49	0.38
Na ₂ O	1.01	0.35	0.62	1.58	1.09
K ₂ O	4.13	5.05	4.48	2.85	3.98
TiO ₂	1.10	0.96	0.97	0.88	1.01
P ₂ O ₅	0.15	0.07	0.19	0.16	0.14
MnO	0.05	0.03	0.06	0.07	0.06
Cr ₂ O ₃	0.01	0.01	0.01	0.01	0.01
LOI	5.10	5.50	6.70	4.70	6.60
Sum	99.40	99.48	99.28	99.61	99.55
CIA value	76.76	79.35	79.29	75.56	78.31
Trace Elements (ppm)					
Ba	1016.00	1175.00	1135.00	717.00	878.00
Ni	42.00	53.00	57.00	32.00	49.00
Sr	138.20	104.30	128.20	98.40	111.20
Zr	310.00	158.00	153.00	199.00	176.00
Y	46.00	41.00	42.00	37.00	41.00
Nb	25.00	16.00	21.00	19.00	17.00
Sc	18.00	23.00	24.00	18.00	21.00

Appendix-C:

Raw data for monitor minerals used in $^{40}\text{Ar}/^{39}\text{Ar}$ geochronology.

Data Monitor Mineral Sanidine FC=2

		^{40}Ar (*+atm)	$^{39}\text{Ar}(\text{K})$	^{38}Ar (Cl+atm)	$^{37}\text{Ar}(\text{Ca})$	$^{36}\text{Ar}(\text{Atm})$	%Rad	R	J-value	%-sd	
au9.4i.san	76	1.1E-13 + 6E-17	9.558E-14 + 3.104E-17	2.14E-16 + 7.099E-19	4.777E-16 + 4.323E-18	1.48E-18 + 1.013E-19	0.9960232	1.1460	0.0136582 + 0.00001	0.0006996	
	77	5.73E-14 + 4E-17	4.945E-14 + 3.63E-17	1.235E-16 + 6.841E-19	2.911E-16 + 3.244E-18	1.199E-18 + 8.417E-20	0.9938144	1.1511	0.0135986 + 0.00001	0.0010932	
	78	9.6E-14 + 7E-17	8.049E-14 + 2.983E-17	2.314E-16 + 1.367E-18	4.193E-16 + 3.924E-18	1.154E-17 + 1.994E-19	0.9644647	1.1497	0.0136141 + 0.00001	0.0010909	
	79	7.6E-14 + 3E-17	6.532E-14 + 4.956E-17	1.662E-16 + 1.085E-18	3.339E-16 + 5.071E-18	1.531E-18 + 1.141E-19	0.9940452	1.1563	0.0135368 + 0.00001	0.0009854	
	80	6E-14 + 5E-17	5.163E-14 + 3.64E-17	1.246E-16 + 5.434E-19	2.768E-16 + 2.656E-18	3.9E-19 + 6.865E-20	0.9980796	1.1600	0.0134941 + 0.00002	0.0011402	
										0.013580 + 0.00003	0.21%
au9.3i.san	86	1.28E-13 + 2E-16	1.104E-13 + 1.834E-16	2.823E-16 + 1.168E-18	6.843E-16 + 9.862E-18	1.63E-18 + 1.283E-19	0.9962265	1.152	0.0135921 + 0.00003	0.002124	
	87	7.41E-14 + 6E-17	6.379E-14 + 7.328E-17	1.604E-16 + 8.886E-19	3.559E-16 + 3.556E-18	6.861E-19 + 9.98E-20	0.9972622	1.1577	0.013521 + 0.00002	0.0015103	
	88	9.39E-14 + 4E-17	8.067E-14 + 6.806E-17	2.069E-16 + 9.793E-19	4.548E-16 + 3.903E-18	2.651E-18 + 1.323E-19	0.9916602	1.1548	0.0135543 + 0.00001	0.0010579	
	89	1.2E-13 + 9E-17	1.021E-13 + 5.093E-17	2.7E-16 + 1.027E-18	6.209E-16 + 6.968E-18	4.877E-18 + 1.311E-19	0.9879887	1.1615	0.0134764 + 0.00001	0.0009784	
	90	1.32E-13 + 7E-17	1.132E-13 + 3.387E-17	2.855E-16 + 1.608E-18	6.439E-16 + 4.47E-18	4.245E-18 + 1.378E-19	0.9904709	1.1520	0.0135876 + 0.00001	0.0006882	
										0.0135463 + 0.00002	0.16%
au9.2i.san	91	3.5E-14 + 2E-17	2.802E-14 + 1.499E-17	6.453E-17 + 3.055E-19	1.728E-16 + 2.773E-18	8.502E-18 + 1.805E-19	0.9282442	1.16	0.0134964 + 0.00003	0.0018908	
	92	8.45E-14 + 5E-17	7.218E-14 + 3.073E-17	1.658E-16 + 6.893E-19	3.99E-16 + 4.185E-18	5.732E-18 + 1.823E-19	0.9799653	1.148	0.0136359 + 0.00001	0.0009939	
	93	7.59E-14 + 6E-17	6.391E-14 + 2.953E-17	1.54E-16 + 9.827E-19	4.966E-16 + 1.086E-17	7.122E-18 + 1.975E-19	0.972273	1.155	0.0135554 + 0.00002	0.0012694	
	94	8.02E-14 + 5E-17	6.857E-14 + 5.714E-17	1.589E-16 + 8.492E-19	3.936E-16 + 6.409E-18	3.391E-18 + 2.208E-19	0.9875099	1.156	0.0135462 + 0.00002	0.0013621	
	95	7.18E-14 + 5E-17	6.235E-14 + 5.175E-17	1.443E-16 + 5.88E-19	3.378E-16 + 2.608E-18	1.136E-18 + 1.343E-19	0.9953291	1.147	0.0136483 + 0.00002	0.0012537	
										0.0135764 + 0.00003	0.21%
au9.1j.san	96	5.24E-14 + 3E-17	4.439E-14 + 3.53E-17	1.064E-16 + 7.292E-19	3.344E-16 + 4.569E-18	1.724E-18 + 8.803E-20	0.9902725	1.168	0.0133956 + 0.00002	0.0011332	
	97	5.47E-14 + 3E-17	4.646E-14 + 2.281E-17	1.28E-16 + 8.064E-19	4.543E-16 + 2.803E-18	2.288E-18 + 9.702E-20	0.9876367	1.163	0.0134619 + 0.00001	0.0009684	
	98	6.6E-14 + 8E-17	5.45E-14 + 5.227E-17	1.827E-16 + 1.161E-18	6.82E-16 + 4.238E-18	7.567E-18 + 1.13E-19	0.9661296	1.17	0.0133736 + 0.00002	0.0016308	
	99	1.08E-13 + 1E-16	9.121E-14 + 6.799E-17	2.449E-16 + 6.84E-19	5.553E-16 + 6.239E-18	9.469E-18 + 1.523E-19	0.9741922	1.158	0.0135167 + 0.00002	0.0013424	
	100	1.12E-13 + 4E-17	9.293E-14 + 4.099E-17	2.378E-16 + 1.03E-18	5.753E-16 + 5.445E-18	9.903E-18 + 2.113E-19	0.9739067	1.175	0.0133177 + 0.00001	0.0008041	
										0.0134131 + 0.00003	0.26%
au9.3g.san	71	1.59E-13 + 4E-17	1.36E-13 + 4.109E-17	3.829E-16 + 8.675E-19	8.156E-16 + 5.129E-18	2.526E-18 + 1.045E-19	0.9953125	1.166	0.0134263 + 6.1E-06	0.0004563	

Notes:

- 1 ^{40}Ar *atm, ^{40}Ar produced from radioactive decay and atmosphere; $^{39}\text{Ar}_{\text{K}}$, ^{39}Ar produced from ^{39}K ; ^{38}Ar produced from atmosphere and chlorine; ^{37}Ar produced from calcium; ^{36}Ar atm, atmospheric ^{36}Ar . %Rad, the percentage of radiogenic ^{40}Ar for $^{40}\text{Ar}_{\text{total}}$; R, the ratio of radiogenic ^{40}Ar to $^{39}\text{Ar}_{\text{K}}$
- 2 All data are in moles
- 3 All uncertainties are quotes at one standard deviation (1σ)
- 4 J values calculated assuming an age of 28.02 ± 0.09 Ma (after Renne et al., 1998)
- 5 Monitor prepared by New Mexico Tech; 20–28 mesh size
- 6 All data are corrected for mass discrimination and interfering argon isotopes produced during $^{39}\text{Ar}_{\text{K}}$

Appendix-C continued:

Cahaba Basin muscovite cooling–ages data.

		⁴⁰ Ar (*+atm)	³⁹ Ar(K)	³⁸ Ar (Cl+atm)	³⁷ Ar(Ca)	³⁶ Ar(Atm)	%Rad	R	Age (Ma)	%-sd						
<i>au9-2b-mus</i>	1	1.46E-14	2.1E-17	8.413E-16	4.5E-18	1.391E-18	7.2E-20	-8.07E-19	1.238E-18	1.277E-18	2.434E-19	97%	16.879146	372.235	2.846	0.007645
<i>CHB-5</i>	2	1.69E-14	3.7E-17	9.749E-16	3.2E-18	1.339E-18	6.09E-20	-1.97E-18	6.638E-19	6.792E-19	2.541E-19	99%	17.100516	376.641	2.259	0.005999
	3	7.56E-15	1.3E-17	3.62E-16	3.5E-18	1.417E-18	1.41E-19	-1.38E-18	9.059E-19	4.831E-18	2.561E-19	81%	16.950945	373.665	6.524	0.017459
	4	6.31E-15	1.9E-17	3.695E-16	2.5E-18	1.506E-18	1.6E-19	4.424E-19	8.397E-19	8.092E-19	2.673E-19	96%	16.427223	363.207	5.501	0.015145
	5	1.16E-14	8E-18	6.717E-16	2.4E-18	1.457E-18	9.5E-20	-1.27E-19	1.183E-18	5.64E-19	2.466E-19	99%	16.990318	374.449	2.750	0.007343
	6	3.74E-15	1.6E-17	2.166E-16	8.8E-19	5.976E-19	1.13E-19	1.352E-18	7.789E-19	5.924E-19	2.516E-19	95%	16.448869	363.641	7.926	0.021796
	7	1.58E-14	1.6E-17	8.812E-16	2.8E-18	2.007E-18	1.09E-19	1.091E-18	1.098E-18	2.618E-18	2.637E-19	95%	17.023598	375.111	2.359	0.006289
	8	4.73E-14	3.5E-17	2.186E-15	4.7E-18	5.034E-18	1.19E-19	1.879E-18	1.062E-18	2.23E-18	2.671E-19	99%	21.322757	458.677	1.315	0.002866
	9	1.8E-15	6.3E-18	1.019E-16	9.8E-19	3.221E-19	1.24E-19	-4.02E-19	8.205E-19	5.612E-19	2.533E-19	91%	16.075444	356.149	16.762	0.047065
	10	1.74E-14	9.7E-18	9.958E-16	4.2E-18	3.5E-18	1.63E-19	2.205E-18	8.578E-19	1.794E-18	2.751E-19	97%	16.938367	373.415	2.428	0.006502
	11	1.54E-14	2.1E-17	7.661E-16	2.8E-18	1.459E-18	8.62E-20	1.215E-18	9.251E-19	7.715E-19	2.51E-19	99%	19.745717	428.470	2.714	0.006335
	12	5.04E-15	6.3E-17	2.994E-16	3E-18	7.352E-19	1.07E-19	1.313E-18	9.464E-19	3.345E-19	2.552E-19	98%	16.517914	365.023	8.152	0.022333
	13	1.53E-14	2E-17	8.9E-16	3E-18	1.411E-18	7.43E-20	4.123E-19	8.4E-19	4.079E-20	2.856E-19	100%	17.174727	378.115	2.513	0.006647
	14	5.28E-15	8.6E-18	3.071E-16	9.9E-19	-2.84E-19	-5.7E-20	-2.6E-19	1.244E-18	3.135E-19	2.86E-19	98%	16.894991	372.551	6.223	0.016703
	15	8.18E-15	1.3E-17	4.352E-16	1.8E-18	5.633E-19	5.56E-20	1.37E-18	1.147E-18	-1.56E-19	-3.09E-19	101%	18.906723	412.192	4.899	0.011884
	16	1.16E-14	3.6E-17	5.357E-16	1.9E-18	1.253E-18	1.07E-19	3.485E-19	1.204E-18	-1.6E-19	-2.88E-19	100%	21.778219	467.307	4.078	0.008726
	17	1.35E-14	1.6E-17	7.989E-16	3.2E-18	1.851E-18	1.17E-19	6.094E-18	1.571E-18	4.199E-20	2.459E-19	100%	16.865255	371.958	2.593	0.006971
	19	7.59E-15	9E-18	4.592E-16	4.6E-18	4.818E-19	4.07E-20	1.216E-18	1.075E-18	2.475E-19	2.257E-19	99%	16.359583	361.852	4.879	0.013483
	20	7.78E-15	8E-18	4.586E-16	1.4E-18	1.113E-18	9.67E-20	1.352E-18	1.712E-18	2.511E-19	2.359E-19	99%	16.795277	365.523	4.371	0.009636
	21	1.32E-14	2.4E-17	7.836E-16	2.9E-18	3.403E-18	2.2E-19	1.791E-18	1.235E-18	3.971E-19	2.405E-19	99%	16.677449	368.211	2.521	0.006845
	22	4.61E-15	6.5E-18	2.819E-16	2.9E-18	8.141E-19	1.04E-19	1.66E-18	1.173E-18	-1.55E-19	-2.45E-19	101%	16.605651	364.799	6.798	0.018635
	23	1.08E-14	1.1E-17	6.375E-16	3.2E-18	8.765E-19	5.66E-20	1.474E-18	1.363E-18	5.356E-19	2.409E-19	99%	16.635788	367.379	3.112	0.00847
	24	3.2E-15	7E-18	1.921E-16	2.3E-18	4.959E-19	9.59E-20	2.266E-18	1.345E-18	-2.17E-20	-2.47E-19	100%	16.714647	368.954	9.313	0.025242
	25	1.17E-14	1.6E-17	6.844E-16	4.3E-18	2.105E-18	1.7E-19	2.776E-18	1.228E-18	1.19E-19	2.213E-19	100%	17.020207	375.044	3.228	0.008607
	26	9.23E-15	1.1E-17	4.96E-16	2.7E-18	5.416E-19	5.36E-20	2.762E-18	1.177E-18	1.955E-19	2.232E-19	99%	18.491525	404.082	3.714	0.009191
	27	9.65E-15	1.4E-17	6.613E-16	4.4E-18	1.93E-18	1.07E-19	3.369E-18	1.209E-18	-4.55E-20	-2.38E-19	100%	14.607532	326.392	4.204	0.009815
	28	6.47E-15	1.2E-17	3.785E-16	2.7E-18	8.061E-19	9.42E-20	1.906E-18	1.404E-18	1.111E-19	2.296E-19	99%	16.998485	374.612	4.853	0.012955
	30	4.86E-15	4.7E-18	2.878E-16	2.1E-18	5.249E-19	7.59E-20	1.195E-18	1.208E-18	2.864E-20	2.235E-19	100%	16.859293	371.673	5.822	0.015663
	31	4.86E-15	8.9E-18	2.863E-16	3.4E-18	1.156E-18	1.38E-19	3.349E-18	1.471E-18	2.721E-19	2.845E-19	98%	16.705814	368.778	4.788	0.021371
	32	7.66E-15	1.3E-17	4.508E-16	3.2E-18	7.288E-19	6.92E-20	1.329E-18	9.025E-19	1.466E-19	2.322E-19	99%	16.891899	372.489	4.341	0.011659
	33	1.55E-14	1.8E-17	8.767E-16	5.9E-18	1.773E-18	9.48E-20	5.585E-18	1.063E-18	4.057E-19	2.439E-19	99%	17.540807	383.372	3.213	0.008338
	34	2.22E-15	5.2E-18	1.295E-16	1.7E-18	-2.06E-22	-7.1E-23	1.674E-18	1.134E-18	1.179E-19	2.353E-19	98%	16.875773	371.407	12.854	0.03461
	35	9.78E-15	1.7E-17	5.463E-16	3.4E-18	1.088E-18	9.01E-20	2.557E-18	8.131E-19	1.35E-19	2.31E-19	100%	17.827392	391.032	3.747	0.009583
	36	1.14E-15	5.2E-18	6.373E-17	6.7E-19	1.295E-18	2.22E-19	2.764E-18	1.432E-18	1.783E-19	2.309E-19	95%	17.098188	376.595	24.114	0.06403
	37	7.1E-15	9.7E-18	4.162E-16	2.9E-18	1.599E-18	8.48E-20	1.884E-18	1.669E-18	8.793E-20	2.225E-19	100%	17.007921	374.799	4.389	0.011711
	39	4.67E-15	7.3E-18	2.675E-16	1.6E-18	1.719E-18	1.04E-19	2.672E-18	1.091E-18	1.739E-19	2.298E-19	99%	17.278412	380.174	6.085	0.016007
	40	2.97E-15	4.9E-18	1.74E-16	2E-18	4.487E-19	6.31E-20	1.108E-18	1.423E-18	2.266E-19	2.23E-19	98%	16.674259	368.148	9.462	0.025702
	41	2.88E-15	6E-18	1.387E-16	5.8E-19	8.883E-19	1.44E-19	3.041E-18	1.164E-18	6.486E-20	2.3E-19	99%	20.640359	445.668	10.917	0.024496
	42	1.34E-14	2.2E-17	7.753E-16	3.2E-18	2.076E-18	8.04E-20	2.128E-18	1.42E-18	5.079E-19	2.341E-19	99%	17.119806	377.024	2.584	0.006853
	43	2.95E-15	8.6E-18	1.744E-16	1.6E-18	7.268E-19	7.82E-20	5.878E-19	1.02E-18	1.342E-19	2.229E-19	99%	16.670419	368.071	6.993	0.024703
	44	6.99E-15	1.2E-17	4.089E-16	3E-18	1.306E-18	7.31E-20	1.305E-18	1.276E-18	-5.75E-19	-3.96E-19	102%	17.50954	384.753	9.001	0.017937
	45	1.87E-14	2.9E-17	1.11E-15	4.1E-18	3.001E-18	1.17E-19	6.204E-18	1.746E-18	9.242E-19	2.68E-19	99%	16.611562	366.895	2.161	0.005889
	46	5.45E-15	5.7E-18	3.206E-16	3.4E-18	9.204E-19	8.67E-20	7.988E-19	1.462E-18	7.766E-20	2.368E-19	100%	16.914892	372.947	6.229	0.016701
	47	3.48E-15	8.2E-18	1.762E-16	1.6E-18	1.244E-18	1.16E-19	3.503E-18	1.14E-18	1.871E-19	2.246E-19	98%	19.430719	422.376	9.153	0.02167
	48	4.42E-15	1.1E-17	2.639E-16	1.7E-18	3.302E-19	3.79E-20	7.285E-19	1.295E-18	9.588E-20	2.205E-19	99%	16.627799	367.220	6.023	0.016402
	49	8.13E-16	3.1E-18	4.651E-17	4.3E-19	4.665E-19	1.32E-19	7.383E-19	1.334E-18	-1.41E-19	-2.26E-19	105%	18.375053	401.839	31.648	0.078758
	50	5E-15	7.9E-18	2.948E-16	1.3E-18	8.626E-19	9.37E-20	1.513E-18	1.448E-18	2.718E-19	2.244E-19	98%	16.679268	368.248	5.260	0.014284
	53	3.49E-16	2E-18	1.885E-17	4.4E-19	-6.23E-19	-7.7E-19	-3.69E-19	9.428E-19	3.055E-19	3.262E-19	74%	13.752545	308.831	115.332	0.373446
	55	3.27E-15	6.3E-18	1.912E-16	1.4E-18	1.811E-19	4.92E-20	1.645E-18	1.139E-18	-2.3E-19	-3.54E-19	102%	17.443421	383.444	12.329	0.032154
	56	5.35E-15	8.9E-18	3.095E-16	3.5E-18	2.44E-19	4.25E-20	1.876E-18	1.111E-18	4.156E-19	3.214E-19	98%	16.883415	372.320	8.081	0.021705
	59	3.42E-15	8.3E-18	2.05E-16	1.7E-18	-1.56E-19	-2.9E-20	7.468E-19	1.216E-18	1.616E-19	2.328E-19	99%	16.433897	363.341	8.077	0.022231
	60	1.4E-15	4.4E-18	9.284E-17	8.2E-19	-2.39E-19	-1.2E-19	-4.84E-18	1.868E-18	4.042E-19	2.333E-19	91%	13.763341	309.054	16.980	0.054942
	61	4.87E-15	1.3E-17	2.853E-16	2.1E-18	1.019E-19	1.02E-20	-9.49E-19	1.147E-18	2.219E-19	2.174E-19	99%	16.846091	371.576	5.805	0.015623
	62	4.16E-15	7.3E-18	2.392E-16	1.3E-18	-4.49E-20	-6E-21	-6.82E-19	1.01E-18	-2.08E-20	-2.89E-19	100%	17.408428	382.751	8.162	0.021324
	63	7.48E-15	8.2E-18	4.484E-16	4.1E-18	5.282E-19	3.57E-20	8.68E-19	1.26E-18	3.149E-19	2.235E-19	99%	16.465728	363.978	4.711	0.012942
	64	1.46E-15	8.8E-18	8.924E-17	1.6E-18	4.69E-19	1.5E-19	-1.05E-18	1.06E-18	3.471E-19	2.201E-19	93%	15.184314	338.143	17.580	0.05199
	65	1.61E-15	3.7E-18	9.151E-17	7.3E-19	5.44E-20	1.91E-20	-2.67E-20	1.066E-18	2.446E-19	2.173E-19	96%	16.815237	370.961	15.809	0.042617
	67	8.5E-16	2E-18	4.872E-17	6.2E-19	-1.56E-19	-1.5E-19	-6.26E-19	1.143E-18	-1.04E-19	-2.17E-19	104%	18.079115	395.989	29.303	0.073999
	68	3.62E-15	1E-17	2.097E-16	7.7E-19	5.672E-19	7.92E-20	-1.43E-18	6.419E-19	-2.43E-19	-2.21E-19	102%	17.586842	386.282	7.069	0.0183
	69	6.11E-15	8.4E-18	3.662E-16	2.											

Appendix–C continued:

Cahaba Basin muscovite cooling–ages data.

	⁴⁰ Ar (*+atm)	³⁹ Ar(K)	³⁸ Ar (Cl+atm)	³⁷ Ar(Ca)	³⁶ Ar(Atm)	%Rad	R	Age (Ma)	%-sd
au9.2a.mus	77	9.45E-15 + 1.2E-17	6.356E-16 + 4.2E-18	1.113E-18 + 3.96E-20	1.743E-21 + 1.437E-18	3.93E-19 + 2.282E-19	99%	14.682789	327.930 + 3.270 0.00997
d2-s2	78	3.27E-14 + 3.6E-17	2.214E-15 + 4.4E-18	6.259E-18 + 2.63E-19	-6.45E-19 + 1.333E-18	8.183E-19 + 2.205E-19	99%	14.640914	327.074 + 0.995 0.003042
	79	2.07E-15 + 5.3E-18	1.372E-16 + 2.3E-18	1.141E-19 + 2.19E-20	1.991E-18 + 1.29E-18	3.348E-19 + 2.232E-19	95%	14.356123	321.246 + 12.156 0.037839
	80	4.55E-15 + 6.4E-18	3.015E-16 + 2.6E-18	1.715E-19 + 2.06E-20	-4.86E-19 + 1.739E-18	4.992E-19 + 2.329E-19	97%	14.599855	326.235 + 5.879 0.01802
	81	5.08E-15 + 7E-18	3.026E-16 + 1.6E-18	1.615E-19 + 1.7E-20	-2E-18 + 1.573E-18	2.215E-19 + 2.279E-19	99%	16.588903	366.442 + 5.338 0.014567
	83	7.3E-15 + 1.2E-17	4.823E-16 + 4.3E-18	5.139E-19 + 3.27E-20	-6.61E-19 + 1.367E-18	-1.38E-19 + -2.85E-19	101%	15.227487	339.019 + 4.923 0.005452
	84	1.04E-14 + 1.5E-17	7.019E-16 + 4.3E-18	1.349E-18 + 5.82E-20	-6.94E-19 + 1.779E-18	5.602E-19 + 2.252E-19	98%	14.562334	325.468 + 2.982 0.009164
	85	2.5E-15 + 5.1E-18	1.705E-16 + 2.3E-18	-1.66E-19 + -2.9E-20	-2.59E-19 + 1.388E-18	3.056E-19 + 2.179E-19	96%	14.109206	316.178 + 9.600 0.030364
	86	1.28E-14 + 1.6E-17	8.637E-16 + 3.1E-18	9.277E-19 + 3.89E-20	-1.77E-18 + 1.503E-18	-1.72E-19 + -3.11E-19	100%	14.883822	332.030 + 2.692 0.008108
	87	1.16E-14 + 1E-17	6.872E-16 + 4.1E-18	8.948E-19 + 4.47E-20	-1.57E-18 + 1.35E-18	-4.44E-19 + -2.76E-19	101%	17.029983	375.238 + 3.438 0.009161
	88	2.08E-14 + 1.5E-17	1.304E-15 + 5.9E-18	3.049E-18 + 9.51E-20	-1.12E-18 + 1.356E-18	5.136E-19 + 2.389E-19	99%	15.812487	350.854 + 2.007 0.00572
	89	1.44E-14 + 1.5E-16	8.328E-16 + 8.4E-18	1.136E-18 + 5.13E-20	7.833E-19 + 1.378E-18	6.095E-19 + 2.273E-19	99%	17.034421	375.327 + 5.819 0.015505
	90	2.29E-14 + 1.8E-16	1.342E-15 + 5.3E-18	1.795E-18 + 6.5E-20	-1.94E-18 + 1.365E-18	3.834E-19 + 2.283E-19	100%	16.982543	374.294 + 3.516 0.009392
	91	3.39E-14 + 2.4E-17	1.902E-15 + 9.9E-18	4.577E-18 + 6.42E-20	4.527E-21 + 1.348E-18	5.434E-19 + 2.417E-19	100%	17.717576	388.865 + 2.210 0.005682
	92	1.63E-14 + 2.1E-17	1.104E-15 + 3.8E-18	1.506E-18 + 4.32E-20	-1.89E-18 + 1.647E-18	4.432E-19 + 2.32E-19	99%	14.620246	326.652 + 1.835 0.005619
	93	3.19E-14 + 2.2E-17	1.517E-15 + 3.5E-18	2.136E-18 + 3.99E-20	8.949E-19 + 1.614E-18	7.066E-20 + 2.874E-19	100%	21.040624	453.310 + 1.634 0.003605
	94	2.17E-14 + 2.2E-17	1.263E-15 + 5.1E-18	1.827E-18 + 3.72E-20	6.102E-18 + 1.447E-18	8.487E-19 + 2.247E-19	99%	17.007377	374.789 + 1.970 0.005256
	95	1.36E-14 + 2.3E-17	9.139E-16 + 3.6E-18	1.528E-18 + 5.16E-20	-5.31E-19 + 1.525E-18	5.091E-19 + 2.398E-19	99%	14.765198	329.612 + 2.242 0.006803
	96	2.42E-14 + 3.6E-17	1.64E-15 + 3.2E-18	3.534E-18 + 1.14E-19	4.793E-18 + 2.396E-18	4.971E-19 + 2.176E-19	99%	14.664475	327.556 + 1.197 0.003656
	97	2.15E-16 + 1.4E-18	1.193E-17 + 5.2E-19	-3.72E-19 + -4.1E-19	5.583E-19 + 1.602E-18	9.348E-20 + 2.325E-19	87%	15.690645	348.396 + 129.254 0.370997
	98	1.26E-14 + 1.3E-17	8.427E-16 + 3.2E-18	1.489E-18 + 5.21E-20	-8.84E-19 + 1.405E-18	3.68E-19 + 2.201E-19	99%	14.766648	329.638 + 2.156 0.006542
	99	1.1E-14 + 1.5E-17	6.682E-16 + 4.9E-18	8.078E-19 + 3.49E-20	5.156E-19 + 1.66E-18	5.075E-20 + 2.248E-19	100%	16.491022	364.485 + 3.508 0.009623
	100	1.79E-14 + 2.2E-17	8.255E-16 + 3.3E-18	1.362E-18 + 6.34E-20	-6.27E-19 + 1.565E-18	4.46E-19 + 2.332E-19	99%	21.574781	463.457 + 2.643 0.005703
	1	2.73E-15 + 7.1E-18	1.794E-16 + 1.6E-18	-5.22E-19 + -1.1E-19	-3.25E-18 + 1.454E-18	-1.34E-19 + -2.8E-19	101%	15.432516	343.176 + 10.732 0.031274
	2	3.77E-15 + 8.7E-18	2.237E-16 + 2.4E-18	-5.05E-19 + -1.6E-19	2.564E-19 + 1.445E-18	3.574E-19 + 2.44E-19	97%	16.3937	362.536 + 8.263 0.022793
	3	2.17E-15 + 7.6E-18	1.468E-16 + 2.2E-18	3.578E-19 + 9.99E-20	3.47E-20 + 1.303E-18	4.362E-19 + 2.404E-19	94%	13.894346	311.756 + 11.976 0.038415
	4	2.12E-15 + 6.6E-18	1.432E-16 + 7.5E-19	-9.72E-19 + -1.1E-18	-1.15E-18 + 1.3E-18	3.737E-19 + 2.379E-19	95%	14.044274	314.842 + 11.189 0.035539
	7	7.98E-16 + 2.6E-18	5.248E-17 + 7.1E-19	-7.86E-19 + -1.5E-18	-3.46E-18 + 1.591E-18	1.213E-19 + 2.354E-19	96%	14.51802	324.562 + 30.008 0.092457
	8	1.19E-15 + 4.3E-17	7.689E-17 + 3E-18	-4.93E-19 + -9.3E-19	-8.99E-19 + 1.256E-18	5.551E-19 + 2.317E-19	86%	13.341372	300.325 + 27.294 0.09088
	9	8.23E-16 + 3.4E-18	3.771E-17 + 5.9E-19	-5.22E-19 + -1.9E-18	-1.63E-18 + 1.427E-18	5.224E-19 + 2.354E-19	81%	17.73826	389.274 + 41.235 0.105929
	11	2.43E-15 + 4.3E-18	1.616E-16 + 1.5E-18	-3.49E-19 + -1.4E-19	-1.97E-18 + 1.399E-18	-2.88E-19 + -3.05E-19	103%	15.587824	346.318 + 12.781 0.036905
	12	1.29E-15 + 3.7E-18	8.786E-17 + 1.3E-18	-6.48E-19 + -1.5E-18	-3.58E-19 + 1.183E-18	5.758E-19 + 2.39E-19	87%	12.762387	288.279 + 18.827 0.065308
	13	9.38E-15 + 1.2E-17	5.375E-16 + 2.5E-18	6.53E-19 + 6.06E-20	-1.29E-18 + 1.16E-18	2.977E-19 + 2.362E-19	99%	17.295818	380.519 + 3.391 0.008911
	14	3.7E-15 + 5.3E-18	2.112E-16 + 1.4E-18	2.564E-19 + 5.88E-20	-1.06E-18 + 1.52E-18	5.417E-19 + 2.427E-19	96%	16.779490	370.247 + 7.949 0.02147
	15	8.16E-15 + 1.3E-17	4.335E-16 + 1.8E-18	8.488E-19 + 8.64E-20	9.206E-19 + 1.422E-18	1.214E-20 + 2.757E-19	100%	18.822388	410.548 + 4.552 0.011089
	17	4.36E-15 + 7E-18	2.915E-16 + 2.1E-18	-2.08E-20 + -3.6E-21	-4.92E-19 + 1.405E-18	9.489E-20 + 2.842E-19	99%	14.875566	331.862 + 6.894 0.020775
	18	3.2E-16 + 4.2E-18	2.036E-17 + 4.9E-19	-1.11E-18 + -6.9E-19	-1.88E-18 + 1.22E-18	4.453E-19 + 2.416E-19	59%	9.2668004	213.788 + 81.569 0.381543
	19	8.26E-15 + 8.9E-18	3.847E-16 + 1.6E-18	-1.17E-19 + -1.8E-20	-1.8E-18 + 1.696E-18	-3.57E-19 + -2.67E-19	101%	21.755453	466.877 + 4.811 0.010305
	21	7.2E-16 + 2.3E-18	4.6E-17 + 4.5E-19	-3.49E-19 + -1.6E-18	-9.61E-19 + 1.295E-18	2.704E-19 + 2.603E-19	89%	13.917567	312.234 + 37.682 0.120685
	22	1.13E-15 + 2.6E-18	7.703E-17 + 1.1E-18	-2.81E-19 + -2.9E-19	-1.47E-18 + 1.4E-18	-1.82E-20 + -2.76E-19	100%	14.796482	330.250 + 24.113 0.073015
	23	1.24E-15 + 3.1E-18	8.377E-17 + 9E-19	-4.14E-19 + -4.8E-19	-1.99E-18 + 1.317E-18	4.503E-19 + 2.436E-19	89%	13.154753	296.451 + 19.716 0.066508
	24	8.87E-16 + 3.2E-18	5.605E-17 + 6.8E-19	-7.75E-19 + -1.8E-18	-1.44E-18 + 1.194E-18	3.842E-19 + 2.324E-19	87%	13.79963	309.803 + 27.873 0.08997
	25	5.84E-16 + 3.5E-18	3.734E-17 + 5.2E-19	-3.11E-19 + -2.6E-18	2.485E-18 + 1.937E-18	3.285E-19 + 2.391E-19	83%	13.052555	294.326 + 43.109 0.146468

Appendix–C continued:

Cahaba Basin muscovite cooling–ages data.

	⁴⁰ Ar (*+atm)	³⁹ Ar(K)	³⁸ Ar (Cl+atm)	³⁷ Ar(Ca)	³⁶ Ar(Atm)	%Rad	R	Age (Ma)	%-sd							
au9.4c.mus	26	3.63E-15	+ 6.9E-18	1.599E-16	+ 2E-18	1.167E-18	+ 2.06E-19	-1.25E-18	+ 1.66E-18	1.352E-18	+ 1.472E-19	89%	20.23374	437.872	+ 8.635	0.01972
D2-S1	27	3.34E-15	+ 5.8E-18	1.843E-16	+ 1.7E-18	1.368E-18	+ 2.08E-19	-1.92E-18	+ 1.593E-18	4.728E-19	+ 1.491E-19	96%	17.346856	381.531	+ 6.434	0.016863
	28	7.39E-15	+ 9.6E-18	3.733E-16	+ 1.9E-18	1.698E-18	+ 1.59E-19	-2.27E-18	+ 1.691E-18	4.837E-20	+ 1.558E-19	100%	19.744729	428.451	+ 3.470	0.0081
	29	2.58E-15	+ 3.7E-18	1.191E-16	+ 1.7E-18	9.412E-19	+ 1.92E-19	-1.76E-18	+ 1.743E-18	1.846E-19	+ 1.591E-19	98%	21.221506	456.753	+ 10.753	0.023541
	30	2.06E-15	+ 5.3E-18	1.278E-16	+ 9.9E-19	1.038E-18	+ 2.06E-19	-1.68E-18	+ 1.544E-18	-3.91E-19	+ -2.61E-19	106%	17.003104	374.703	+ 13.630	0.036374
	31	1.28E-14	+ 1.4E-17	7.631E-16	+ 1.7E-18	1.337E-18	+ 8.96E-20	1.073E-18	+ 1.401E-18	1.694E-19	+ 2.586E-19	100%	16.769858	370.056	+ 2.404	0.006496
	32	7.57E-14	+ 4.5E-17	3.567E-15	+ 5.6E-18	8.145E-18	+ 1.24E-19	5.299E-19	+ 1.442E-18	1.248E-18	+ 2.284E-19	100%	21.119098	454.804	+ 0.869	0.001911
	34	1.98E-14	+ 1.7E-17	9.615E-16	+ 5.5E-18	2.458E-18	+ 1.08E-19	-2.21E-19	+ 1.536E-18	5.353E-19	+ 3.117E-19	99%	20.412563	441.305	+ 3.315	0.007513
	35	3.99E-15	+ 7.5E-18	1.906E-16	+ 1.7E-18	9.4E-20	+ 2.37E-20	4.647E-19	+ 1.248E-18	7.077E-20	+ 2.456E-19	99%	20.829709	449.287	+ 9.228	0.020539
	36	1.75E-14	+ 2E-17	8.323E-16	+ 3.6E-18	2.291E-18	+ 1.04E-19	-4.93E-19	+ 1.251E-18	7.862E-19	+ 2.256E-19	99%	20.766233	448.075	+ 2.680	0.005982
	37	8.71E-15	+ 1.7E-17	4.071E-16	+ 2.9E-18	1.03E-18	+ 9.47E-20	6.111E-19	+ 1.596E-18	-8.64E-19	+ -3.2E-19	103%	22.020115	471.874	+ 6.044	0.012809
	38	9.46E-16	+ 4.1E-18	4.271E-17	+ 6.6E-19	-7.63E-20	+ -8.1E-20	-1.23E-18	+ 1.03E-18	-4.72E-20	+ -2.42E-19	101%	22.473761	480.408	+ 36.593	0.07617
	39	2.42E-14	+ 2E-17	1.148E-15	+ 4.9E-18	2.86E-18	+ 1.05E-19	-3.08E-18	+ 1.495E-18	1.262E-19	+ 2.435E-19	100%	21.065086	453.776	+ 2.395	0.005279
	40	7.16E-15	+ 7.9E-18	3.359E-16	+ 3.3E-18	5.407E-19	+ 5.21E-20	3.916E-20	+ 1.035E-18	3.477E-19	+ 2.561E-19	99%	21.024364	453.000	+ 6.643	0.014664
	41	1.07E-14	+ 1.3E-17	6.031E-16	+ 1.9E-18	1.417E-18	+ 9.7E-20	-9.72E-19	+ 1.18E-18	1.7E-19	+ 2.657E-19	100%	17.657254	387.674	+ 3.151	0.008127
	42	1.47E-14	+ 2E-17	6.844E-16	+ 3E-18	1.292E-18	+ 7.39E-20	-1.98E-18	+ 1.165E-18	2.519E-19	+ 2.496E-19	99%	21.312856	458.489	+ 3.130	0.006827
	44	2.72E-14	+ 2.4E-17	1.283E-15	+ 4.2E-18	2.564E-18	+ 8.26E-20	3.276E-18	+ 1.291E-18	1.351E-18	+ 2.795E-19	99%	20.903532	450.696	+ 2.091	0.004639
	45	1.6E-14	+ 1.8E-17	7.684E-16	+ 3.4E-18	1.308E-18	+ 5.22E-20	3.965E-18	+ 1.007E-18	1.475E-19	+ 2.775E-19	100%	20.82924	449.278	+ 3.103	0.006907
	46	4.36E-15	+ 7.9E-18	2.08E-16	+ 1.8E-18	6.204E-19	+ 6.28E-20	2.254E-18	+ 1.121E-18	-1.51E-19	+ -2.72E-19	101%	21.181194	455.986	+ 9.211	0.020199
	47	6.89E-15	+ 8.9E-18	3.383E-16	+ 2.4E-18	6.879E-19	+ 7.22E-20	2.693E-18	+ 1.286E-18	5.383E-20	+ 2.757E-19	100%	20.311297	439.362	+ 6.171	0.014045
	48	1.12E-15	+ 2.5E-18	7.154E-17	+ 5.2E-19	-1.5E-19	+ -8.1E-20	2.937E-18	+ 1.373E-18	5.873E-20	+ 2.668E-19	98%	15.454946	343.630	+ 24.979	0.072692
	49	1.12E-14	+ 8.7E-18	5.775E-16	+ 2.9E-18	5.036E-19	+ 2.73E-20	1.828E-18	+ 9.784E-19	3.351E-19	+ 2.873E-19	99%	19.136165	416.658	+ 3.850	0.00924
	50	5.03E-15	+ 8E-18	2.362E-16	+ 1.3E-18	6.839E-19	+ 9.8E-20	2.625E-18	+ 1.152E-18	-1.98E-19	+ -3.16E-19	101%	21.539254	462.784	+ 8.869	0.019165
	51	2.24E-14	+ 9.1E-18	1.063E-15	+ 3E-18	1.923E-18	+ 5.51E-20	3.847E-18	+ 1.365E-18	3.497E-19	+ 2.728E-19	100%	20.977035	452.098	+ 2.078	0.004595
	52	1.35E-14	+ 2E-17	6.471E-16	+ 3.4E-18	1.602E-18	+ 7.01E-20	2.751E-18	+ 1.131E-18	2.268E-19	+ 2.848E-19	100%	20.797722	448.676	+ 3.722	0.008296
	53	3.1E-14	+ 3.3E-17	1.46E-15	+ 4.5E-18	3.427E-18	+ 9.6E-20	9.891E-19	+ 1.213E-18	1.298E-19	+ 2.168E-19	100%	21.226524	456.848	+ 1.763	0.003858
	54	5.7E-15	+ 8.9E-18	3.365E-16	+ 1.8E-18	1.039E-18	+ 9.03E-20	-4.31E-19	+ 1.192E-18	8.538E-20	+ 2.296E-19	100%	16.86359	371.925	+ 4.896	0.013164
	55	2.79E-15	+ 1E-17	1.723E-16	+ 8.8E-19	6.589E-19	+ 1.06E-19	-1.15E-19	+ 7.578E-19	-1.38E-19	+ -2.22E-19	101%	16.43442	363.351	+ 8.720	0.023998
	56	6.83E-15	+ 8.8E-18	3.29E-16	+ 2.2E-18	1.817E-18	+ 2.07E-19	6.766E-19	+ 1.335E-18	8.294E-20	+ 2.334E-19	100%	20.674581	446.323	+ 5.453	0.012129
	58	6.06E-15	+ 1E-17	3.994E-16	+ 3.8E-18	1.853E-18	+ 2.15E-19	1.343E-18	+ 1.156E-18	2.117E-19	+ 2.233E-19	99%	15.00337	334.465	+ 4.911	0.014683
	59	5.96E-15	+ 1.2E-17	3.209E-16	+ 2E-18	4.796E-19	+ 5.82E-20	8.116E-19	+ 9.222E-19	1.905E-19	+ 2.167E-19	99%	18.38521	401.999	+ 5.093	0.012669
	60	7.11E-15	+ 9E-18	3.437E-16	+ 1.8E-18	1.048E-18	+ 8.75E-20	4.879E-18	+ 1.409E-18	1.635E-19	+ 2.247E-19	99%	20.538089	443.711	+ 4.861	0.010956
	62	4.73E-15	+ 6.7E-18	2.21E-16	+ 3.3E-18	4.351E-19	+ 9.19E-20	5.4E-19	+ 1.242E-18	3.643E-19	+ 2.561E-19	98%	20.92838	451.170	+ 10.114	0.022417
	64	2.66E-15	+ 5.6E-18	7.612E-16	+ 2.6E-18	1.274E-18	+ 6.48E-20	1.358E-18	+ 6.396E-19	6.421E-19	+ 2.143E-19	93%	3.2489306	77.871	+ 2.024	0.025986
	66	2.7E-15	+ 5E-18	1.261E-16	+ 1.7E-18	5.929E-19	+ 1.42E-19	-2.98E-19	+ 7.587E-19	-7.72E-19	+ -2.96E-19	108%	23.217995	494.321	+ 15.952	0.032271
	67	4.31E-15	+ 7.4E-18	3.102E-16	+ 2.6E-18	1.937E-18	+ 2.32E-19	-3.46E-19	+ 8.997E-19	4.368E-19	+ 2.228E-19	97%	13.94924	303.492	+ 5.475	0.01804
	68	9.27E-16	+ 4.3E-18	3.843E-17	+ 4.9E-19	9.945E-19	+ 3.52E-19	1.425E-18	+ 7.982E-19	3.378E-19	+ 2.174E-19	89%	21.534005	462.685	+ 36.656	0.079224
	69	3.51E-15	+ 8.8E-18	1.695E-16	+ 1.8E-18	3.56E-19	+ 7.82E-20	1.776E-18	+ 1.391E-18	-2.53E-19	+ -2.06E-19	102%	21.147315	455.341	+ 9.094	0.019971
	70	1.09E-14	+ 1.6E-17	5.115E-16	+ 3.5E-18	5.022E-20	+ 5.09E-21	1.789E-19	+ 1.109E-18	-5.17E-21	+ -2.2E-19	100%	21.330471	458.823	+ 4.183	0.009117
	72	2.92E-15	+ 5.6E-18	1.368E-16	+ 1.6E-18	-1.63E-20	+ -5.8E-21	1.958E-19	+ 1.479E-18	7.243E-20	+ 2.334E-19	99%	21.193779	456.225	+ 12.122	0.02657
	73	5.42E-15	+ 1.6E-17	2.597E-16	+ 1.5E-18	8.484E-19	+ 1.28E-19	-1.19E-18	+ 1.233E-18	-3.02E-19	+ -2.35E-19	102%	21.230048	456.915	+ 6.428	0.014608
	77	1.04E-14	+ 2.1E-17	5.144E-16	+ 2.4E-18	7.629E-19	+ 5.36E-20	-3.39E-18	+ 1.269E-18	-5.38E-21	+ -2.75E-19	100%	20.174476	436.738	+ 4.001	0.00916
	78	3.21E-14	+ 9.9E-17	1.495E-15	+ 6.6E-18	2.895E-18	+ 8.52E-20	-2.31E-18	+ 1.278E-18	1.778E-19	+ 2.635E-19	100%	21.460755	461.296	+ 2.351	0.005096
	79	8.26E-15	+ 6.8E-18	5.013E-16	+ 2.8E-18	1.631E-18	+ 1.17E-19	1.597E-19	+ 1.074E-18	3.012E-19	+ 2.442E-19	99%	16.308713	360.832	+ 3.801	0.010534
	80	5.28E-15	+ 1.2E-17	2.474E-16	+ 1.3E-18	6.307E-19	+ 7.66E-20	-2.68E-18	+ 1.004E-18	7.149E-20	+ 2.42E-19	100%	21.263438	457.550	+ 6.722	0.014691
	81	1.01E-14	+ 1.1E-17	4.789E-16	+ 5.2E-18	6.814E-19	+ 4.97E-20	-1.62E-18	+ 1.082E-18	1.322E-19	+ 3.134E-19	100%	21.087869	454.210	+ 6.493	0.014294
	82	1.26E-14	+ 1.3E-17	1.286E-15	+ 2.2E-18	4.089E-18	+ 1.84E-19	-2.41E-18	+ 1.077E-18	8.165E-20	+ 2.467E-19	100%	9.773966	224.789	+ 1.380	0.006141
	83	1.95E-15	+ 6.1E-18	9.345E-17	+ 1.8E-18	1.271E-19	+ 4.69E-20	-2.91E-18	+ 9.226E-19	2.16E-19	+ 2.431E-19	97%	20.143638	436.140	+ 18.850	0.043221
	84	3.18E-15	+ 7.4E-18	1.529E-16	+ 2.3E-18	5.661E-20	+ 1.53E-20	-1.68E-18	+ 1.086E-18	-2.29E-19	+ -2.87E-19	102%	21.263476	457.550	+ 13.672	0.029882
	85	4.78E-15	+ 1.1E-17	2.279E-16	+ 1.8E-18	9.16E-19	+ 1.1E-19	1.677E-18	+ 9.574E-19	-7.16E-20	+ -2.06E-19	100%	21.072061	453.909	+ 6.819	0.015023
	86	2.82E-15	+ 1.1E-17	1.373E-16	+ 7.6E-19	5.811E-19	+ 1.1E-19	7.563E-19	+ 1.046E-18	3.967E-19	+ 2.598E-19	96%	19.707076	427.724	+ 12.508	0.029243
	88	9.23E-15	+ 1.7E-17	6.53E-16	+ 3E-18	1.238E-18	+ 4.05E-20	-7.43E-19	+ 1.149E-18	-8.56E-19	+ -1.88E-19	103%	14.521795	324.639	+ 2.474	0.00762
	90	3.45E-15	+ 1.2E-17	1.613E-16	+ 1.6E-18	9.598E-19	+ 1.16E-19	-1.92E-19	+ 9.718E-19	2.032E-19	+ 1.256E-19	98%	21.028626	453.081	+ 6.912	0.015255